A High–Level Investigation of the Energetics and Kinetics of Cyano Radical Reactions

by

Alexandra Diann Burke

(Under the Direction of Henry F. Schaefer III)

Abstract

Highly accurate quantum chemical methods may be utilized to characterize small molecule reactions with accuracy rivaling experiment. This type of study may provide understanding of reactions that are difficult to investigate via experimental methods, thus providing guidance to experiment. The first project in this dissertation investigates a variety of hydrogen abstractions by the cyano radical with a large set of different hydrogen donors. It concludes that the methodology developed for this study has excellent agreement with experiment, and it may be used for future studies of hydrogen abstractions, particularly with larger hydrogen donors. The second project in this dissertation builds on the first as it investigates hydrogen abstractions by the cyano radical of slightly larger hydrogen donors. It shows that a similar methodology provides results that may be relied upon to guide future studies of these same reactions. The final chapter of this dissertation provides a summary of the overall findings of this study.

INDEX WORDS: Computational Chemistry, Coupled–Cluster Theory, Focal Point Analysis, Basis Set Extrapolation, Transition State Theory, Cyano Radical, Hydrogen Abstraction

A High–Level Investigation of the Energetics and Kinetics of Cyano Radical Reactions

by

Alexandra Diann Burke

B.S. Taylor University, 2019

A Dissertation Submitted to the Graduate Faculty
of the University of Georgia in Partial Fulfillment
of the Requirements for the Degree

Doctor of Philosophy

Athens, Georgia

2023

A High–Level Investigation of the Energetics and Kinetics of Cyano Radical Reactions

by

Alexandra Diann Burke

Major Professor: Henry F. Schaefer III

Committee: Melanie A. Reber

Steven E. Wheeler

Electronic version approved:

Ron Walcott

Dean of the Graduate School

University of Georgia

August 2023

Dedication

To my fiancé, Alexander, and to my mom and dad. Thank you for pushing me to grow into a better scientist and for your undying love and support as I have worked toward the culmination of this dissertation.

Acknowledgements

The publication of this dissertation was made possible by numerous friends, colleagues, and family members.

- My faith and commitment to Jesus have been the most important parts of my life. This would not have been possible without the strength He has mercifully given me. I would not be who I am today without Him, and I am eternally grateful for all that He has done for me.

- The best part of my time in graduate school has been my relationship with Alexander Heide, the man I love and will be marrying in a couple months. His love, support, and encouragement have been a wonderful blessing that have made this process so much easier.

- I am so grateful to my parents, Matt and Jill Burke. They have been a constant source of encouragement and support over the last 4 years. Moving 600 miles away from home was so difficult, but it has been a wonderful experience and it has brought a lot of blessing to my life. Without their support, I would not have been able to do this.

- I would also like to thank Jacob, Grace, Claire, and Levi Burke, my lifelong partners in crime for always believing in me and encouraging me. I even thank them for all the times they have called me a nerd.

- The professors at my undergraduate institution, Taylor University, greatly influenced me and taught me how to be a student and scientist and how to make my faith part of my academic pursuits.

- Over the past several years, Dr. Henry F. Schaefer has been a wonderful mentor and encouragement as I have navigated the difficulties of graduate school.
- My committee members, Dr. Steven Wheeler and Dr. Melanie Reber, have been giving of their time and their feedback, which have made me into the scientist I am today.
- I would like to thank Dr. Justin Turney for all of his assistance with the numerous projects and assignments I attempted over the past several years.
- I would like to thank the many other students I have worked alongside in the Center for Computational Quantum Chemistry. Your friendship and knowledge have made the last 4 years a blast and very educational.
- I would like to thank the administrative team at the CCQC, Sybil Zimmerman, Kathryn Juras, Amber Lahm, Megan Reeves, Emory Grace Smith, and Carroll Williams. Their support with all of the paperwork and administrative processes have made it possible for me to focus on my education without getting bogged down by the bureaucracy.
- Graduate school would have been impossible for me if not for my community outside of school. I would like to thank all of the lifelong friends I have made throughout my life for their friendship and community over the past several years. You have kept me steady and balanced as I've gone through all the craziness.
- There are many more people to whom I am forever grateful for their encouragement and belief that I could accomplish this goal. Thank you all for your kind words and many prayers.

Table of Contents

List of Tables

List of Figures

List of Symbols or Abbreviations

ATcT	Active Thermochemical Tables
aug–cc–pVXZ	augmented correlation consistent polarized valence X–ζ basis set
CBS	Complete basis set
CC	Coupled cluster
cc–pCVXZ	correlation consistent polarized core–valence X–ζ basis set
cc–pVXZ	correlation consistent polarized valence X–ζ basis set
CCSD(T)	Coupled cluster with single, double, and perturbative triple excitations
CCSDT	Coupled cluster with single, double, and triple excitations
CCSDT(Q)	Coupled cluster with single, double, triple, and perturbative quadruple excitations
CGTO	Contracted Gaussian–type orbital
CISD	Configuration interaction with single and double excitations
CORE	Core–valence correlation correction
CVT	Canonical variational transition state theory
DBOC	Diagonal Born–Oppenheimer correction
FCI	Full configuration interaction
FPA	Focal point analysis
GTO	Gaussian–type orbital
HF	Hartree–Fock
ISM	Interstellar Medium
LCAO	Linear combination of atomic orbitals
MO	Molecular orbital
MP2	Second–order Møller–Plesset perturbation theory
PRC	Pre–reactive complex or post–reactive complex
REL	Scalar relativistic correction
RHF	Restricted Hartree–Fock
ROHF	Restricted open–shell Hartree–Fock
RRHO	Rigid–rotor harmonic oscillator
SCT	Small curvature tunneling
SO	Spin–orbit coupling
STO	Slater–type orbital
TS	Transition state
TST	Transition state theory
UHF	Unrestricted Hartree–Fock
VPT2	Second–order vibrational perturbation theory
VTST	Variational transition state theory
X2C–1e	Exact two–component one electron
ZPVE	Zero–point vibrational energy

Chapter 1

Introduction

The Schrödinger Equation

The time–independent Schrödinger equation[1] is the fundamental equation that governs the properties of molecular systems:

$$\hat{H}\boldsymbol{\Psi} = E\boldsymbol{\Psi} \tag{1.1}$$

where $\hat{H}$ is the quantum mechanical Hamiltonian operator, $\boldsymbol{\Psi}$ is the molecular wavefunction, and $E = \langle\boldsymbol{\Psi}|\hat{H}|\boldsymbol{\Psi}\rangle$ is the total energy. The Hamiltonian operator may be written in terms of the following kinetic and potential energy operators:

$$\hat{H} = \hat{T}_N + \hat{T}_e + \hat{V}_{Ne} + \hat{V}_{ee} + \hat{V}_{NN} \tag{1.2}$$

where $\hat{T}_N$ is the kinetic energy operator of the nuclei, $\hat{T}_e$ is the kinetic energy operator of the electrons, $\hat{V}_{ee}$ is the electron–electron repulsion operator, $\hat{V}_{Ne}$ is the nuclear–electron attraction operator, and $\hat{V}_{NN}$ is the nuclear–nuclear repulsion operator. The operators, when neglecting relativistic effects, are simple generalizations of the classical hamiltonian for charged particles. The kinetic energy operator takes on the general form $\frac{-\hbar^2}{2m}\nabla^2_{\boldsymbol{r}}$ where m is the mass of a particle, $\hbar$ is Planck's constant divided by 2π, $\nabla^2_{\boldsymbol{r}}$ is the Laplacian operator $\frac{\partial^2}{\partial x^2} + \frac{\partial^2}{\partial y^2} + \frac{\partial^2}{\partial z^2}$ where $\boldsymbol{r}$ denotes the three–dimensional Cartesian coordinates of a particle (x, y, z), and the potential energy operator takes on the form $\frac{q_i q_j}{4\pi\epsilon_0|\boldsymbol{r_i}-\boldsymbol{r_j}|}$, where ϵ_0 is the vacuum permittivity constant and q is the charge of the particle. The Hamiltonian operator may be written as a sum of the

following kinetic and potential energy operators:

$$\hat{T}_N = -\sum_A \frac{\hbar^2}{2M_A}\nabla^2_{\boldsymbol{R}_A} \tag{1.3}$$

$$\hat{T}_e = -\sum_i \frac{\hbar^2}{2m_e}\nabla^2_{\boldsymbol{r}_i} \tag{1.4}$$

$$\hat{V}_{Ne} = -\sum_i \sum_A \frac{Z_A e^2}{|\boldsymbol{r_i} - \boldsymbol{R_A}|} \tag{1.5}$$

$$\hat{V}_{ee} = \sum_i \sum_{j>i} \frac{e^2}{4\pi\epsilon_0 |\boldsymbol{r_i} - \boldsymbol{r_j}|} \tag{1.6}$$

$$\hat{V}_{NN} = \sum_A \sum_{B>A} \frac{Z_A Z_B e^2}{4\pi\epsilon_0 |\boldsymbol{R_A} - \boldsymbol{R_B}|} \tag{1.7}$$

where $\boldsymbol{r}_i$ corresponds to the coordinates of a particular electron indexed by i and $\boldsymbol{R}_A$ denotes the coordinates of a particular nucleus indexed by A. M_A denotes the mass of nucleus A, m_e denotes the mass of an electron, Z denotes the atomic number of an atom, and e is the charge of a proton or electron. For simplicity, it is convenient to define these operators in atomic units, such that $m, \hbar, e,$ and $4\pi\epsilon_0$ are set equal to 1. This provides energy eigenvalues in units of Hartrees. This results in the following simplified operators:

$$\hat{T}_N = -\sum_A \frac{1}{2M_A}\nabla^2_{\boldsymbol{R}_A} \tag{1.8}$$

$$\hat{T}_e = -\sum_i \frac{1}{2}\nabla^2_{\boldsymbol{r}_i} \tag{1.9}$$

$$\hat{V}_{Ne} = -\sum_i \sum_A \frac{Z_A}{|\boldsymbol{r_i} - \boldsymbol{R_A}|} \tag{1.10}$$

$$\hat{V}_{ee} = \sum_i \sum_{j>i} \frac{1}{|\boldsymbol{r_i} - \boldsymbol{r_j}|} \tag{1.11}$$

$$\hat{V}_{NN} = \sum_A \sum_{B>A} \frac{Z_A Z_B}{|\boldsymbol{R_A} - \boldsymbol{R_B}|} \tag{1.12}$$

Thus, the Hamiltonian operator in atomic units is

$$\hat{H} = -\sum_{A} \frac{1}{2M_A} \nabla^2_{\boldsymbol{R}_A} - \sum_{i} \frac{1}{2} \nabla^2_{\boldsymbol{r}_i} - \sum_{i} \sum_{A} \frac{Z_A}{|\boldsymbol{r_i} - \boldsymbol{R_A}|} \tag{1.13}$$

$$+ \sum_{i} \sum_{j>i} \frac{1}{|\boldsymbol{r_i} - \boldsymbol{r_j}|} + \sum_{A} \sum_{B>A} \frac{Z_A Z_B}{|\boldsymbol{R_A} - \boldsymbol{R_B}|}$$

Within a system, the nuclei move on a much larger timescale than the electrons due to their mass. Because of this, it may be assumed the nuclei are frozen, and the electrons can be treated within the static electric field of the nuclei. This reduces the dimensionality of the solution to the Schrödinger Equation. This is known as the Born–Oppenheimer approximation.[2] Under this approximation, the nuclear kinetic energy term becomes 0 and the nuclear repulsion energy becomes a constant that can be added on to the total energy later. The result of this approximation is known as the electronic Hamiltonian:

$$\hat{H}_e = -\sum_{i} \frac{1}{2} \nabla^2_i - \sum_{i} \sum_{A} \frac{Z_A}{|\boldsymbol{r_i} - \boldsymbol{R_A}|} + \sum_{i} \sum_{j>i} \frac{1}{|\boldsymbol{r_i} - \boldsymbol{r_j}|} \tag{1.14}$$

This Hamiltonian can be written in terms of one and two–electron operators.

$$\hat{H}_e = \sum_{i} \hat{h}(i) + \sum_{i<j} \hat{g}(i,j) \tag{1.15}$$

$$\hat{h}(i) = -\frac{1}{2} \nabla^2_i - \sum_{A} \frac{Z_A}{|\boldsymbol{r_i} - \boldsymbol{R_A}|}$$

$$\hat{g}(i,j) = \sum_{i} \frac{1}{|\boldsymbol{r_i} - \boldsymbol{r_j}|}$$

This Hamiltonian has been obtained by only considering electronic interactions, by utilizing unit–based simplifications, and by implementing the Born–Oppenheimer approximation. Due to these simplifications, this Hamiltonian does not exactly describe a given molecular system. The lowest energy eigenvalue of this Hamiltonian is known

as the electronic ground state energy. For hydrogenic (one electron) systems, the Schrödinger equation may be solved analytically; however, the world is made up of many–electron systems for which the Schrödinger equation cannot be solved analytically. Methods have been developed to numerically approximate solutions to the Schrödinger equation with varying levels of accuracy. These will be discussed in the following sections.

The Wavefunction

The wavefunction of a given system is an eigenfunction which contains all possible information about that system. It is a function that describes the behavior of the electrons as they interact with each other and the nuclei. For an N–electron system the N–electron wavefunction is built by a product of molecular orbitals (MO). Because of the Pauli principle, each molecular orbital can hold up to two electrons with opposite spins.[3] It is experimentally known that the wavefunctions we write must adhere to the antisymmetry principle and the indistinguishability of electrons. Therefore, each molecular orbital can hold up to two electrons with opposite spins, the wavefunction must change signs upon interchange of electrons, and the wavefunction must not distinguish between particles. This is accomplished with molecular spin orbitals, frequently referred to as spin orbitals.

$$\psi_i(\boldsymbol{x_j}) = \phi_i(r_j)\omega_i(s_j) \tag{1.16}$$

where $\boldsymbol{x_j} = (r_j, s_j)$, r_j represents the spatial coordinates of electron j, which are generally in Cartesian coordinates, s_j represents the spin coordinate of electron j, ϕ_i is a spatial orbital, and ω_i is a spin orbital. By convention, the spin coordinate (s_j) is either spin up (α) or spin down (β), and the spin orbitals are orthonormal. The wavefunction is often represented as a Slater determinant because of its incorpo-

ration of the antisymmetry property of the wavefunction and indistinguishability of electrons.[4] For a generalized system with N electrons, this takes the form:

$$\Phi = \frac{1}{\sqrt{N!}} \begin{vmatrix} \psi_1(\boldsymbol{x_1}) & \psi_2(\boldsymbol{x_1}) & \dots & \psi_N(\boldsymbol{x_1}) \\ \psi_1(\boldsymbol{x_2}) & \psi_2(\boldsymbol{x_2}) & \dots & \psi_N(\boldsymbol{x_2}) \\ \vdots & \vdots & \ddots & \vdots \\ \psi_1(\boldsymbol{x_N}) & \psi_2(\boldsymbol{x_N}) & \dots & \psi_N(\boldsymbol{x_N}) \end{vmatrix} \tag{1.17}$$

where $\boldsymbol{x_N}$ represents the position r_N and spin s_N of electron N. Expression of the wavefunction as a Slater determinant satisfies the Pauli principle because exchanging two electrons is equivalent to swapping two rows of a determinant. Moreover, the linear combination of products of orbitals from the determinant satisfies the indistinguishability of electrons. For a two electron system with molecular orbitals ψ_1 and ψ_2, the Slater determinant expands to:

$$\Phi(\boldsymbol{x_1}, \boldsymbol{x_2}) = \frac{1}{\sqrt{2}} \begin{vmatrix} \psi_1(\boldsymbol{x_1}) & \psi_2(\boldsymbol{x_1}) \\ \psi_1(\boldsymbol{x_2}) & \psi_2(\boldsymbol{x_2}) \end{vmatrix} = \frac{1}{\sqrt{2}} \left[\psi_1(\boldsymbol{x_1})\psi_2(\boldsymbol{x_2}) - \psi_1(\boldsymbol{x_2})\psi_2(\boldsymbol{x_1})\right] \tag{1.18}$$

Hartree–Fock Theory

Hartree–Fock (HF) theory is a critical approximation that allows chemists to determine approximate molecular orbitals for a wavefunction. It is foundational to other more accurate approximations that include the effects of electron correlation. The correlated methods that will be utilized and discussed later in this work are built upon the foundations of Hartree–Fock theory. To derive the Hartree–Fock equations, we begin at the time–independent Schrödinger equation.

$$\hat{H} \left|\Psi\right\rangle = E \left|\Psi\right\rangle \tag{1.19}$$

Left multiplying each side by $\langle\Psi|$ and integrating over all space gives

$$\langle\Psi|\hat{H}|\Psi\rangle = E\,\langle\Psi|\Psi\rangle \tag{1.20}$$

Here the wavefunction takes the assumed form of a Slater determinant Φ, and the Hamiltonian is the electronic hamiltonian previously described.

$$\langle\Phi|\hat{H}|\Phi\rangle = E\,\langle\Phi|\Phi\rangle \tag{1.21}$$

Assuming the wavefunction is normalized, this simplifies to the expectation value of the electronic Hamiltonian, which is the electronic energy:

$$E = \langle\Phi|\hat{H}|\Phi\rangle \tag{1.22}$$

Substituting Equation 1.15 in for $\hat{H}$

$$E = \langle\Phi|\sum_i \hat{h}(i) + \sum_{i<j} \hat{g}(i,j)|\Phi\rangle \tag{1.23}$$

Expanding this equation and applying spin orbital orthonormality, this becomes:

$$E = \sum_i \langle\psi_i|\hat{h}(i)|\psi_i\rangle + \sum_{i<j}\left[\langle\psi_i^i\psi_j^j|\hat{g}(i,j)|\psi_i^i\psi_j^j\rangle - \langle\psi_i^i\psi_j^j|\hat{g}(i,j)|\psi_j^i\psi_i^j\rangle\right] \tag{1.24}$$

The notation ψ_i^i represents the labeling of the electrons (subscript) and the labeling of the spin orbitals (superscript). The two terms in the two electron integrals are referred to as the Coulomb integrals

$$\langle\psi_i^i\psi_j^j|\hat{g}(i,j)|\psi_i^i\psi_j^j\rangle \tag{1.25}$$

and the Exchange integrals

$$\langle \psi_i^i \psi_j^j | \hat{g}(i,j) | \psi_j^i \psi_i^j \rangle \tag{1.26}$$

Equation 1.24 is often written as an unrestricted sum over antisymmetrized two electron integrals.

$$E = \sum_i \langle \psi_i | \hat{h}(i) | \psi_i \rangle + \frac{1}{2} \sum_{ij} \langle \psi_i^i \psi_j^j || \psi_i^i \psi_j^j \rangle \tag{1.27}$$

The Hartree–Fock equations are obtained by minimizing this energy under the constraint that the orbitals are orthonormal. This is done by varying the spin orbitals (the wavefunction) until the energy reaches a minimum. This is known as a variational method, which begins with a trial wavefunction depending on some number of parameters, then optimizing the parameters until the expectation value of the Hamiltonian, the energy, reaches the lowest possible value. Varying the orbitals such that the energy is lowest will give the best wavefunction, and best energy approximation. Any chosen trial wavefunction will always result in an energy eigenvalue that is greater than or equal to the true ground state energy.

$$E_{\mathrm{HF}} \geq E_{\mathrm{Exact}} \tag{1.28}$$

A system with all molecular orbitals doubly occupied is referred to as closed–shell. The HF molecular orbitals can be restricted such that $N = 2n$ electrons in n doubly–occupied spatial orbitals. This restriction of Hartree–Fock is known as the restricted Hartree–Fock (RHF) formalism.[5] The energy expression for RHF is modified such that

$$E_{\mathrm{RHF}} = 2 \sum_i^{MO} \langle \phi_i | \hat{h}_i | \phi_i \rangle + \sum_i^{MO} \sum_j^{MO} \left[2 \langle \phi_i \phi_j | \hat{g}(i,j) | \phi_i \phi_j \rangle - \langle \phi_i \phi_j | \hat{g}(i,j) | \phi_j \phi_i \rangle \right] \tag{1.29}$$

Equation 1.29 may be written more concisely by utilizing some definitions.

The Coulomb operator, typically denoted with $\hat{J}$, may be written as:

$$\hat{J}_j \left|\phi^\mu\right\rangle = \langle\phi_j^\nu|\hat{g}(\mu,\nu)|\phi_j^\nu\phi^\mu\rangle \tag{1.30}$$

The exchange operator, typically denoted with $\hat{K}$, may be written as:

$$\hat{K}_j \left|\phi^\mu\right\rangle = \langle\phi_j^\nu|\hat{g}(\mu,\nu)|\phi^\nu\phi_j^\mu\rangle \tag{1.31}$$

This simplifies E_{RHF} to

$$E_{\mathrm{RHF}} = 2\sum_i^{N/2}\langle\phi_i|\hat{h}_i|\phi_i\rangle + \sum_i^{N/2}\sum_j^{N/2}\left[2\left\langle\phi_i|\hat{J}_j|\phi_i\right\rangle - \langle\phi_i|\hat{K}_j|\phi_i\rangle\right] \tag{1.32}$$

All of the operators in the RHF energy expression are now written as one–electron operators.

By Lagrangian minimization of the energy with respect to molecular orbitals with the constraint of orthonormality, it my be shown that the best set of molecular orbitals satisfy the following equations:

$$\left[\hat{h} + \sum_j\left(2\hat{J}_j - \hat{K}_j\right)\right]\phi_i = \epsilon_i\phi_i \tag{1.33}$$

where ϵ_i represents the orbital energy. The term in square brackets is referred to as the Fock operator $\hat{f}$

$$\hat{f}\phi_i = \epsilon_i\phi_i \tag{1.34}$$

The MO's which give the best Slater determinant and lowest energy are all eigenfunctions of the hermitian operator $\hat{f}$. However, from the definitions of the Coulomb and exchange operators, the Fock operator itself is defined in terms of the molecular orbitals. Therefore, solving the Hartree–Fock equations requires an iterative procedure. It is typical to approximate the molecular orbitals via a linear combination of

atomic orbital basis functions (LCAO).

$$\phi_i = \sum_q \chi_q C_{qi} \tag{1.35}$$

where χ_q are atomic orbitals and C_{qi} are expansion coefficients for the atomic orbitals. The set of atomic orbitals composing the LCAO is known as a basis set. This will be further discussed in the following section. Plugging this new MO expression into the Hartree–Fock equations yields:

$$\hat{f} \sum_q \chi_q C_{qi} = \epsilon_i \sum_q \chi_q C_{qi} \tag{1.36}$$

Left–multiplying both sides by some other atomic orbital χ_p^*, integrating, and defining $F_{pq} = \langle \chi_p | \hat{f} | \chi_q \rangle$ and $S_{pq} = \langle \chi_p | \chi_q \rangle$ gives:

$$\sum_q F_{pq} C_{qi} = \epsilon_i S_{pq} C_{qi} \tag{1.37}$$

In order to simplify this into a single equation which determines all possible ϕ_i in terms of χ, this can be redefined in matrix notation

$$\boldsymbol{F_{pq} C_{qi} = S_{pq} C_{qi} \epsilon_i} \tag{1.38}$$

It is typical to drop the subscripts for simplicity.

$$\boldsymbol{FC = SC\epsilon} \tag{1.39}$$

Here $\boldsymbol{F}$ is the Fock matrix, $\boldsymbol{C}$ is the expansion coefficients matrix, $\boldsymbol{S}$ is the atomic orbital overlap matrix, and $\boldsymbol{\epsilon}$ is a diagonal matrix of orbital energies. These are known as the Roothan–Hall equations. This is almost a typical eigenvalue problem that can be solved by diagonalizing $\boldsymbol{F}$. Because the atomic orbitals are not guaranteed to be

orthogonal, $\boldsymbol{S}$ is generally a non–diagonal matrix. Therefore, these equations must be transformed into an orthonormal basis before $\boldsymbol{F}$ can be diagonalized. One strategy to accomplish this is to left multiply both sides of the equation by $\boldsymbol{S^{-1/2}}$ and insert the identity matrix $\boldsymbol{I} = \boldsymbol{S^{-1/2}S^{1/2}}$ twice.

$$\boldsymbol{S^{-1/2}FS^{-1/2}S^{1/2}C} = \boldsymbol{S^{-1/2}SS^{-1/2}S^{1/2}C\epsilon} \tag{1.40}$$

To write Equation 1.40 as a simple eigenvalue equation, we define $\tilde{\boldsymbol{F}} = \boldsymbol{S^{-1/2}FS^{-1/2}}$ and $\tilde{\boldsymbol{C}} = \boldsymbol{S^{1/2}C}$.

$$\tilde{\boldsymbol{F}}\tilde{\boldsymbol{C}} = \tilde{\boldsymbol{C}}\boldsymbol{\epsilon} \tag{1.41}$$

Now it is straightforward to diagonalize $\tilde{\boldsymbol{F}}$. Afterwards, $\tilde{\boldsymbol{C}}$ can be transformed back to the original, unorthogonal basis, and a new Fock matrix can be formed. This process is continued until the coefficients and energy have converged.

In the case of open–shell molecules, which have an odd number of electrons, unrestricted Hartree–Fock (UHF) may be utilized.[6] UHF uses different sets of molecular orbitals for the α and β electrons, rather than using a single molecular orbital twice as in the case of RHF. However, with open–shell molecules UHF can suffer from spin–contamination where the energy is artificially lowered by the ground state mixing with higher energy spin states and the required spin symmetry of the wavefunction is broken. The expectation value of $\hat{S}^2$ will deviate from the expected value based on the multiplicity in such cases. To combat this issue, restricted open–shell Hartree–Fock (ROHF) may be used.[7,8] ROHF uses doubly occupied molecular orbitals for the paired electrons, like RHF does, but for the unpaired electrons it utilizes singly occupied molecular orbitals. UHF gives a better description of the unpaired electron density distribution than ROHF, however it suffers from the breaking of spin–symmetry and artificial lower energies. The breaking of spin–symmetry is unphysical since the ground state is required to be an eigenfunction of the total symmetry operator, and

the lower energies are unphysical as they are simply an artifact of the mathematics behind the method. Therefore, it is important to use discernment when choosing between UHF and ROHF for open–shell systems.

Hartree–Fock is a mean–field theory, meaning that the individual interactions in a given system are replaced with an average or effective interaction. This essentially reduces the many–body problem to a one–body problem. More sophisticated methods have been created to account for electron correlation, and they are referred to as post–Hartree–Fock methods. Before discussing these methods, an examination of the wavefunction approximation with an atomic orbital basis set is appropriate.

Basis Sets

Generally, a basis set refers to a set of simple functions (or vectors) which can be used to express more complex functions (or vectors) as a linear combination. In the context of quantum chemistry, atomic orbitals, the known solutions to the Schrödinger equation for the two body problem, are chosen as the basis for the solution to the many body problem. For a given molecule, each atom is described by an atomic orbital. In order to describe the molecule as a whole, the linear combination of atomic orbitals is used to construct molecular orbitals, as shown in Equation 1.35. With an infinite basis set, an exact expansion of the wavefunction is guaranteed; however, a finite basis set is required for computational tractability. Therefore, a basis set is sought such that adding any new basis functions would not change the wavefunction or its properties – this is the infinite basis set or complete basis set (CBS) limit. However, the amount of time required to solve the Schrödinger equation critically depends on the basis set size. While large basis sets close to the CBS limit are computationally feasible, certain families of basis sets have been designed to systematically approach this limit.

Computationally, an ideal basis set is as small as possible. To maintain an accurate expansion, the basis sets should be highly similar to the expected form of the wavefunction. Slater type orbitals (STO) might be expected to be appropriate based on the solutions to the hydrogen atom.

$$\phi_{\mu}^{\mathrm{STO}}(r;\xi,n,l,m) = Nx^{l}y^{m}z^{n}e^{-\xi r} \tag{1.42}$$

STOs are characterized by a sharp cusp at the center and by exponential decay as r increases or decreases. However, there is no general analytic solution for the two electron integrals using basis functions with $e^{-\xi r}$ dependence, so using STOs as basis functions is not computationally efficient. It was discovered that STOs could be approximated using linear combinations of Gaussian type orbitals (GTO).[9] GTOs have the general form:

$$\phi_{\mu}^{\mathrm{GTO}}(r;\alpha,n,l,m) = Nx^{l}y^{m}z^{n}e^{-\alpha r^{2}} \tag{1.43}$$

An individual GTO gives a poor description of the electron near the nucleus, so they are almost always contracted into contracted Gaussian type orbitals (CGTO)[10] which are generated from linear combinations of GTOs of the form:

$$\phi_{\mu}^{\mathrm{CGTO}}(r;n,l,m) = \sum_{i} c_{i}^{\mu}\phi_{\mu}^{\mathrm{GTO}}(r;\alpha_{i},n,l,m) \tag{1.44}$$

where c_i^{μ} is a contraction coefficient, and α_i is the orbital exponent. These are determined via variationally minimizing the electronic energy for a given atomic center.

The first instance of systematically determining optimal contraction coefficients and orbital exponents is the STO–MG basis set family.[11] The STO–MG, or "Slater–Type orbital approximated by M Gaussians," series was optimized for use with HF for many of the atoms on the periodic table and with $M = 2-6$ Gaussians. Of the chosen

values of M, STO–3G was discovered to be optimal in terms computational speed and accuracy. This basis set is known as a single–ζ or minimal basis set, which means that only one basis function is included for each atomic orbital. Solutions utilizing a minimal basis set will be far from the CBS limit. Including more basis functions per atomic orbital will increase the accuracy of the solution while generally increasing the computational cost. For example, a double–ζ basis set includes two basis functions for each atomic orbital, a triple–ζ includes three, and so on. In addition to increasing the number of basis functions in a basis set, the addition of polarization functions is also necessary to accurately describe molecular systems. These functions are higher angular momentum basis functions that are used to describe the polarization of the electron density of an atom in a molecule.[12] For example, the only basis function in a minimal basis for hydrogen would be a function describing the $1s$ orbital. To add polarization to the basis set, a p function would be included. These functions describe the shift in electron density needed for bonding orbitals and generally add more of the mathematical flexibility needed for an accurate wavefunction.

The Dunning basis sets, also known as the correlation–consistent polarized valence basis sets (cc–pVXZ), is a basis set family that was designed to systematically converge toward the CBS limit.[13,14] This series is an example of a split–valence basis set, which utilizes one basis function for each core atomic orbital and multiple basis functions for the valence atomic orbitals, and adds greater flexibility for the orbitals involved in bonding. The contraction coefficients and orbital exponents of the Dunning basis functions were variationally optimized for post–HF methods, which include treatment of electron correlation and will be discussed in the next section. This family of basis sets was designed with a built–in hierarchy. The simplest Dunning basis set, cc–pVDZ, includes one basis function for the core orbitals, two for the valence orbitals, and one polarization function. As the cardinality increases from double–ζ to triple–ζ, and so on, each step adds an additional set of valence orbitals, another

set of the current polarization functions, and a set of polarization functions of higher angular momentum. The design of this hierarchy gives these basis sets the ability to be used in basis set extrapolation methods, which are used to converge electronic energies to the complete basis set limit. The ability to be used in basis set extrapolations makes them attractive for obtaining highly accurate energetics, as will be demonstrated in Chapters 2 and 3.

The standard Dunning basis sets have been amended in multiple ways to include a variety of added features that can better describe specific situations in molecular systems. In order to better describe core electron correlation, as the standard basis sets were designed for valence–only calculations, functions describing core correlation have been added. These basis sets are denoted with an added " C," such that the naming convention becomes cc–pCVXZ. Elements in the second row require extra d polarization functions to be more accurately described as the original polarization functions were found to not be tight enough. These added functions are sometimes referred to as "tight d" functions, and are denoted by cc–pV(X+d)Z. Tight d functions are small exponent Gaussians that describe electron density close to the nucleus. Diffuse functions are also sometimes necessary, particularly when describing orbitals far away from the nucleus. Adding diffuse functions is sometimes referred to as "augmenting" the basis set, and in the Dunning nomenclature these basis sets are denoted with an "aug–" prefix. Some applications of this include calculations for anions, dipole moments, and the accurate modeling of intramolecular and intermolecular bonding. Additionally, there is a set of Dunning basis sets referred to with cc–pVXZ–F12. These basis sets are designed to be used in conjunction with explicitly correlated methods which accelerate convergence to the CBS limit.

Correlated Methods

Hartree–Fock accounts for about 99% of a system's absolute energy, leaving about 1% uncaptured. It turns out that 1% is particularly important to obtain in order to accurately describe what is happening in nature. Hartree–Fock does not fully account for electron correlation, which is defined as the instantaneous, mutual repulsion of an electron with all other electrons in the system. The more simplified definition of electron correlation is the amount of energy that Hartree–Fock fails to capture even though HF, as previously described, includes first–order correlation. Many post–Hartree–Fock methods have been designed and implemented in order to treat this electron correlation.

$$E_{\text{Corr}} \equiv E_{\text{Exact}} - E_{\text{HF}} \leq 0 \tag{1.45}$$

Electron correlation can be divided into dynamic correlation and static correlation. Dynamic correlation accounts for correlation caused by the movement of electrons, and it is significant for all molecular systems. Static correlation is a result of the single–determinant nature of Hartree–Fock theory. This is particularly important in systems where the different orbitals or configurations have near–degenerate energies. This occurs when there are multiple important determinants which interact strongly, and dynamical correlation must be considered in both configurations simultaneously.

The exact solution to the Schrödinger equation can be obtained by taking linear combinations of a reference determinant or configuration and all possible excited configurations from that reference. This wavefunction would include all possible configurations of electrons and is referred to as the full configuration interaction (FCI) wavefunction:

$$|\Psi_{\text{FCI}}\rangle = (c_0 + C_1 + C_2 + C_3 + \cdots + C_N)\,|\Phi\rangle \tag{1.46}$$

where C_1 generates all possible single excitations from the reference, C_2 generates

all possible double excitations, and so on to include all possible excitations from the reference configuration. Including all possible configurations in a computation is very computationally expensive. This issue is further exacerbated by the choice of basis set. The computational time required for FCI grows factorially with the number of electrons and basis functions.[15] Due to this computational scaling, FCI with a moderate basis set is not feasible for systems containing more than a few atoms. As the basis set size increases, the computation would become more accurate while simultaneously becoming more cost prohibitive. If one chose a hypothetical infinite basis set, the resulting FCI/CBS result would be theoretically exact, however the computation would never finish.

In order to combat this computational cost issue, it is common to truncate the FCI wavefunction to only include up to a certain size of excited configurations in order to achieve a sufficiently accurate energy while being an affordable computation. A common truncation is referred to as CISD, which includes single and double excitations.

$$|\Psi_{\mathrm{CISD}}\rangle = (c_0 + C_1 + C_2)\,|\Phi\rangle \tag{1.47}$$

This allows a nice progression of methods approaching FCI as more and more excitations are added into the solution. However, as FCI is truncated, the properties of size–consistency and size–extensivity are lost. Additionally, as the system size increases, the error caused by the loss of size–consistency is further exacerbated. A method is size–consistent if the energy of non–interacting systems is the same as the result of summing the individual energies of the systems separately, such that

$$E(A, B) = E(A) + E(B) \tag{1.48}$$

It is common to include a correction to account for this, the most common of which is the Davidson correction, which is denoted by a "+Q."[16] A method is size–extensive

if the obtained energy scales linearly with the number of electrons.

Because the size–consistency and size–extensivity have been lost in truncated configuration interaction, it is necessary to find another method that maintains these properties while accounting for a truncated set of excitations. The premier correlation method, coupled cluster (CC), was devised to resolve this issue.[17] The coupled cluster wavefunction *ansatz* uses an exponential operator to generate the excited configurations from the reference determinant:

$$|\Psi_{\mathrm{CC}}\rangle = \exp\left(T_1 + T_2 + T_3 + \cdots + T_N\right)|\Phi\rangle = \exp(T)\,|\Phi\rangle \tag{1.49}$$

where T_N corresponds to a set of N–electron excitations. For example, the T_2 operator includes all possible double excitations. This method can also be truncated to a given excitation level as appropriate. The CCSDT wavefunction,[18] which contains all possible single, double, and triple excitations may be written as

$$|\Psi_{\mathrm{CCSDT}}\rangle = \exp\left(T_1 + T_2 + T_3\right)|\Phi\rangle \tag{1.50}$$

This method has been shown to quickly approach the exact solution as more excitations are included. This truncation maintains the quality of size consistency. Unfortunately, the computational scaling of CCSDT is $O(N^8)$, which is computationally infeasible for systems with more than a few dozen electrons. To improve the computational scaling, CCSD(T) was developed which yields accurate results for many systems. This method includes all single, double, and a perturbative correction for triple excitations. The CCSD(T) method has been well established in the field of computational chemistry, and the CCSD(T)/cc–pVTZ level of theory has been set as the "gold standard."[19] As such, it is common to see this method utilized.

Focal Point Analysis

As mentioned in previous sections, the inability to utilize an infinite basis set and the infeasibility of incorporating all possible excited configurations into the wavefunction limits the achievable accuracy when solving the multi–electron Schrödinger equation. The full configuration interaction energy includes all possible configurations and, when paired with an infinite basis set, provides the exact electronic energy. For molecules of a few atoms, it is possible to approach the FCI and CBS limits. With larger molecules this becomes cost–prohibitive. In order to obtain FCI/CBS quality energies without spending the required time and computing resources, alternatives have been introduced. Extrapolation methods, such as HEAT,[20] W3 and W4,[21,22] and Focal Point Analysis (FPA),[23,24] have been developed in pursuit of chemical accuracy ($\leq$ 1.0 kcal mol^{-1}). HEAT utilizes HF and CCSD(T) extrapolated to the complete basis set limit, a CCSDT correction to account for deficiencies of the triple excitations in CCSD(T), and a CCSDTQ correction to approximate the difference between the CCSDT and FCI correlation energies. It also includes corrections for the zero–point vibrational energy, the Born–Oppenheimer approximation, a spin–orbit coupling correction, and the scalar relativistic contribution to the energy. W3 and W4 are basis set extrapolation methods that have been developed from the original W1 and W2 extrapolation methods.[25] HEAT, W3, and W4 are all specific computational protocols that have been developed in an effort to achieve chemical accuracy, and in some cases subchemical accuracy ($\leq$ 1.0 kJ mol^{-1}). FPA is more flexible than these methods as it is a general strategy for approaching the FCI/CBS limit rather than a set protocol. Due to its flexibility, it has been selected as the extrapolation method used in the research present later in this work.

Focal Point Analysis, also known as the Focal Point Approach, was developed by Allen and coworkers.[23,24] It is a composite method which systematically approaches

both the FCI and CBS limits, estimating FCI/CBS. The Dunning basis sets are necessary for this method because of their systematic convergence to the CBS limit, as discussed previously. Because of the difference in convergence between methods, it is necessary to utilize a different extrapolation equation for the Hartree–Fock energy. A three–point extrapolation is utilized, shown in Equation 1.51.[26]

$$E_{\text{ref}}(X) = E_{\text{HF}}^{\infty} + ae^{-bX} \tag{1.51}$$

Due to previously seen unreliability in the Hartree–Fock double–ζ quality energy, it is necessary to utilize at least a quintuple–ζ basis set. For the correlation energy, a two–point extrapolation may be used (Equation 1.52).[27]

$$E_{\text{corr}}(X) = E_{\text{corr}}^{\infty} + aX^{-3} \tag{1.52}$$

In the FPA method, a series of energies are computed at an array of methods and basis sets in order to obtain the relative energy of a given stationary point along the potential energy surface. See Table 1.1 for an example. The columns in the incremental focal point analysis table correspond to the different methods utilized and the rows correspond to the different basis sets utilized.

Table 1.1: Representative incremental focal point analysis table for the barrier height of the $CN + H_2$ reaction.

Basis Set	HF	$+\delta$MP2	$+\delta$CCSD	$+\delta$(T)	$+\delta$T	$+\delta$(Q)	Net
aug–cc–pVDZ	+12.50	−11.14	+2.87	−0.77	+0.21	−0.13	[+3.55]
aug–cc–pVTZ	+13.48	−11.60	+3.07	−0.84	[+0.21]	[−0.13]	[+4.20]
aug–cc–pVQZ	+13.71	−11.67	+3.11	−0.85	[+0.21]	[−0.13]	[+4.38]
aug–cc–pV5Z	+13.74	−11.65	+3.12	−0.85	[+0.21]	[−0.13]	[+4.44]
CBS Limit	[+13.74]	[−11.62]	[+3.12]	[−0.85]	[+0.21]	[−0.13]	[+4.48]

In Table 1.1, each column is the relative energy difference that method achieved relative to the previous column. Moving across the columns of an incremental FPA table, the amount of correlation treatment is increased and the energy increments should approach 0, signifying convergence to the FCI limit. Moving down the rows, the energy should converge toward one energy value, signifying convergence toward the CBS limit for a given level of theory. As seen in the table, the energy differences across columns can be positive or negative. It is common for the energy differences to oscillate between positive and negative as they converge. The increment at the highest level of theory should ideally be less than or equal to $|0.1|$ kcal mol,$^{-1}$ signifying that the energy has converged toward the FCI limit.

As shown in the table, the numbers in brackets were obtained using the extrapolation equations. The CCSD(T) method recovers a majority of the correlation energy, but not all. It is important to continue past this method to achieve chemical accuracy for many systems.[28] This example utilized methods up to CCSDT(Q). Methods such as CCSDT and CCSDT(Q) are typically only utilized with double zeta and triple zeta basis sets, depending on computational cost. When affordable, coupled cluster methods with higher excitations and larger Dunning basis sets than those demonstrated above may be utilized in order to achieve satisfactory convergence to the FCI/CBS limit.

In FPA, a series of additive energy corrections may be included which account for approximations that were made when computing electronic energies and during the optimization. It is typical for electronic structure packages to by default use the frozen–core approximation, which assumes that determinants where core electrons have been excited may be ignored. The core–valence correlation (δ_{CORE}) can be accounted for as the difference between an all–electron and frozen–core computation with an appropriate basis set such as a cc–pCVXZ basis set which includes core electron correlation. As mentioned in Section 1.1, the Born–Oppenheimer approximation

assumes that the nuclei are frozen as a result of the large time–scale difference between nuclei and electrons. It is simple to account for this approximation by including the diagonal Born–Oppenheimer correction (δ_{DBOC}) using HF and an appropriate basis set, such as aug–cc–pVTZ.[29] It is typical for δ_{DBOC} corrections to be small, typically on the scale of 0.01 kcal mol^{-1}. Some systems will exhibit much larger δ_{DBOC} corrections, which may be evidence of a nearby conical intersection or may correspond to a transition state with a large imaginary frequency.[30] Relativistic effects have the greatest effect on heavy elements as the electrons in these elements have the ability to achieve speeds approaching the speed of light. The Schrödinger equation does not account for relativity, so relativistic effects can be accounted for (δ_{REL}) as the difference between a computation with and without relativistic effects included. To convert electronic energies into comparable relative enthalpies, it is necessary to include the zero–point vibrational energy (δ_{ZPVE}). Compiling the FPA energy and all of the additive energy corrections gives the reaction enthalpy.

$$\Delta H_{0\mathrm{K}} = \Delta E_{\mathrm{CCSDT(Q)/CBS}} + \delta_{\mathrm{CORE}} + \delta_{\mathrm{DBOC}} + \delta_{\mathrm{REL}} + \delta_{\mathrm{ZPVE}} \tag{1.53}$$

Transition State Theory

Of particular interest in quantum chemistry is the determination of accurate rate constants for reactions at various temperatures and pressures.[31] Theoretical calculations can be used where experimental rate constants have not been determined or could be exceedingly difficult. A common method for computing rate constants is canonical transition state theory (TST). In order to utilize TST, it is necessary to have highly accurate knowledge of the reaction's potential energy surface. *Ab initio* methods, like FPA, are excellent for providing this high level of accuracy. Due to the nature of TST, as the error in the activation barrier height increases, the error in the

rate constants will increase exponentially. Thus, knowing the barrier heights of these reactions to chemical accuracy is of the utmost importance for obtaining accurate rate constants.

Consider a hypothetical bimolecular reaction where the reactants first form a pre–reactive complex (PRC) before reacting:

$$\text{Reactants} \underset{\text{k}_{-1}}{\overset{\text{k}_1}{\rightleftharpoons}} \text{PRC} \xrightarrow{\text{k}_2} \text{Products} \tag{1.54}$$

The total rate constant for the forward direction of this reaction is equal to the product of the rate constants for each step. The rate constant for PRC formation is the ratio between the rate of step one (k_1) and the sum of the reverse of step one (k_{-1}) and the rate of step two (k_2), and the rate constant for irreversible product formation is (k_2):

$$k_{\text{Total}} = \frac{k_1}{k_{-1} + k_2} k_2 \tag{1.55}$$

If we assume the transition state between the PRC and the products lies above the relative enthalpy of the reactants, we can assume $k_{-1} \gg k_2$, which simplifies the total rate equation:

$$k_{\text{Total}} = \frac{k_1}{k_{-1}} k_2 = K_{eq} k_2 \tag{1.56}$$

where K_{eq} is the equilibrium constant for the reaction between the reactants and the PRC. K_{eq} may also be represented here as the ratio between the canonical partition functions for the PRC and the reactants (R).

$$K_{eq} = \frac{Q^{\text{PRC}}}{Q^{\text{R}}} \tag{1.57}$$

The rate constant for the second step of the hypothetical reaction (k_2) can be expressed as:[32,33]

$$k_2 = \kappa(T) \frac{k_B T}{h} \frac{Q^{TS}(T)}{Q^{PRC}(T)} \tag{1.58}$$

where k_B is the Boltzmann distribution, T is temperature in Kelvin, h is Planck's constant, $\kappa(T)$ is the temperature dependent transmission coefficient, and $Q(T)$ is the canonical partition function either for the transition state (TS) or the pre–reactive complex. Combining the equations for K_{eq} and k_2 results in the following expression for k_{Total}:

$$k_{Total}(T) = k^{\mathrm{TST}}(T) = \kappa(T)\frac{k_B T}{h}\frac{Q^{\mathrm{TS}}(T)}{Q^{\mathrm{R}}(T)}\exp\left(\frac{-\Delta H^{\ddagger}}{k_B T}\right) \tag{1.59}$$

where $\Delta H^{\ddagger}$ is the barrier height of the transition state.

There are multiple ways to represent $\kappa(T)$. Wigner proposed a simple approximation:[34]

$$\kappa(T) = 1 + \frac{1}{24}\left[\frac{h\omega^{\ddagger}}{k_B T}\right]^2 \tag{1.60}$$

where $\omega^{\ddagger}$ is the imaginary frequency associated with the transition state. This approximation is most successful when $h\omega^{\ddagger} \gg k_B T$. Tunneling may also be accounted for by fitting the reaction coordinate corresponding to the minimum energy reaction path to an Eckart potential.[35] This method provides an excellent estimate of $\kappa(T)$ in the limit of single–dimensional tunneling. An even more sophisticated model for treating one–dimensional tunneling is via small curvature tunneling (SCT). This method is designed to take into account the curvature of the reaction–path, thus providing a better approximation of the tunneling contributions present in a reaction.[36] This type of model becomes more important for reactions where tunneling effects are quite dominant. Even though SCT can provide an excellent tunneling model, Eckart tunneling has proven to be a sufficient model for numerous reactions, particularly at moderate to high temperatures.[37–42]

In order to represent the canonical partition functions necessary for the calculation of rate constants via TST, the rigid–rotor harmonic oscillator approximation is generally utilized. The partition function $Q(T)$ can be represented as a product of

the partition functions of the individual degrees of freedom in a molecule.

$$Q(T) = Q_{Trans}(T)Q_{Elec}(T)Q_{Rot}(T)Q_{Vib}(T) \tag{1.61}$$

The vibrational modes of the smallest magnitude frequencies contribute the most to the vibrational partition function at all temperatures. The smallest harmonic frequencies often correspond to bending modes or hindered rotations which typically have a lot of anharmonicity. Treating these small modes as harmonic oscillators leads to overestimation of the vibrational partition function, especially at higher temperatures.

Canonical transition state theory is not the only method that provides theoretical rate constants. TST is convenient because the rigid–rotor harmonic oscillator approximation (RRHO) may be used to compute the partition functions in order to define its free energy. Variational transition state theory (VTST) variationally moves the reference point along the surface that is used to obtain the free energy until the rate constant is minimized. VTST is defined via the following:

$$k_{VTST}(T) = \min_{s} \frac{k_B T}{h} \frac{Q_{TS}(T,s)}{Q_{Reactants}(T)} e^{\left(\frac{-\Delta H^{\ddagger}}{k_B T}\right)} \tag{1.62}$$

where s is the path length along the reaction path where $k_{VTST}(T)$ is evaluated and $s = 0$ at the first–order saddle point. At high temperatures, variational transition state theory outperforms TST, however TST still performs well at those temperatures. At lower temperatures, TST generally outperforms VTST due to some fortuitous cancellation of error. For these reasons, canonical transition state theory is generally sufficient for providing rate constants for reactions with well–defined barriers like those that will be discussed in this dissertation.

Chapter 2

Energetics and Kinetics of Various Cyano Radical Hydrogen Abstractions[1]

[1] Burke, A.D., Bowman, M.C., Turney, J.M., and Schaefer III, H.F., *Physical Chemistry Chemical Physics*, 2021, 23, 3389. Reprinted here with permission of the publisher. https://pubs.rsc.org/en/content/articlehtml/2021/cp/d0cp06228f

Abstract

The cyano radical (CN) is an abundant, open–shell molecule found in a variety of environments, including the atmosphere, the interstellar medium and combustion processes. In these environments, it often reacts with small, closed–shell molecules via hydrogen abstraction. Both carbon and nitrogen atoms of the cyano radical are reactive sites, however the carbon is more reactive with reaction barrier heights generally between $2-15$ kcal mol^{-1} lower than those of the analogous nitrogen. The CN + HX $\rightarrow$ HCN/HNC + X, with X = H, CH_3, NH_2, OH, F, SiH_3, PH_2, SH, Cl, C_2H, CN reactions have been studied at a high–level of theory, including CCSD(T)–F12a. Furthermore, kinetics were obtained over the $100-1000$ K temperature range, showing excellent agreement with those rate constants that have been determined experimentally.

Introduction

In addition to being one of the first radicals to be detected in the interstellar medium (ISM), the cyano radical (CN $^2\Sigma^+$) is also one of the most abundant open–shell molecules found in the ISM.[43,44] The CN radical has been identified in Titan's atmosphere[45] as well as the atmospheres of the outer planets and some of their satellites.[46] Furthermore, it is involved in the chemistry of hot molecular cores and the outflow of dying carbon stars.[47] Also, the reactions of CN radicals with unsaturated hydrocarbons are important steps in the production of long chain nitrile species.[46] Because hydrogen cyanide is a common intermediate in hydrocarbon flames containing a nitrogen source, the CN radical is also particularly relevant to the combustion of hydrocarbons.[48] The cyano radical often reacts via hydrogen abstraction with small, closed–shell molecules also found in interstellar and combustion environments.[43,49]

The reaction of CN radical with H_2 to form HCN and the subsequent reaction between HCN and atomic oxygen to form NO is an important aspect of NO formation from atmospheric nitrogen and nitrogen–containing fuels.[50,51] Additionally, the cyano radical is a by–product of the decomposition of nitrogen oxide compounds.[49] The production of HCN via the abstraction of H_2 by the cyano radical has been observed at very low temperatures, such as those in the ISM.[52] Other hydrogen abstractions by the cyano radical, such as $CN^{\bullet} + CH_4 \rightarrow HCN + CH_3$, are among the proposed reactions that take place in Titan's atmosphere[45] and HCN is an important intermediate in combustion environments and can be produced through cyano radical hydrogen abstractions. Accurately determining the energetics and rate constants of these reactions can provide insight into what is taking place in both combustion environments and the ISM.

In these hydrogen abstractions, either the carbon or nitrogen can abstract the hydrogen. HCN is an important intermediate in the combustion of hydrocarbons, but the isomer HNC has a lower stability and is rare on earth. The abundance ratio of these two molecules in space is quite different. HNC has been observed to be as abundant as HCN, and in some cases moreso. The HNC/HCN abundance ratio has even been observed to be 1.55 in cold clouds with temperatures as low as 10 K.[53,54] While the carbon terminal is more reactive, reactions with the nitrogen end are still feasible and have been considered in previous studies.[43,55–59] Therefore, reactions with the nitrogen end will be examined as well. In this work, the following hydrogen abstraction reactions of the cyano radical with various small closed–shell molecules will be investigated using high–level *ab–initio* methods:

$$CN + HX \rightarrow HCN + X \quad \text{(R1)}$$

$$CN + HX \rightarrow HNC + X \quad \text{(R2)}$$

where X = H, CH_3, NH_2, OH, F, SiH_3, PH_2, SH, Cl, C_2H, and CN. In this study, we are primarily concerned with the energetics of the stationary points and kinetics

of these reactions. Our primary goal with this work is to achieve accurate barrier heights which paint a picture of the potential energy surfaces of each reaction pathway. After accurately determining the barrier heights for these reactions, we can produce reliable rate constants over a wide range of temperatures which mimic the conditions in which these reactions occur. These highly accurate results may then be used by experimentalists when examining yet–uncharacterized reactions involving the cyano radical.

Methods

Equilibrium geometries of stationary points (both minima and transition states) were optimized using the CCSD(T)–F12a[60] method with the aug–cc–pVTZ basis set[61] in Molpro 2010.[62] Electronic energies of stationary points along all reactions were computed according to the focal point approach of Allen and coworkers.[23,24] Methods that describe electron correlation up to CCSDT(Q)[63] and basis sets as large as aug–cc–pV5Z[61] were used in this study. CCSD(T)/aug–cc–pVXZ (X = D, T, Q, 5)[14] single point energies were computed using Molpro 2010[62] whereas the CCSDT/aug–cc–pVDZ and CCSDT(Q)/aug–cc–pVDZ corrections were obtained using Mrcc 2018.[64] For third row elements (Si – – Cl), aug–cc–pV(X+d)Z (X = D, T, Q, 5)[14] basis sets were used to compute the CCSD(T) single point energies. As seen in Table 2.1, there is excellent convergence to the CBS limit and good convergence to the FCI limit. The CCSD(T) complete basis set energies were obtained by extrapolating the Hartree–Fock energy and correlation energies using a three–point exponential equation[65] and a two–point inverse cubic equation,[66] respectively:

$$E_{\text{ref}}(X) = E_{\text{HF}}^{\infty} + ae^{-bX} \tag{2.1}$$

$$E_{\text{corr}}(X) = E_{\text{corr}}^{\infty} + aX^{-3} \tag{2.2}$$

The focal point energies were obtained with the following formula:

$$\Delta E_{\mathrm{CCSDT(Q)/CBS}} = \Delta E_{\mathrm{CCSD(T)/CBS}} + \delta E_{\mathrm{T(Q)}} \tag{2.3}$$

Table 2.1: Representative incremental focal point analysis table for the barrier height of the $CN + H_2$ reaction.

Basis Set	HF	$+\delta$MP2	$+\delta$CCSD	$+\delta$(T)	$+\delta$T	$+\delta$(Q)	Net
aug–cc–pVDZ	+12.48	−11.10	+2.86	−0.77	+0.22	−0.13	[+3.56]
aug–cc–pVTZ	+13.46	−11.57	+3.06	−0.84	[+0.22]	[−0.13]	[+4.20]
aug–cc–pVQZ	+13.69	−11.64	+3.10	−0.85	[+0.22]	[−0.13]	[+4.38]
aug–cc–pV5Z	+13.72	−11.62	+3.10	−0.85	[+0.22]	[−0.13]	[+4.45]
CBS Limit	[+13.72]	[−11.59]	[+3.11]	[−0.84]	[+0.22]	[−0.13]	[+4.49]

Additional corrections were made to account for approximations made during the focal point computations. To account for the core–correlation neglected under the frozen–core approximation, the difference between the CCSD(T)/aug–cc–pCVQZ energies with and without core–electrons correlated was determined (δ_{CORE}). A scalar relativistic correction was obtained using X2C–CCSD(T)/aug–cc–pCVTZ–X2C (δ_{REL}).[67,68] The clamped nuclei approximation was treated via diagonal Born–Oppenheimer corrections (δ_{DBOC})[69,70] evaluated at the ROHF/aug–cc–pVTZ level of theory.[61] Both the relativistic correction and the diagonal Born–Oppenheimer correction were carried out with CFOUR 2.0.[71] An experimental shift (δ_{SO}) was included for the OH, F, Cl, and SH products to account for the splitting of the electronic ground state due to spin–orbit coupling.[72,73] Finally, zero–point vibrational energies (δ_{ZPVE}) were obtained from the CCSD(T)–F12a/aug–cc–pVTZ harmonic vibrational frequencies. Anharmonic contributions for the zero–point vibrational energies of the reactants and products were also determined at the MP2/cc–pVDZ[74–76] level of theory by applying VPT2[77–82] using CFOUR 2.0.[71] These corrections were included if they were considered significant ($\geq$0.1 kcal mol^{-1}). These corrections were added together to

obtain the relative enthalpy at 0 K:

$$\Delta H_{0\mathrm{K}} = \Delta E_{\mathrm{CCSDT(Q)/CBS}} + \delta_{\mathrm{CORE}} + \delta_{\mathrm{REL}} + \delta_{\mathrm{DBOC}} + \delta_{\mathrm{ZPVE}}(+\delta_{\mathrm{SO}}) \tag{2.4}$$

Rate constants were calculated over a range of temperatures using canonical transition state theory:[83,84]

$$k^{\mathrm{TST}}(T) = \kappa(T)\frac{k_B T}{h}\frac{Q^{\mathrm{TS}}(T)}{Q^{\mathrm{R}}(T)}\exp\left(\frac{-\Delta H^{\ddagger}}{k_B T}\right) \tag{2.5}$$

where $Q^{\mathrm{TS}}(T)$ and $Q^{\mathrm{R}}(T)$ are the partition functions of the transition state (TS) and reactants (R) and $\Delta H^{\ddagger}$ is the barrier height for the reaction. The transmission coefficient, $\kappa(T)$, was determined with an asymmetric Eckart potential barrier given the relative enthalpies of the pre–reactive complex, transition state, and products for each reaction as well as the imaginary harmonic vibrational frequency corresponding to the reaction mode of the transition state.[37] Eckart tunneling was used because of its past success accurately describing the tunneling of hydrogen transfer reactions at moderate to high temperatures.[37–40] The methods we have used are the most accurate in the $200 - 2000$ K range.

Results

Energies and Geometries

Tables 2.2 and 2.3 show the reaction enthalpies at 0 K for CN H–abstractions from the carbon and nitrogen terminals. As seen in the final two columns of each table, the agreement between our computed reaction enthalpies and the reaction enthalpies taken from the Active Thermochemical Tables (ATcT) (version 1.122e) is excellent.[85–87] The latter results were unavailable for the reactions between CN and

SiH_4, PH_3, and H_2S. All of our energy values for the carbon terminal abstractions lie within 0.20 kcal mol^{-1} of the ATcT values, while those of the corresponding nitrogen abstractions lie within 0.30 kcal mol^{-1}. The mean absolute error of the carbon terminal abstraction reaction enthalpies is 0.09 kcal mol^{-1} and 0.11 kcal mol^{-1} for the nitrogen abstractions. The root mean square error for the carbon abstractions is 0.11 kcal mol^{-1} and 0.14 kcal mol^{-1} for the nitrogen abstractions. The largest deviation for both the carbon and nitrogen abstractions is that for HF, with differences of 0.20 kcal mol^{-1} and 0.29 kcal mol^{-1}, respectively.

Table 2.2: Enthalpies at 0 K ($\Delta H_{0\mathrm{K}}$) in kcal mol^{-1} for products relative to reactants ($CN + HX \rightarrow HCN + X$).

Donor	CBS[a]	$\delta_{\mathrm{T(Q)}}$	δ_{CORE}	δ_{REL}	δ_{DBOC}	δ_{ZPVE}[b]	δ_{SO}	Total	ATcT[c]
H_2	−22.64	0.65	−0.52	0.07	0.00	0.78		−21.66	−21.76
CH_4	−19.78	0.65	−0.34	0.05	0.00	−2.35(0.93)		−21.77	−21.66
NH_3	−16.92	0.64	−0.22	−0.03	0.09	−2.52(0.18)		−18.95	−19.02
H_2O	−6.50	0.72	−0.30	−0.07	0.02	−1.06(0.16)	−0.20	−7.38	−7.38
HF	9.32	0.81	−0.34	−0.14	0.03	1.15	−0.39	10.44	10.24
SiH_4	−35.55	0.63	−0.36	−0.06	−0.04	0.77		−34.60	
PH_3	−44.54	0.67	−0.36	−1.63	−0.01	0.43		−45.44	
H_2S	−36.08	0.68	−0.32	−1.93	−0.01	−2.46	−0.54	−40.11	
HCl	−24.63	0.70	−0.29	−0.47	0.00	2.79	−0.84	−22.74	−22.82
C_2H_2	7.12	0.38	−0.18	−0.07	0.02	−0.72		6.56	6.69
HNC	−14.91	−0.17	−0.20	−0.03	0.07	0.32		−14.93	−14.89

[a] CBS denotes the CCSD(T)/CBS relative energy.
[b] Zero–point vibrational energies computed with the harmonic oscillator treatment, contributions from anharmonic treatment of the ZPVEs at the MP2/cc–pVDZ level of theory are in parentheses.
[c] Data taken from the Active Thermochemical Tables.[85–87]

Table 2.4 shows the enthalpies of the carbon terminal abstraction transition states relative to their respective reactants. According to the results in Table 2.2, we may expect these barrier heights to be accurate within an uncertainty of 0.20 kcal mol^{-1}. The transition states with NH_3, PH_3, and H_2S have submerged barriers below the relative enthalpies of their respective reactants. This suggests that these reactions will be fast even at low temperatures. On the other hand, reactions with

Table 2.3: Enthalpies at 0 K (ΔH_{0K}) in kcal mol^{-1} for products relative to reactants ($CN + HX \rightarrow HNC + X$).

Donor	CBS[a]	$\delta_{T(Q)}$	δ_{CORE}	δ_{REL}	δ_{DBOC}	δ_{ZPVE}[b]	δ_{SO}	Total	ATcT[c]
H_2	−7.73	0.82	−0.32	0.11	−0.10	0.46		−6.76	−6.86
CH_4	−4.87	0.82	−0.14	0.09	−0.02	−2.67(0.94)		−6.79	−6.77
NH_3	−2.00	0.81	−0.02	0.01	0.07	−2.84(0.20)		−3.97	−4.13
H_2O	8.41	0.90	−0.10	−0.04	0.04	−1.38(0.18)	−0.20	7.64	7.51
HF	24.24	0.98	−0.14	−0.10	0.01	0.83	−0.39	25.43	25.14
SiH_4	−20.64	0.80	−0.16	−0.03	−0.05	0.45		−19.62	
PH_3	−29.63	0.84	−0.16	−1.60	−0.10	0.11(0.10)		−30.54	
H_2S	−21.16	0.85	−0.12	−1.89	−0.02	−2.78(0.10)	−0.54	−25.13	
HCl	−9.72	0.87	−0.09	−0.43	−0.03	2.47	−0.84	−7.77	−7.92
C_2H_2	22.04	0.55	0.02	−0.03	0.01	−1.04		21.54	21.58
HCN	14.92	0.16	0.20	0.03	−0.10	−0.32		14.93	14.89

[a] CBS denotes the CCSD(T)/CBS relative energy.

[b] Zero–point vibrational energies computed with the harmonic oscillator treatment, contributions from anharmonic treatment of the ZPVEs at the MP2/cc–pVDZ level of theory are in parentheses.

[c] Data taken from the ATcT.[85–87]

HF, C_2H_2, HCN, and HNC have barriers larger than 10 kcal mol^{-1} so it is unlikely that these reactions will take place at room temperature. Reactions with H_2, CH_4, H_2O, HCl, and SiH_4 have barriers between 0 and 8 kcal mol^{-1} so these reactions will proceed at a modest but non–negligible rate at moderate temperatures. For the reactions with moderate barriers, it is important to determine the barrier height to a high–level of accuracy in order to elucidate exactly how fast each reaction will occur.

Table 2.5 shows the nitrogen terminal abstraction transition state reaction enthalpies relative to their respective reactants. According to the results in Table 2.3, we may expect these barrier heights to be reliable within an uncertainty of 0.3 kcal mol^{-1}. None of the nitrogen terminal abstractions studied have submerged barriers, and in every case the transition state barriers for these abstractions are higher than those of the corresponding carbon terminal abstractions.

Table 2.4: Enthalpies in 0 K in kcal mol^{-1} of carbon terminal abstraction transition states relative to reactants ($CN + HX \rightarrow HCN + X$).

Donor	CBS[a]	$\delta_{T(Q)}$	δ_{CORE}	δ_{REL}	δ_{DBOC}	δ_{ZPVE}	Total
H_2	4.40	0.08	−0.02	0.03	0.11	−0.37	4.24
CH_4	2.43	0.17	−0.06	−0.08	0.10	−1.37	1.19
NH_3	−0.79	0.00	−0.11	−0.01	0.03	−1.53	−2.41
H_2O[b]	10.14	−0.55	−0.13	−0.05	0.16	−2.42	7.15
HF	24.67	−0.64	0.09	−0.09	0.02	−1.53	22.53
SiH_4	−0.69	0.03	−0.04	0.02	0.01	1.02	0.35
PH_3	−4.24	0.08	−0.15	0.36	0.01	0.35	−3.59
H_2S	−1.15	0.05	−0.17	0.33	0.10	0.09	−0.75
HCl	5.09	−0.01	−0.09	0.06	0.06	−1.64	3.47
C_2H_2	18.64	0.20	−0.11	0.05	0.02	−3.55	15.25
HCN	18.47	0.00	0.02	0.00	0.15	−2.87	15.77
HNC	13.99	0.14	0.04	−0.08	0.02	−2.83	11.27

[a] CBS denotes the CCSD(T)/CBS relative energy.
[b] The transition state for the $CN + H_2O \rightarrow HCN + OH$ reaction was optimized at the CCSD(T)/aug–cc–pVTZ level of theory.

Table 2.5: Enthalpies in 0 K in kcal mol^{-1} of nitrogen abstraction transition states relative to reactants ($CN + HX \rightarrow HNC + X$).

Donor	CBS[a]	$\delta_{T(Q)}$	δ_{CORE}	δ_{REL}	δ_{DBOC}	δ_{ZPVE}	Total
H_2	17.69	−0.28	0.04	0.01	0.38	−1.25	16.59
CH_4	16.02	−0.20	0.13	0.04	0.06	−3.26	12.79
NH_3	8.91	0.00	0.04	−0.01	0.01	−1.68	7.27
H_2O	21.59	−1.69	−0.09	−0.05	0.01	−2.86	16.91
HF	32.72	−0.94	−0.03	−0.08	−0.01	−3.40	28.25
SiH_4	8.57	−0.22	−0.01	−0.04	0.15	−2.09	6.36
PH_3	4.90	0.04	0.06	0.33	0.25	−1.33	4.25
H_2S	9.03	−0.76	−0.04	0.67	0.03	−1.45	7.47
HCl	11.60	−0.41	0.07	−0.15	0.09	−1.73	9.47
C_2H_2	32.76	−0.17	0.07	−0.04	−0.01	−4.71	27.91
HCN	28.90	0.31	0.04	−0.08	0.02	−2.81	26.37
HNC	16.13	−0.33	0.06	0.00	0.07	−2.08	13.85

[a] CBS denotes the CCSD(T)/CBS relative energy.

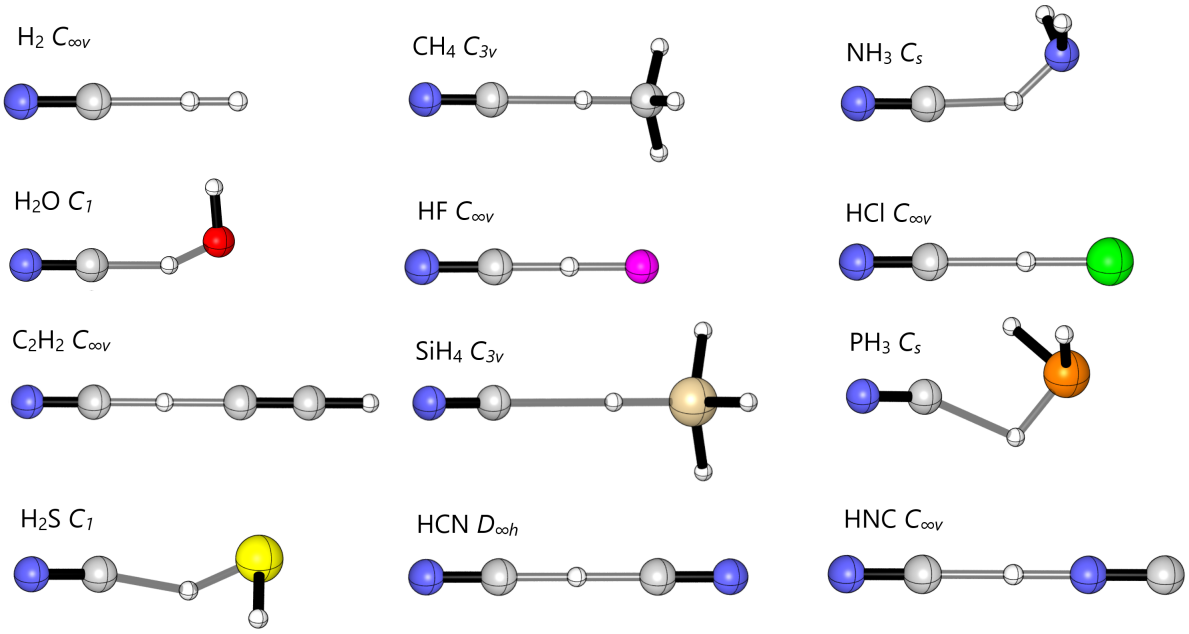

Figure 2.1: Geometries of R1 transition states

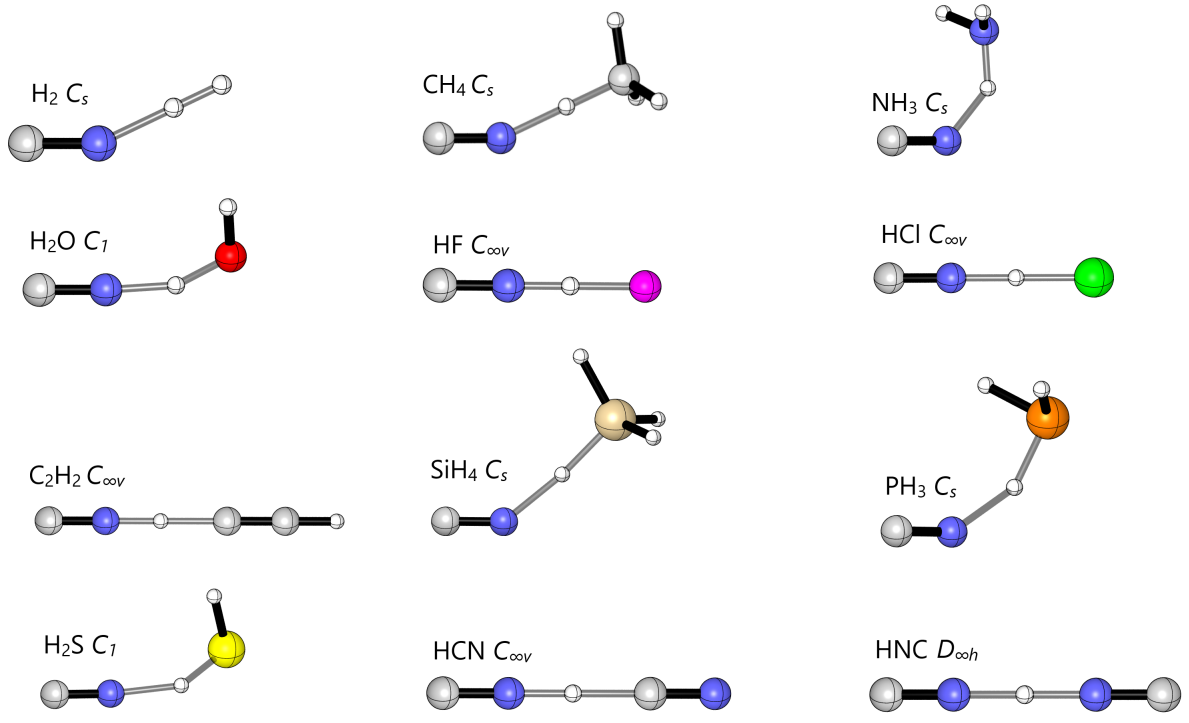

Figure 2.2: Geometries of R2 transition states

The nitrogen terminal abstractions with $H_2, CH_4, H_2O, HF, C_2H_2, HCN,$ and HNC all have barriers greater than 10 kcal mol^{-1} and in some cases the barriers are greater than 20 kcal mol^{-1}. Because of this, these reactions are unlikely to take place at most temperatures. The remaining reactions, $NH_3, HCl, SiH_4, PH_3,$ and H_2S, have barriers less than 10 kcal mol^{-1}. These reactions are more likely to take place than the others; but in most cases the carbon terminal abstraction will dominate.

Of the corrections reported in Tables 2.4 and 2.5, δ_{ZPVE} is the largest, suggesting that accurate barrier heights require accurate electronic energies as well as reliable vibrational frequencies. As expected, δ_{REL} is larger for the third row donors $PH_3, H_2S,$ and HCl. The diagonal Born–Oppenheimer corrections for the reaction enthalpies in Tables 2.2 and 2.3 were consistently small (≤ 0.1 kcal mol^{-1}) while for the transition state barriers this is not the case, where δ_{DBOC} values are as large as 0.4 kcal mol^{-1}. The latter value is artifactual, almost surely due to a conical intersection involving the A $^2\Pi$ state of the CN radical.

The isomerization energy barrier for HNC $\rightarrow$ HCN has been extensively studied in previous theoretical studies.[88–98] In this work, it was predicted to be 44.61 kcal mol^{-1}, which is in agreement with the energy value range of $44.5 - 48.2$ kcal mol^{-1} reported by previous studies.[88,90–93,97] This large energy barrier makes it unlikely that the HCN formed will isomerize into HNC at low temperatures. It will become more likely at higher temperatures, but we did not consider this in the present research.

Comparison between Hydrogen Abstractions by C_2H and CN

The ethynyl radical (C_2H) is another radical present in the interstellar medium and combustion environments. It is isoelectronic with the cyano radical and also has a high affinity for hydrogen abstraction from small closed–shell molecules. The transition state barrier enthalpies in Figure 2.3 were taken from a recent paper studying many of the same reactions with ethynyl radical as the abstraction agent instead.[42] This

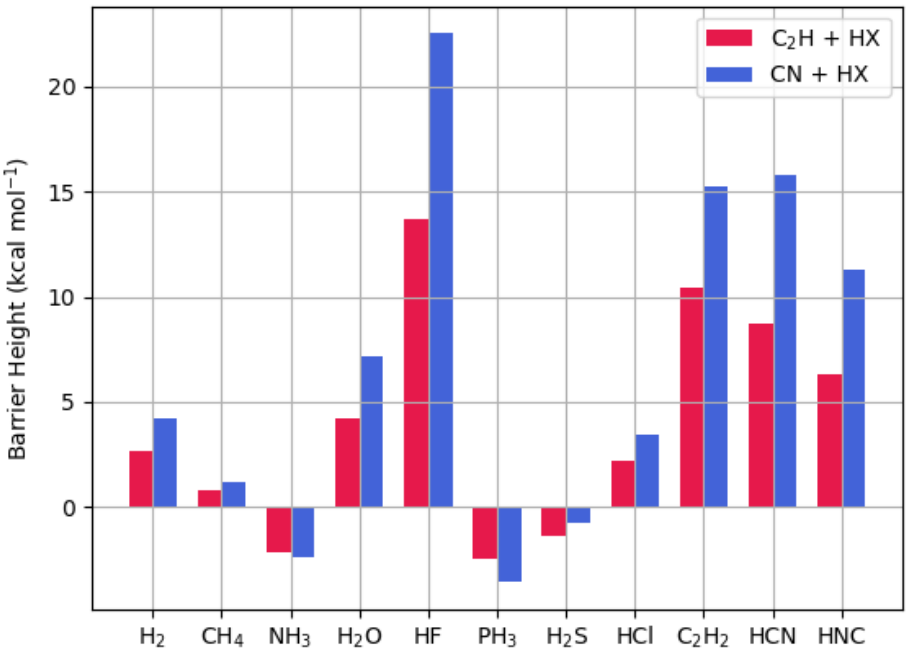

Figure 2.3: Comparison of enthalpies at 0 K in kcal mol^{-1} of the $C_2H + HX \rightarrow C_2H_2 + X$ transition states, optimized at the CCSD(T)–F12a/aug–cc–pVTZ–F12 level of theory, and the $CN + HX \rightarrow HCN + X$ transition states, optimized at the CCSD(T)–F12a/aug–cc–pVTZ level of theory, relative to their respective reactants. Barrier height ($\Delta H^{\ddagger}$) values can be found in Table 2.4 herein and in the study by Bowman and coworkers.[42]

---

work on the ethynyl radical employed a very similar level of theory which allows us to make accurate direct comparisons. The transition state barriers of the cyano radical nitrogen terminal abstractions are significantly larger than the corresponding barriers for both the cyano radical carbon terminal abstractions and the ethynyl radical abstractions. Therefore, we have chosen to only draw comparisons between the ethynyl radical abstractions and the cyano radical carbon terminal abstractions. When comparing reactions, we see that abstractions of NH_3, PH_3, and H_2S by the ethynyl radical and the cyano radical all have submerged barriers. In every case except for the abstractions of NH_3 and PH_3, the barrier of the cyano radical carbon

abstraction is higher than the analogous ethynyl barrier. The difference between the barrier heights of the ethynyl radical and cyano radical is less than 5 kcal mol^{-1} for all reactions except for the abstraction of HF and HCN. Therein the cyano radical abstraction of HF has a barrier height 8.80 kcal mol^{-1} higher than that of the ethynyl radical, and the cyano radical abstraction of HCN has a barrier height 7.05 kcal mol^{-1} higher than the corresponding ethynyl barrier.

Kinetics

Thus far, only the kinetics for the reactions resulting in the production of HCN have been studied. As discussed previously, in nearly every case, the reaction resulting in the production of HCN will be significantly faster than the corresponding reaction producing HNC. For this reason we chose to only report rate constants for a subset of reactions. Table 2.6 contains the rate constants for CN + $H_2, H_2O, HCl,$ and SiH_4 using the rigid–rotor harmonic oscillator approximation. The reactions of CN + $NH_3, PH_3,$ and H_2S have submerged barriers, and as such the rate constants for these reactions at all temperatures will be large as most collisions result in the products $NH_2, PH_2,$ and HS. On the other hand, the abstractions from C_2H_2, HCN, HNC, and HF encounter barriers in excess of 10 kcal mol^{-1} and are not expected to be very important at most temperatures. Because of these considerations, we have only examined the rate constants for the abstractions from $H_2, CH_4, H_2O,$ HCl, and SiH_4. Table 2.6 displays the rate constants for the CN + $H_2, CH_4, H_2O,$ HCl, and SiH_4 reactions.

$CN + H_2$

Due to the simplicity of this system and its importance in interstellar and combustion chemistry, $CN + H_2 \rightarrow HCN + H$ has been extensively studied in numerous previous experimental[99–104] and theoretical studies.[58,89,105–114] Figure 2.4 shows fea-

Table 2.6: Rate constants for CN + HX → HCN + X abstractions in cm^3 $molecule^{-1}$ s^{-1}. Rate constants are obtained with the harmonic oscillator approximation unless stated otherwise.

T(K)	H_2	CH_4[a]	H_2O	HCl	SiH_4
50	3.61×10^{-19}	1.34×10^{-17}	8.36×10^{-19}	5.03×10^{-21}	2.68×10^{-13}
100	7.25×10^{-18}	2.71×10^{-14}	1.13×10^{-18}	5.87×10^{-19}	2.52×10^{-13}
150	1.26×10^{-16}	1.33×10^{-13}	2.50×10^{-18}	3.21×10^{-17}	2.81×10^{-13}
175	4.30×10^{-16}	2.29×10^{-13}	4.14×10^{-18}	1.31×10^{-16}	2.99×10^{-13}
200	1.24×10^{-15}	3.57×10^{-13}	7.20×10^{-18}	4.05×10^{-16}	3.17×10^{-13}
225	3.03×10^{-15}	5.21×10^{-13}	1.29×10^{-17}	1.03×10^{-15}	3.37×10^{-13}
250	6.54×10^{-15}	7.21×10^{-13}	2.34×10^{-17}	2.25×10^{-15}	3.57×10^{-13}
275	1.27×10^{-14}	9.59×10^{-13}	4.22×10^{-17}	4.38×10^{-15}	3.77×10^{-13}
295	2.03×10^{-14}	1.18×10^{-12}	6.99×10^{-17}	7.01×10^{-15}	3.93×10^{-13}
298	2.17×10^{-14}	1.21×10^{-12}	7.15×10^{-17}	7.49×10^{-15}	3.95×10^{-13}
300	2.27×10^{-14}	1.24×10^{-12}	7.48×10^{-17}	7.83×10^{-15}	3.97×10^{-13}
325	3.78×10^{-14}	1.56×10^{-12}	1.29×10^{-16}	1.30×10^{-14}	4.17×10^{-13}
350	5.95×10^{-14}	1.92×10^{-12}	2.16×10^{-16}	2.05×10^{-14}	4.38×10^{-13}
375	8.95×10^{-14}	2.33×10^{-12}	3.49×10^{-16}	3.08×10^{-14}	4.58×10^{-13}
400	1.29×10^{-13}	2.79×10^{-12}	5.47×10^{-16}	4.44×10^{-14}	4.78×10^{-13}
500	4.23×10^{-13}	5.11×10^{-12}	2.50×10^{-15}	1.46×10^{-13}	5.59×10^{-13}
1000	8.71×10^{-12}	3.20×10^{-11}	1.55×10^{-13}	3.36×10^{-12}	9.20×10^{-13}
1500	3.82×10^{-11}	9.25×10^{-11}	1.15×10^{-12}	1.63×10^{-11}	1.22×10^{-12}
2000	1.01×10^{-10}	1.93×10^{-10}	4.15×10^{-12}	4.57×10^{-11}	1.48×10^{-12}
3000	3.69×10^{-10}	5.30×10^{-10}	2.12×10^{-11}	1.78×10^{-10}	1.91×10^{-12}
4000	8.84×10^{-10}	1.05×10^{-9}	6.05×10^{-11}	4.38×10^{-10}	2.27×10^{-12}
5000	1.70×10^{-9}	1.77×10^{-9}	1.30×10^{-10}	8.58×10^{-10}	2.59×10^{-12}

[a] C−H−C bending motion treated as an anharmonic vibration.

tures of the potential energy surface we obtained for this reaction. The reaction proceeds through a linear transition state at 4.24 kcal mol^{-1} and then continues to the products at −21.66 kcal mol^{-1}. Further results for this reaction as studied in this work can be found in the supporting information. Comparisons may be drawn between the theoretical results presented in this work and previous theoretical studies of this reaction; see Table 2.7. In Table 2.7, our results may be considered as the current highest level of theory incorporating a robust geometry as well as various incremental corrections to the electronic energy. The CAS+1+2+QC(3E,3O)/cc–pVTZ

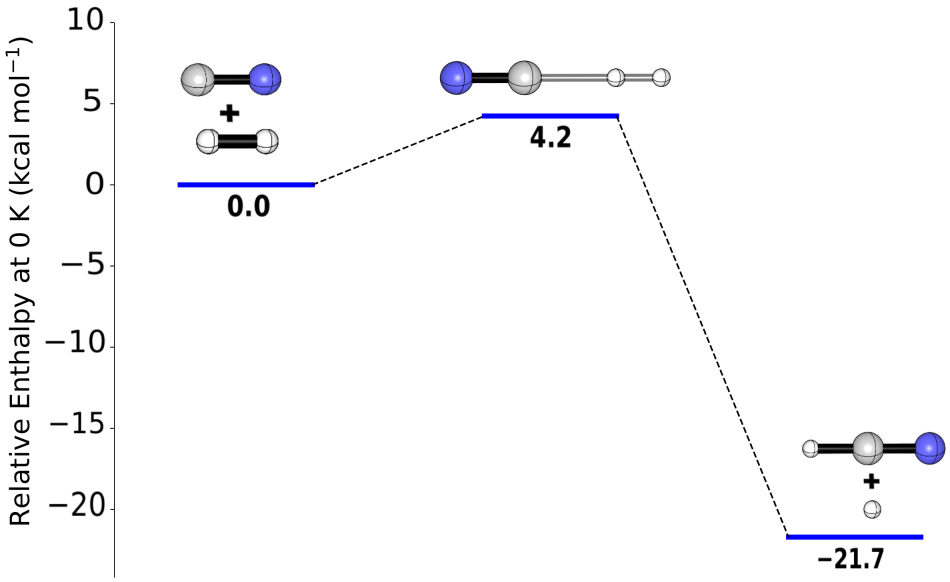

Figure 2.4: Potential energy surface of the $CN + H_2 \rightarrow HCN + H$ reaction at 0 K at the CCSDT(Q)/CBS//CCSD(T)–F12a/aug–cc–pVTZ level of theory. Internal coordinates for all structures can be found in the supporting information.

---

results from ter Horst et al.,[58] the HFB/6–311G(2d,2p) results from Carvalho–Silva et al.,[107] and the MR–CI,3E,3O–CAS+1+2/cc–pVTZ results from He et al.[111] all agree reasonably well with our results. The barrier heights from these studies fall within 0.20 kcal mol^{-1} of the barrier height we found in this study.

Table 2.6 contains the rate constants obtained for the reaction $CN + H_2 \rightarrow HCN + H$. Rate constants were obtained using canonical transition state theory with Eckart tunneling corrections.[37,83,84] Furthermore, to account for the uncertainty in the barrier height, we evaluated rate constants with transition state barriers 0.3 kcal mol^{-1} higher and lower than the barrier height of 4.24 kcal mol^{-1} that we reported. The rate constants with the increased barrier height of 4.54 kcal mol^{-1} seem to match experiment the best in the range $300 - 700$ K. The rate constants with the decreased barrier of 3.94 kcal mol^{-1} overestimate the experimental rate constants over the $100 - 1000$

Table 2.7: Comparison of the $CN + H_2 \rightarrow HCN + H$ abstraction at various levels of theory. Enthalpies are given in kcal mol^{-1}, bond distances and angles of the transition state are given in Angstroms and degrees, respectively, and frequencies in cm^{-1}.

Method	$\Delta H^{\ddagger}$	ΔH_r	R_{CH}	$\omega^{\ddagger}$
CCSDT(Q)/CBS//CCSD(T)–F12a/aug–cc–pVTZ[a]	4.24	−21.66	1.593	$750i$
QCISD(T)/6–311++G**//B3LYP/6–311++G**[b]	1.43	−20.18		
CAS+1+2+QC(3E,3O)/cc–pVTZ[c]	4.3	−20.0	1.62	$684i$
MRCI/cc–pVQZ[d]	3.49	−20.46		$690i$
HFB/6–311G(2d,2p)[e]	4.41			$596i$
MP2/6–311G(2d,2p)[e]	3.19			$572i$
MR–CI,3E,3O–CAS+1+2/cc–pVTZ[f]	4.44		1.685	$644i$
G3[g]	3.85	−22.83	1.701	$1415i$
Active Thermochemical Tables		−21.76		

[a] This work.
[b] Zhao et al.[113]
[c] ter Horst et al.[58] (QC here means a Davidson correction has been included).
[d] Ju et al.[112]
[e] Carvalho–Silva et al.[107]
[f] He et al.[111]
[g] Albernaz and Barreto.[106]

K range, suggesting a lower barrier height is not as reliable for this reaction.

We compared our computed rate constants with previous theoretical and experimental works, as can be seen in Figure 2.5. Wagner and Bair[105] computed their rate constants using conventional transition state theory with Wigner tunneling. They originally found a barrier height of 6.0 kcal mol^{-1} (without zero–point vibrational correction) which they suspected was too high to be consistent with experimental rate constants. Instead, they reported constants using a barrier height of 4.1 kcal mol^{-1}, which reproduced experimental rate constants.[105] However, it appears their rate constants are a bit higher than experiment, suggesting their barrier height is not high enough. Albernaz and Barreto[106] obtained their rate constants using canonical

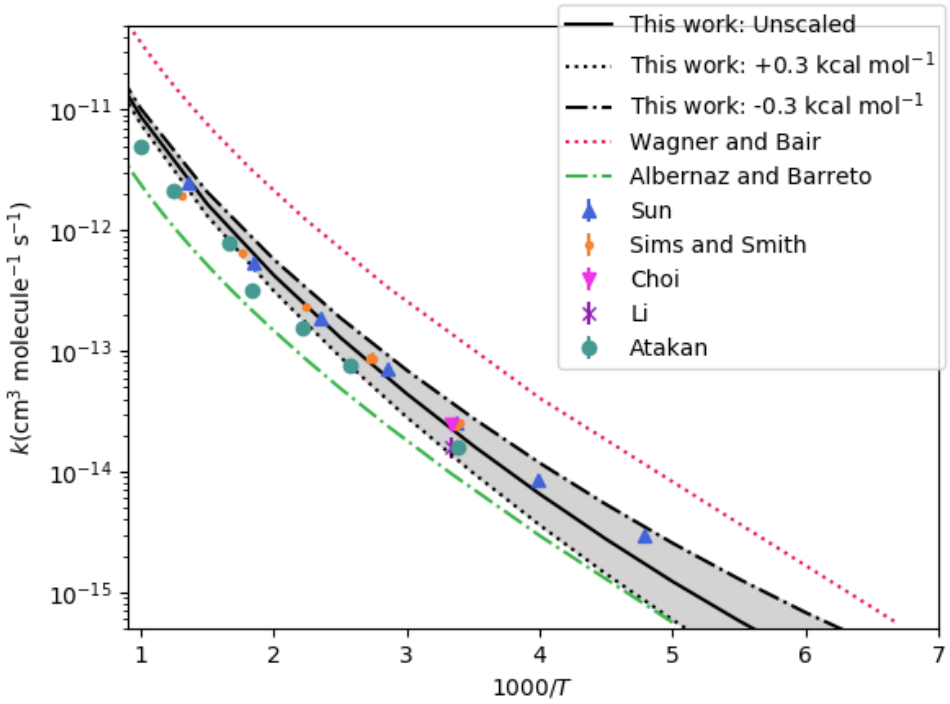

Figure 2.5: Comparison between CN + H_2 → HCN + H rate constants obtained in this work and previously reported experimental (markers)[99–102,104] and theoretical rate constants (lines).[105,106]

---

variational transition state theory with Wigner tunneling. They reported a zero–point corrected barrier height for the reaction CN + H_2 → HCN + H of 3.85 kcal mol^{-1} which is 0.39 kcal mol^{-1} lower than the barrier found in this research.[106] This smaller barrier height along with the variational treatment of their rate constants likely lead to a slight underestimation of the experimental rate constants.

We also investigated the branching ratio for the reactions CN + H_2 → HCN + H and CN + H_2 → HNC + H. The branching ratio between the formation of HNC versus HCN for these reactions is simply given as the ratio between canonical transition state theory rate constants between R2 and R1 for the H_2 donor at a certain temperature. At higher temperatures, the branching ratio becomes more evenly distributed between the production of HCN and HNC. In most cases, the barrier of the nitrogen

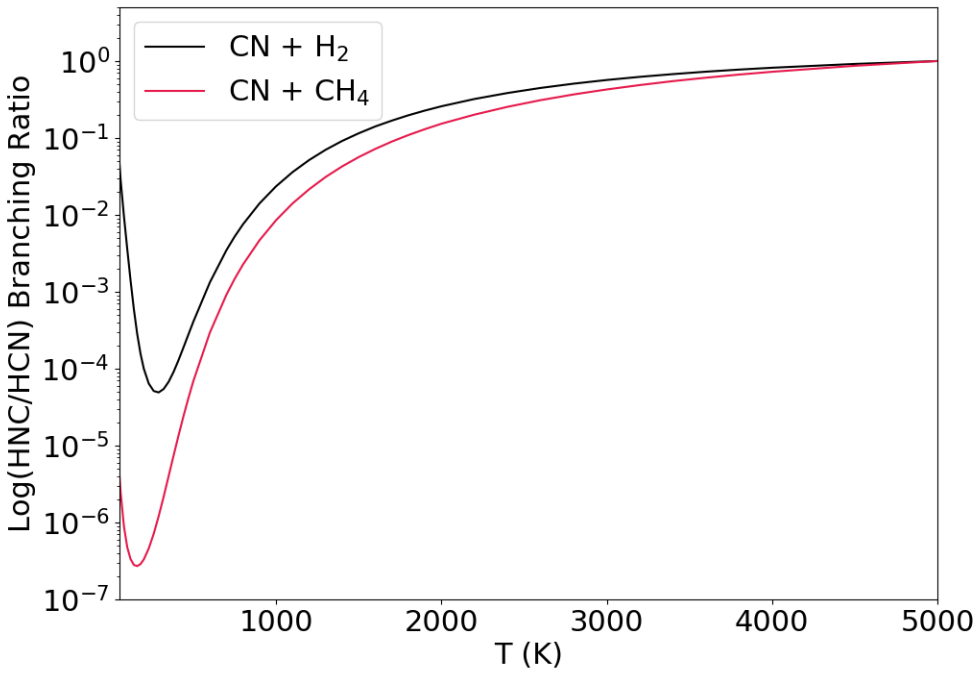

Figure 2.6: Theoretical branching ratios for $CN + H_2 \rightarrow HNC/HCN + H$ and $CN + CH_4 \rightarrow HNC/HCN + CH_3$ as a function of temperature (40–5000 K) (this research).

---

terminal abstraction is at least 5 kcal mol^{-1} greater than the barrier of the corresponding carbon terminal abstraction. Therefore the production of HCN is expected to dominate the HNC production pathway at moderate to low temperatures.

Albernaz and Barreto[106] also reported theoretical HNC/HCN branching ratios for the reaction $CN + H_2 \rightarrow HNC/HCN + H$. They predicted the branching ratio to be temperature dependent over the range $200 - 4000$ K with the $CN + H_2 \rightarrow HCN + H$ reaction as the dominant channel. As the temperature increases to 4000 K, Albernaz and Barreto found the HCN channel remains dominant with the probability $> 99\%$ in the range of temperatures they analyzed.[106] We found similar results for the branching ratio of this reaction, as may be seen in Figure 2.6. As the temperature increases from 40 K up to about 350 K, the HNC/HCN branching ratio quickly decreases to a minimum of less than 10^{-4}, suggesting that the $CN + H_2 \rightarrow HNC + H$ reaction channel

is not as important at low temperatures. As the temperature increases past this point, the branching ratio begins to increase again, showing an increased favorability for the production of HNC. We agree with the findings of Albernaz and Barreto that the $CN + H_2 \rightarrow HCN + H$ pathway is the dominant reaction channel for this range of temperatures. However, as the temperature increases, the probability of this reaction channel decreases as the probability of the $CN + H_2 \rightarrow HNC + H$ increases.

$CN + CH_4$

The $CN + CH_4 \rightarrow HCN + CH_3$ reaction has also been studied in previous experimental[59,99–102,104] and theoretical studies[115] due to its importance in both combustion environments and the ISM. Figure 2.7 shows the stationary points we obtained for this reaction. This reaction proceeds through a transition state of C_{3v} symmetry with a small barrier height of 1.19 kcal mol^{-1}. The reaction then continues to the products HCN and CH_3 at -21.77 kcal mol^{-1}. Further results for this reaction as studied in this work can be found in the supporting information. Rate constants for this reaction are provided in Table 2.6. In a previous study, we found that anharmonic treatments of low frequency vibrational modes may be necessary for highly accurate TST rate constants.[42] For the reaction $CN + CH_4 \rightarrow HCN + CH_3$ we also found this type of treatment to be necessary and it has been included. Our rate constants were obtained using canonical transition state theory with Eckart tunneling corrections using an anharmonic treatment of the first degenerate vibrational mode. Additionally, we computed rate constants for this reaction with barrier heights 0.3 kcal mol^{-1} higher and lower than the barrier height we reported for this reaction. The rate constants computed with the reduced (1.19 - 0.30) barrier height of 0.89 kcal mol^{-1} significantly overestimated the experimental rate constants, while the rate constants computed with the higher (1.19 + 0.30) barrier height of 1.49 kcal mol^{-1} had excellent agreement with experimental rate constants in the range $100 - 500$ K.

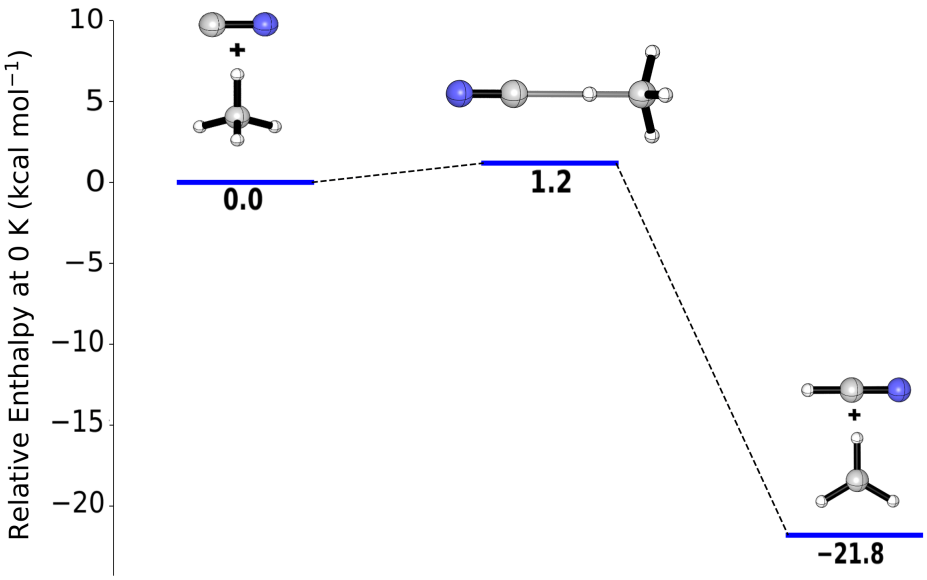

Figure 2.7: Potential energy surface of CN + CH_4 → HCN + CH_3 reaction at 0 K at the CCSDT(Q)/CBS//CCSD(T)–F12a/aug–cc–pVTZ level of theory. Internal coordinates for all structures can be found in the supporting information.

The latter result is a bit surprising because higher levels of electronic structure theory (than those used here) tend to *decrease* barrier heights. However, our simple procedures for predicting the rate constants may be an important part of the disagreement between the 1.19 and 1.49 kcal mol^{-1} barrier results.

We compared our computed rate constants with previous theoretical and experimental works, as shown in Figure 2.8. Espinosa–Garcia et al.[115] computed their rate constants using canonical variational transition state theory (CVT) with multidimensional tunneling, and again with ring polymer molecular dynamics (RPMD). They computed their rate constants with a transition state barrier of 2.5 kcal mol^{-1}. Their CVT results seem to reproduce experimental data well in the range $300 - 1000$ K while the RPMD seem to slightly overestimate the experimental rates in the same temperature range. Our results seem to match the experimental trend qualitatively,

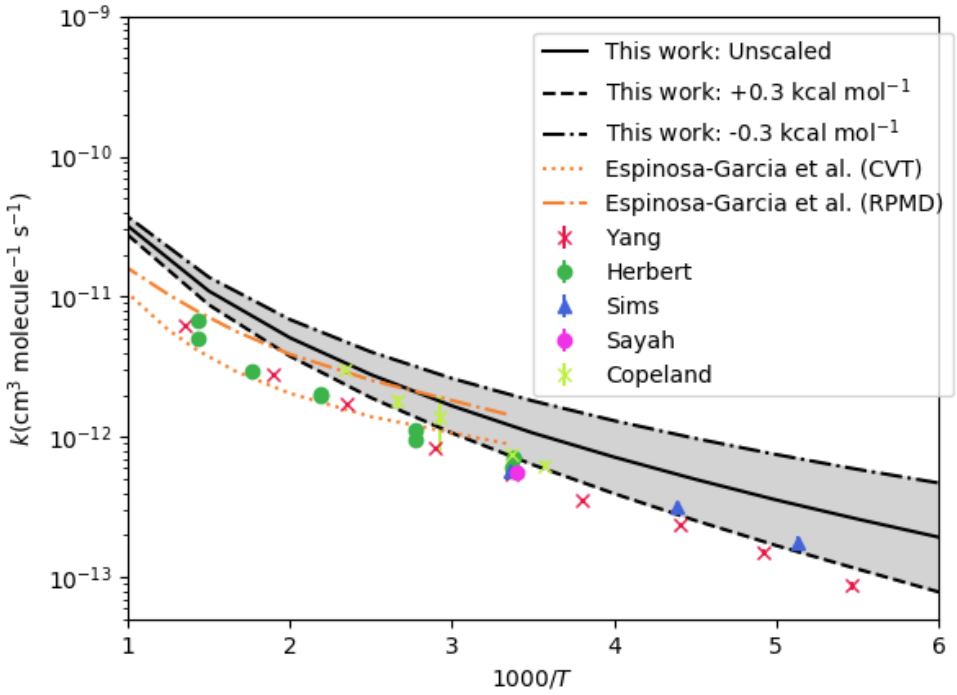

Figure 2.8: Comparison between $CN + CH_4 \rightarrow HCN + CH_3$ rate constants obtained in this work and previously reported experimental (markers)[49,116–119] and theoretical data (solid and dashed lines).[115]

---

but our rate constants overestimate the experimental rates in this same temperature range. If we had used a variational treatment for our rate constants, it is possible they would have matched experiment better at high temperatures. At lower temperatures, the rate constants we computed with the barrier height 1.49 kcal mol^{-1} have excellent agreement with experiment.

We investigated the branching ratio between the $CN + CH_4 \rightarrow HCN + CH_3$ and $CN + CH_4 \rightarrow HNC + CH_3$ reactions using the same methodology described before. Bethardy et al.[120] reported a HNC/HCN branching ratio for the reaction $CN + CH_4 \rightarrow HNC/HCN + CH_3$ of less than 10^{-4} at room temperature, which we have found to be true at low temperatures.[120] As the temperature increases from 40 K up to around 350 K, we found there is a decrease in the branching ratio, leading to a minimum

of less than 10^{-6} at around room temperature. This value is in agreement with the results reported by Bethardy and coworkers. As the temperature increases past this point, the HNC/HCN branching ratio increases and approaches 1 as the temperature approaches 5000 K, showing that the reaction between $CN + CH_4$ may proceed over the 12.79 kcal mol^{-1} barrier resulting in the production of $HNC + CH_3$. However, the $CN + CH_4 \rightarrow HCN + CH_3$ reaction will remain the dominant reaction pathway of the two. The relationship between branching ratio and temperature is illustrated in Figure 2.6, presented earlier.

$CN + NH_3$

The reaction $CN + NH_3 \rightarrow HCN + NH_2$ has a submerged barrier of -2.41 kcal mol^{-1}. Because of this submerged barrier, rate constants for this reaction at all temperatures will be large, as most collisions will result in the products. The experiment of De Juan et al.[121] agrees with this. The rate constants they obtained for this reaction were so large that they concluded the absence of any significant potential barrier.[121] Other previous experimental and theoretical studies similarly found that this reaction has a rapid rate.[56,122–124] Comparisons may be drawn between the theoretical results presented in this work and previous theoretical studies on this reaction, found in Table 2.8. Our results may be considered as the current highest level of theory incorporating a robust geometry as well as various incremental corrections to the electronic energy. The next highest level of theory [CCSD(T)] is the work by Talbi and Smith found in Table 2.8.[125] The transition state we found is in reasonable agreement with that which Talbi and Smith reported for the low energy pathway from $CN + NH_3$ to $HCN + NH_2$ using their potential energy surface. Our transition state barrier is -2.41 kcal mol^{-1}, which is within 0.2 kcal mol^{-1} of the transition state reported by Talbi and Smith.[125] However, our exothermicity (-18.95 kcal mol^{-1}) is in near perfect agreement with the ATcT result (-19.02 kcal mol^{-1}) but quite distant

from the earlier theoretical result (-20.78 kcal mol^{-1}). Additionally, the geometric parameters of our transition state are in good agreement with those of Talbi and Smith, as can be seen in Table 2.8.

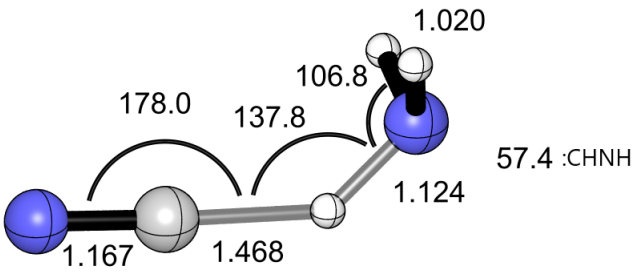

Figure 2.9: C_s symmetric $CN + NH_3$ transition state found in this work optimized at the CCSD(T)–F12a/aug–cc–pVTZ level of theory. Bond angles and bond distances are given in degrees and in Angstroms, respectively.

Table 2.8: Comparison of $CN + NH_3 \rightarrow HCN + NH_2$ abstraction at various levels of theory. Enthalpies are given in kcal mol^{-1}, bond distances and angles of the transition state are given in Angstroms and degrees, respectively, and frequencies in cm^{-1}.

Theory	$\Delta H^{\ddagger}$	ΔH_r	R_{CH}	R_{NH}	$\angle$CHN	$\omega^{\ddagger}$
CCSDT(Q)/CBS//CCSD(T)–F12a/aug–cc–pVTZ[a]	-2.41	-18.95	1.46	1.12	137.8°	$1068i$
CCSD(T)/6–311++G(3df,2pd)//CCSD/6–311G(d,p)[b]	-2.60	-20.78	1.54	1.09	133.9°	$846i$
Active Thermochemical Tables		-19.02				

[a] This work.
[b] Talbi and Smith.[125]

$CN + H_2O$

Due to its importance in the ISM and combustion environments, the $CN + H_2O \rightarrow HCN + OH$ reaction has been studied in previous experimental[126–128] and theoretical studies.[129] Figure 2.10 shows the stationary point energies we obtained for this reaction. This reaction proceeds through a transition state of C_1 symmetry with a barrier height of 7.15 kcal mol^{-1}. The reaction then proceeds to the products

HCN and OH at -7.38 kcal mol^{-1}. Further results for this reaction as studied in this work can found in the supporting information. Rate constants for this reaction can be found in Table 2.6. Our rate constants were obtained using canonical transition state theory with Eckart tunneling corrections. Additionally, we computed rate constants for this reaction with a barrier height 0.3 kcal mol^{-1} higher and lower than the barrier height we reported for this reaction. The rate constants computed with both modified barrier heights and those computed with our actual barrier height of 7.15 kcal mol^{-1} fall between the two sets of experimental results, seen in Figure 2.11.

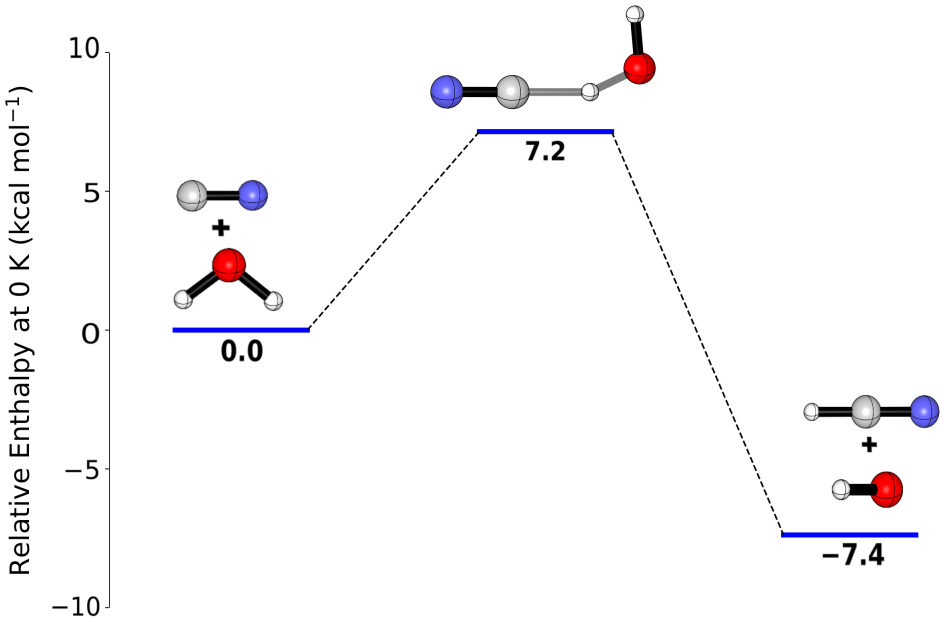

Figure 2.10: Potential energy surface features for the CN + $H_2O \rightarrow$ HCN + OH reaction at 0 K at the CCSDT(Q)/CBS//CCSD(T)/aug–cc–pVTZ level of theory. Internal coordinates for all structures can be found in the supporting information.

We compared our computed rate constants with previous theoretical and experimental studies, as illustrated in Figure 2.11. Wang et al.[129] computed their rate constants using both conventional transition state theory and canonical variational transition state theory. They further corrected their CVT rate constants with small–

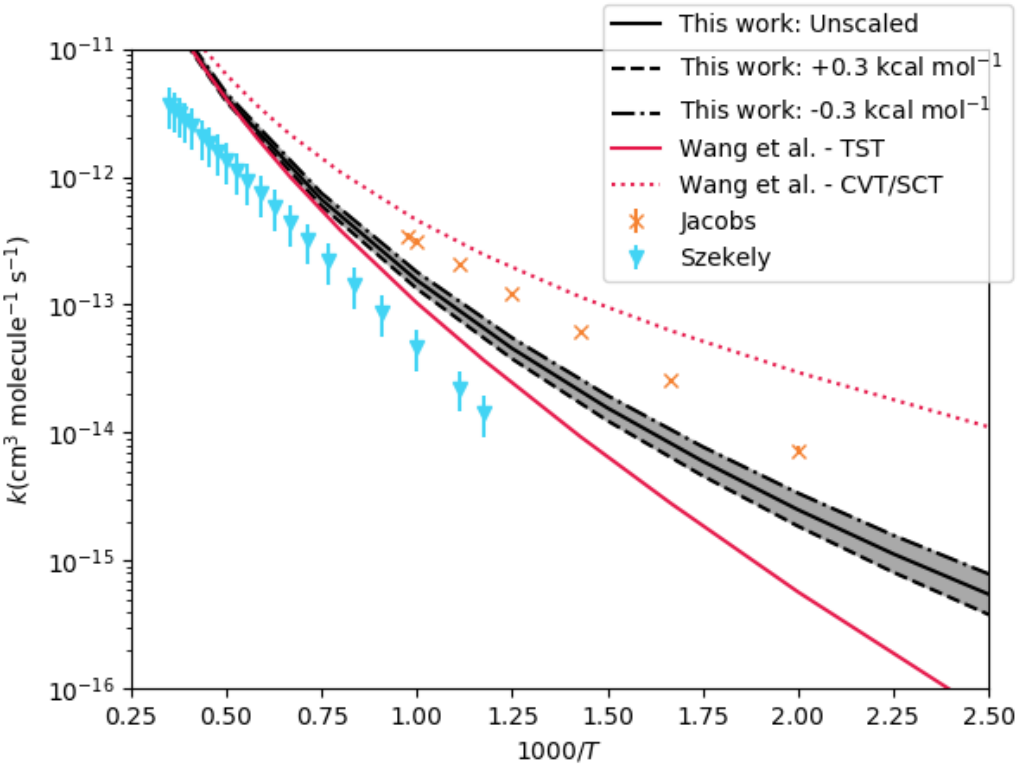

Figure 2.11: Comparison between $CN + H_2O \rightarrow HCN + OH$ rate constants obtained in this work and previously reported experimental (markers)[126,128] and theoretical data (solid and dashed lines).[129]

---

curvature tunneling (SCT).[129] They optimized their stationary points for this reaction at the QCISD(T)/6–311+G(2df,2p)//QCISD/6–311G(d,p) level of theory. They reported a transition state barrier height of 7.51 kcal mol^{-1} with zero–point energy included. Based on their results, Wang et al. concluded that the variational effect is very small in the calculation of the rate constants. They also concluded that the SCT corrections were necessary, so they consider their CVT/SCT results to be the most reliable.[129] The TST results they reported fall between the experimental results while their CVT/SCT results fall slightly above the experimental results reported by Jacobs et al.[126] Our results seem to match the experimental trend well qualitatively, falling between the experimental rate constants reported by Jacobs et al. and Szekely

et al.[126,128] We also obtained rate constants with modified barrier heights 0.3 kcal mol^{-1} higher and lower than our reported barrier height to explore whether our barrier was too high or too low. As can be seen in Figure 2.11, these modified barrier heights do not significantly alter our rate constants with respect to the experimental results. At high temperatures, our rate constants match well with the transition state theory results reported by Wang et al.[129] We obtained a transition state barrier for this reaction of 7.15 kcal mol^{-1}, which is slightly lower than their transition state barrier of 7.51 kcal mol^{-1}.[129] Future experimental studies of this reaction may be necessary. The two experimental studies compared in this work disagree significantly, and the theoretical results found in this study are not in excellent agreement with either set of experimental results.

Conclusion

The energetics of the cyano radical hydrogen abstractions of H_2, CH_4, NH_3, H_2O, HF, SiH_4, PH_3, H_2S, HCl, C_2H_2, HCN, and HNC with both the carbon and nitrogen terminals have been determined using highly accurate *ab initio* methods. We were able to achieve sub–chemical accuracy through a variety of additive energy corrections and we obtained excellent agreement with the Active Thermochemical Table values. Accurate transition state barriers have been obtained for all reactions with the carbon and nitrogen terminals. It was found that the carbon terminal abstractions of NH_3, PH_3, and H_2S have submerged barriers below the relative enthalpies of their respective reactants. Abstractions of H_2, CH_4, H_2O, HCl, and SiH_4 have barriers between 0 and 8 kcal mol^{-1}. Abstractions of HF, C_2H_2, HCN, and HNC have barriers larger than 10 kcal mol^{-1}. It was also found that the nitrogen terminal abstractions have higher barrier heights and are almost always slower than the analogous carbon terminal abstractions. The energetics for the nitrogen terminal abstractions presented

in this research may aid any future experimental studies of these reactions. Accurate rate constants were obtained for the $CN + H_2/CH_4/H_2O/HCl/SiH_4 \rightarrow HCN + H/CH_3/OH/Cl/SiH_3$ reactions. Excellent agreement was demonstrated for the computed rate constants for the $CN + H_2 \rightarrow HCN + H$ reaction with current experimental rate constants without adjusting the barrier height. Good agreement for the computed rate constants for the $CN + CH_4 \rightarrow HCN + CH_3$ and $CN + H_2O \rightarrow HCN + OH$ reactions with current experimental rate constants was also demonstrated. Based on the agreement of these rate constants with experiment, the computed rate constants for the $CN + HCl \rightarrow HCN + Cl$ and $CN + SiH_4 \rightarrow HCN + SiH_3$ reactions are expected to be reliable. The $CN + HCl \rightarrow Cl$ reaction has not been as extensively studied as the $CN + H_2/CH_3/H_2O \rightarrow H/CH_3/OH$ reactions, and the $CN + SiH_4 \rightarrow HCN + SiH_3$ reaction has not yet been studied, so these results will be useful to guide future experimental and theoretical studies.

Acknowledgements

The authors gratefully acknowledge support from the US Department of Energy (DOE), Office of Basic Energy Sciences (BES), Computational and Theoretical Chemistry (CTC) Program, under Grant No. DE-SC0018412.

Chapter 3

A High–Level Theoretical Study of Various Cyano Radical Hydrogen Abstractions from Mid–Sized Donors[2]

[2] To be submitted to *Physical Chemistry Chemical Physics.*

Abstract

Hydrogen abstraction with small, closed–shell molecules is one of the most prevalent reactions the cyano radical undergoes. These reactions have been well–studied in previous works. This study investigated the energetics and kinetics of hydrogen abstractions by the cyano radical with mid–size hydrogen donors. Both abstractions by the carbon and nitrogen terminals were studied as both terminals of the cyano radical are reactive sites. In most cases, the carbon terminal abstraction barrier height was found to be lower in energy than the corresponding nitrogen terminal abstraction barrier. The CN + HX → HCN/HNC + X reactions where HX = HNCO, HOCN, *trans*–HONO were studied at a high–level of theory, including CCSD(T)–F12a. Rate constants were obtained for these reactions over a wide range of temperatures. Excellent agreement with the ATcT values was achieved via the methods outlined in this study. The energetics and kinetics obtained here may be used to guide future studies of these reactions as well as hydrogen abstractions by the cyano radical of larger hydrogen donors, such as benzene or naphthalene.

Introduction

The cyano radical (CN $^2\Sigma^+$) is one of the most abundant open–shell molecules found in the interstellar medium.[43,44] It has been identified in the atmospheres of Titan and the outer planets and some of their satellites, and it has been known to be involved in the chemistry of hot molecular cores and the outflow of dying carbon stars.[45–47] Additionally, it has been found to be important in the combustion of hydrocarbons as HCN is a common intermediate in hydrocarbon flames containing a nitrogen source,[48] and the reactions of CN radicals with unsaturated hydrocarbons are important steps in the production of long chain nitrile species.[46] The cyano radical

often reacts with small, closed–shell molecules found in these same environments via hydrogen abstraction.[43,49] It has been found that the cyano radical can abstract the hydrogen, forming either HCN or HNC. Reactions of this kind have been well–studied in the past.[41,100–110,115,116,122,127] The prototypical $CN + H_2 \rightarrow HCN/HNC + H$ reaction has been studied extensively theoretically and experimentally.[41,99–110] A previous study investigated this reaction and numerous other hydrogen abstractions of small hydrogen–donors at a high level of theory to obtain highly accurate energetics and kinetics for these reactions.[41] In this study, similar high level methods will be applied to hydrogen abstractions by the cyano radical of slightly larger hydrogen–donors. The following reactions will be studied:

$$CN + HX \rightarrow HCN + X \quad \text{(R1)}$$

$$CN + HX \rightarrow HNC + X \quad \text{(R2)}$$

where HX = HNCO, HOCN, and *trans*–HONO. These hydrogen donors have been chosen because of their importance in the interstellar and combustion environments in which the cyano radical is present. Understanding how the cyano radical hydrogen abstraction behaves with mid–size hydrogen donors may inform future studies of the hydrogen abstractions of much larger molecules like benzene or naphthalene. HNC is more rare than HCN on earth. However, in space HNC has been observed at times to be as abundant as HCN. In cold clouds with temperatures as low as 10 K the HNC/HCN abundance ratio was observed to be 1.55.[53,54] While the carbon terminal of the cyano radical is generally more reactive than the nitrogen terminal, the HNC–producing reactions will also be studied due to the observed abundance of HNC in space.

This study will provide highly accurate barrier heights for the listed reactions to illustrate a picture of the potential energy surfaces of these reaction pathways. Additionally, reliable theoretical rate constants will be obtained for these reactions over a wide range of temperatures which mimic the conditions in which these reactions

occur. These results may be used to guide future studies of reactions involving the cyano radical.

Methods

Equilibrium geometries of all stationary points were optimized using the CCSD(T)–F12a[60] method with the cc–pVTZ–F12[130] basis set as implemented in Molpro 2010.[62] Harmonic vibrational frequencies were obtained for each stationary point at this same level of theory. Electronic energies of the stationary points along all the reactions were computed according to the focal point approach of Allen and coworkers.[23,24] Methods that describe electron correlation up to CCSDT(Q)[63] and basis sets as large as aug–cc–pV5Z[61] were used in this study. CCSD(T)/aug–cc–pVXZ[14,131,132] (X = D, T, Q, 5) single point energies were computed using Molpro 2010 and the CCSDT/aug–cc–pVDZ and CCSDT(Q)/aug–cc–pVDZ energies were obtained using MRCC 2018.[18] Good convergence to the complete basis set limit was demonstrated for all stationary points; an example is shown in Table 3.1. A three–point exponential equation[65] (Equation 3.1) was used to estimate the CBS limit for the SCF energies, and a two–point inverse cubic equation[66] (Equation 3.2) was used to extrapolate post–Hartree–Fock energies.

$$E_{\mathrm{ref}}(X) = E_{\mathrm{HF}}^{\infty} + ae^{-bX} \tag{3.1}$$

$$E_{\mathrm{corr}}(X) = E_{\mathrm{corr}}^{\infty} + aX^{-3} \tag{3.2}$$

Additive high–order energy corrections were included for the CCSDT and CCSDT(Q) correlation. The focal point energies were obtained with the following formula:

$$\Delta E_{\mathrm{CCSDT(Q)/CBS}} = \Delta E_{\mathrm{CCSD(T)/CBS}} + \delta E_{\mathrm{T(Q)}} \tag{3.3}$$

Table 3.1: Representative incremental focal point analysis table for the products of the CN + HNCO → HCN + NCO reaction relative to the reactants. Additional focal point tables can be found in the supporting information.

Basis Set	HF	+δ MP2	+δCCSD	+δ(T)	+δT	+δ(Q)	Net
aug–cc–pVDZ	−24.69	+12.18	−4.42	+1.77	+0.18	+0.06	[−14.92]
aug–cc–pVTZ	−25.15	+12.01	−4.67	+2.03	[+0.18]	[+0.06]	[−15.55]
aug–cc–pVQZ	−24.90	+12.18	−4.67	+2.08	[+0.18]	[+0.06]	[−15.08]
aug–cc–pV5Z	−24.89	+12.23	−4.68	+2.10	[+0.18]	[+0.06]	[−15.01]
CBS Limit	[−24.90]	[+12.28]	[−4.69]	[+2.12]	[+0.18]	[+0.06]	[−14.96]

Additional energy corrections were included to account for various approximations made during the focal point computations. To account for the core–correlation neglected under the frozen–core approximation, the difference between the CCSD(T)/aug–cc–pCVQZ energies with and without core–electrons correlated was determined (δ_{CORE}). A scalar relativistic correction was obtained using X2C–CCSD(T)/aug–cc–pCVTZ–X2C (δ_{REL}).[67,68] The clamped nuclei approximation was treated via a diagonal Born–Oppenheimer correction[69,70] at the ROHF/aug–cc–pVTZ level of theory (δ_{DBOC}). Both the relativistic correction and the diagonal Born–Oppenheimer correction were carried out with CFOUR.[71] A spin–orbit coupling constant (δ_{SO}) was included for NCO to account for the splitting of the electronic ground state.[133] Zero–point vibrational energies were obtained from the CCSD(T)–F12a/cc–pVTZ–F12 harmonic vibrational frequencies (δ_{ZPVE}). These corrections were added together to obtain the relative enthalpy of each stationary point at 0 K:

$$\Delta H_{0\mathrm{K}} = \Delta E_{\mathrm{CCSDT(Q)/CBS}} + \delta_{\mathrm{CORE}} + \delta_{\mathrm{REL}} + \delta_{\mathrm{DBOC}} + \delta_{\mathrm{ZPVE}}(+\delta_{\mathrm{SO}}) \tag{3.4}$$

Rate constants were calculated over a range of temperatures using canonical transition state theory:[83,84]

$$k^{\mathrm{TST}}(T) = \kappa(T)\frac{k_B T}{h}\frac{Q^{\mathrm{TS}}(T)}{Q^{\mathrm{R}}(T)}\exp\left(\frac{-\Delta H^{\ddagger}}{k_B T}\right) \tag{3.5}$$

where $Q^{\mathrm{TS}}(T)$ and $Q^{\mathrm{R}}(T)$ are the partition functions of the transition state (TS) and reactants (R), respectively, and $\Delta H^{\ddagger}$ is the barrier height for the reaction. The transmission coefficient, $\kappa(T)$, was determined with an asymmetric Eckart potential barrier given the relative enthalpies of the pre–reactive complex, transition state, and products for each reaction as well as the imaginary harmonic vibrational frequency corresponding to the reaction mode of the transition state.[37] This tunneling treatment was used because of its past success accurately describing the tunneling of hydrogen abstraction reactions at moderate to high temperatures.[37–40] These methods have been observed to be the most accurate in the $200-2000$ K range.[41,42] Previous studies of the rate constants of hydrogen abstractions by the cyano radical and the ethynyl radical, which is isoelectronic, have found that the use of canonical transition state theory with an asymmetric Eckart potential is useful for reproducing experimental results.[41,42]

Results

Energies and Geometries

Table 3.2 contains the energetic breakdown for each set of products for each investigated reaction producing HCN and HNC. As seen in the final two columns of these tables, there is excellent agreement between our computed energies and the values taken from the Active Thermochemical Tables (ATcT) (version 1.122r).[85–87] The mean absolute error with respect to the ATcT values of the carbon terminal abstraction reaction enthalpies is 0.09 kcal mol^{-1} and 0.13 kcal mol^{-1} for the nitrogen terminal abstractions. The root mean square error for the carbon terminal abstractions when compared to the ATcT is 0.11 kcal mol^{-1} and 0.15 kcal mol^{-1} for the nitrogen terminal. The largest deviation occurs for the HCN–producing reaction involving HOCN at 0.16 kcal mol^{-1} and the HNC–producing reaction involving

trans–HONO at 0.22 kcal mol^{-1}. The $\delta_{\mathrm{T(Q)}}$ corrections are notably large, ranging from 0.23 to 0.69 kcal mol^{-1}. A CCSDT/aug–cc–pVTZ correction may have improved the observed convergence for the FPA of these stationary points, however, this computation was determined to be too cost prohibitive for the transition states and pre– and post–reactive complexes, therefore was not included for the products. The δ_{CORE} correction is quite large for both sets of products including *trans*–HONO. The δ_{REL} and δ_{DBOC} corrections are within the expected range with average magnitudes of 0.09 and 0.02 kcal mol^{-1}, respectively. No transition state for the CN + HOCN → HNC + NCO reaction has been found, so it is not included in this study.

Table 3.2: Enthalpies at 0 K ($\Delta H_{0\mathrm{K}}$) in kcal mol^{-1} for products relative to reactants.

HCN Production	CBS[a]	$\delta_{\mathrm{T(Q)}}$	δ_{CORE}	δ_{REL}	δ_{DBOC}	δ_{ZPVE}	δ_{SO}[b]	Total	ATcT[c]
HNCO	−15.19	0.23	−0.10	−0.09	0.02	−0.08	−0.137	−15.34	−15.34
HOCN	−39.74	0.33	−0.19	−0.07	0.04	−0.18	−0.137	−39.95	−40.11
t–HONO	−46.81	0.53	−0.65	0.09	0.03	−0.18		−46.99	−47.14
HNC Production	CBS[a]	$\delta_{\mathrm{T(Q)}}$	δ_{CORE}	δ_{REL}	δ_{DBOC}	δ_{ZPVE}	δ_{SO}[b]	Total	ATcT[c]
HNCO	−0.28	0.40	0.10	−0.05	0.00	−0.40	−0.137	−0.37	−0.43
t–HONO	−31.89	0.69	−0.45	0.13	0.01	−0.50		−32.01	−32.23

[a] CBS denotes the CCSD(T)/CBS relative energy.
[b] Spin–orbit coupling constants are included for NCO.[133]
[c] Data taken from the Active Thermochemical Tables.[85–87]

Optimized geometries for each transition state are shown in Figure 3.1. Further details for each stationary point can be found in the supporting information. Table 3.3 contains the energetic breakdown for each of the transition states for the investigated reactions producing HCN and HNC. According to these results, the barrier heights for the HCN–producing reactions may be considered accurate within an uncertainty of 0.16 kcal mol^{-1} and the HNC–producing reactions may be considered accurate within an uncertainty of 0.22 kcal mol^{-1}. The $\delta_{\mathrm{T(Q)}}$ corrections observed for the transition states have magnitudes between 0.02 and 0.69 kcal mol^{-1}. The CN + HOCN reaction and the *trans*–HONO abstractions have the largest corrections suggesting these barrier heights may benefit from the inclusion of a CCSDT/aug–cc–

pVTZ, however as mentioned before this was determined to be too cost prohibitive. Regardless, there is still confidence that these barrier heights are within an uncertainty of 0.16 and 0.22 kcal mol^{-1} for the HCN–producing and HNC-producing reactions, respectively. The core valence correction for both *trans*–HONO transition states is larger than expected with a magnitude of 0.28 and 0.29 kcal mol^{-1} for the carbon and nitrogen abstractions, respectively. The δ_{DBOC} correction for all transition states except for $\mathrm{CN} + \mathrm{HNCO} \rightarrow \mathrm{HCN} + \mathrm{NCO}$ are within a reasonable range. The diagonal Born–Oppenheimer correction for the $\mathrm{CN} + \mathrm{HNCO} \rightarrow \mathrm{HCN} + \mathrm{NCO}$ transition state is notably large with a quantity of 1.62 kcal mol^{-1}. An investigation into the significance of this correction can be found in the corresponding subsection. In each transition state, the carbon terminal abstraction barrier height is lower than the corresponding nitrogen terminal abstraction barrier height, except for the *trans*–HONO transition state. Further explanation of this can be found in the corresponding subsection. According to the results in Table 3.2, it is expected that the HCN and HNC–producing barrier heights are accurate within uncertainties of 0.16 kcal mol^{-1} and 0.22 kcal mol^{-1}, respectively. Pre– and post–reactive complexes for relevant reactions are discussed in the following subsections.

Table 3.3: Enthalpies at 0 K ($\Delta H_{0\mathrm{K}}$) in kcal mol^{-1} for the transition states relative to the reactants.

HCN Production	CBS[a]	$\delta_{\mathrm{T(Q)}}$	δ_{CORE}	δ_{REL}	δ_{DBOC}	δ_{ZPVE}	Total
HNCO	9.43	0.02	0.06	−0.20	(1.62)	−3.08	6.23[b]
HOCN	8.19	−0.69	−0.03	−0.03	0.18	−3.40	4.22
t–HONO	11.59	−0.49	−0.29	0.05	0.03	−0.78	10.12
HNC Production	CBS[a]	$\delta_{\mathrm{T(Q)}}$	δ_{CORE}	δ_{REL}	δ_{DBOC}	δ_{ZPVE}	Total
HNCO	16.15	−0.14	0.15	−0.07	0.24	−3.01	13.33
t–HONO	8.14	−0.23	−0.28	0.12	0.15	−1.27	6.64

[a] CBS denotes the CCSD(T)/CBS relative energy.
[b] Does not include diagonal Born–Oppenheimer correction.

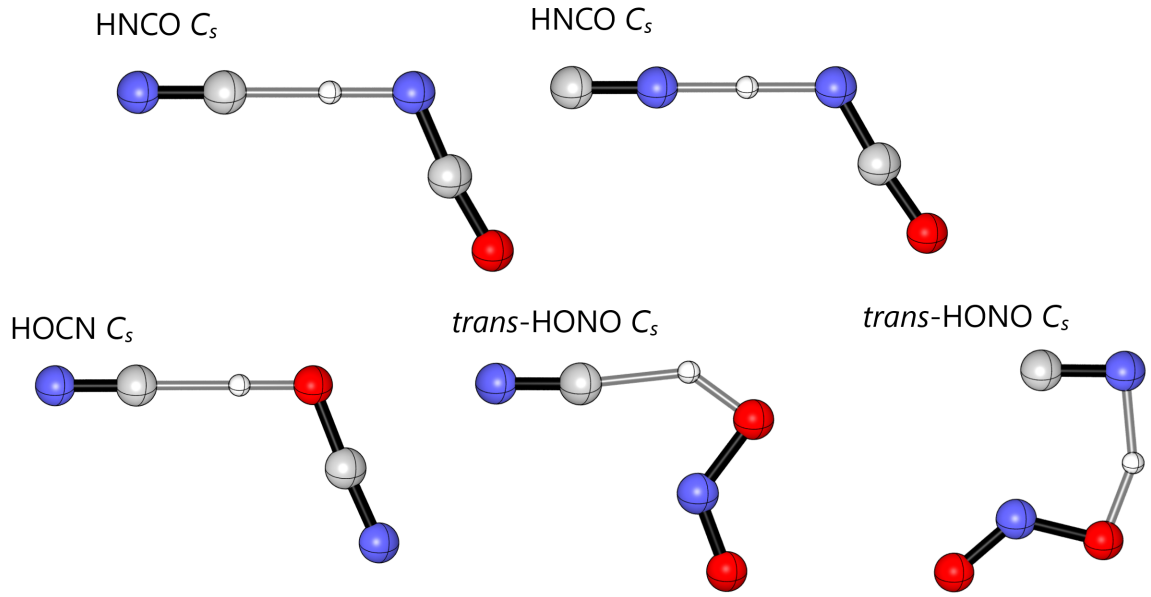

Figure 3.1: Geometries of (R1 and R2) transition states

Table 3.4: Reaction enthalpies ($\Delta_r H$), transition state barrier heights ($\Delta H^{\ddagger}$), geometric parameters, and transition state imaginary frequencies ($\omega^{\ddagger}$) for the CN + HX abstractions at the CCSDT(Q)/CBS//CCSD(T)–F12a/cc–pVTZ–F12 level of theory. The HCN and HNC Donor sections of the table reference the CN + HX → HCN + X and CN + HX → HNC + X reactions, respectively.

HCN Donor	$\Delta_r H$	$\Delta H^{\ddagger}$	R_{CH}	$\Delta R^{\mathrm{a}}_{\mathrm{XH}}$	θ_1	θ_2	$\omega^{\ddagger}$
t–HONO	−46.99	10.12	1.517	15.8%	173.6	137.4	$2194i$
HOCN	−39.95	4.22	1.486	10.4%	180.0	180.0	$2134i$
HNCO	−15.34	6.23	1.428	12.8%	180.0	180.0	$1361i$
HNC Donor	$\Delta_r H$	$\Delta H^{\ddagger}$	R_{NH}	$\Delta R^{\mathrm{a}}_{\mathrm{XH}}$	θ_1	θ_2	$\omega^{\ddagger}$
t–HONO	−32.01	6.64	1.330	23.6%	95.6	154.2	$1779i$
HNCO	−0.37	13.33	1.248	22.0%	180.0	180.0	$3439i$

[a] $\Delta R_{\mathrm{XH}} = (R_{\mathrm{XH,TS}} - R_{\mathrm{XH,eq}})/R_{\mathrm{XH,eq}}$

Table 3.4 contains energetic and geometric parameters for the various reactions investigated in this study. The ΔR_{XH} variable in Table 3.4 shows the percent change between the XH bond length in the optimized donor molecule and the XH bond length in the transition state, where X = O, N for *trans*–HONO and HOCN or HNCO, re-

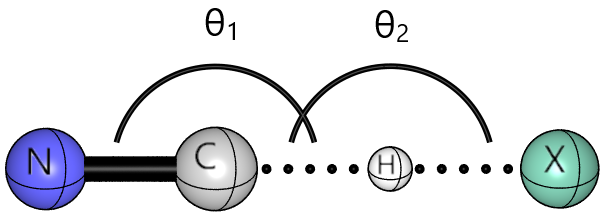

Figure 3.2: General geometric parameters of the transition states investigated in this work.

---

spectively. The bond lengths used to calculate ΔR_{XH} can be found in the supporting information. A general transition state figure with appropriate labeling corresponding to Table 3.4 is shown in Figure 3.2.

An example calculation of ΔR_{XH} is as follows. For the CN + *trans*–HONO → HCN + NO_2 reaction, the ΔR_{XH} value is calculated to be:

$$\Delta R_{\mathrm{XH}} = \frac{(R_{\mathrm{OH,TS}} - R_{\mathrm{OH,eq}})}{R_{\mathrm{OH,eq}}} * 100 = \frac{\left(1.119\ \text{Å} - 0.966\ \text{Å}\right)}{0.966\ \text{Å}} * 100 = 15.8\% \qquad (3.6)$$

where $R_{\mathrm{OH,TS}}$ corresponds to the OH bond distance in the optimized transition state geometry and $R_{\mathrm{OH,eq}}$ corresponds to the OH bond distance in the optimized geometry of *trans*–HONO. The larger the value of ΔR_{XH}, the more the transition state XH bond distance has increased from the original XH bond distance from the reactant geometry. If a transition state more closely resembles the reactants than the products, the ΔR_{XH} value should be less than 50%, and it should be greater than 50% for the opposite. The Hammond postulate describes how the relationship between the geometric parameters of the transition state and the reactants is dependent on the exothermicity of the reaction. Via the Hammond postulate, the transition state should geometrically resemble either the reactants or the products, whichever it is closer to in energy. The reactions investigated in this work follow this postulate. The value for ΔR_{XH} for the CN + HNCO → HCN + NCO reaction is 12.8%, and the energy difference between the reactants and transition state is 6.23 kcal mol^{-1} while

the energy difference between the transition state and the products is 21.57 kcal mol^{-1}. The transition state lies energetically closer to the reactants than the products, which corresponds to the calculated ΔR_{XH} value. The same principle holds for the CN + HNCO $\rightarrow$ HNC + NCO reaction. The reactants and transition state lie 13.33 kcal mol^{-1} apart while the transition state and products lie 13.70 kcal mol^{-1} apart. The value of ΔR_{XH} for the HNC–producing reaction is 10.8% higher than that of the HCN–producing reaction, which corresponds with the observed magnitude of the energy differences. However, it still corresponds with the observed geometric parameters indicating the transition state more closely resembles the reactants than the products. For the CN + *trans*–HONO $\rightarrow$ HCN + NO_2 reaction, the energy difference between the reactants and the transition state is 10.12 kcal mol^{-1} and the energy difference between the transition state and the products is 57.11 kcal mol^{-1}. As seen with the HNCO transition states, the CN + *trans*–HONO $\rightarrow$ HCN + NO_2 transition state lies energetically closer to the reactants than the products, which corresponds with the calculated ΔR_{XH} value of 15.8%. For the CN + *trans*–HONO $\rightarrow$ HNC + NO_2 reaction, the energy difference between the reactants and transition state is 6.64 kcal mol^{-1} and the transition state is 38.65 kcal mol^{-1} higher than the products. This again corresponds with the ΔR_{XH} value of 23.6%, which indicates that the transition state more closely resembles the reactants than the products.

The Evans–Polanyi principle states that the activation energy for similar reactions is proportional to the reaction enthalpy. For the abstractions of HNCO, the HCN–producing reaction proceeds through a 6.23 kcal mol^{-1} barrier and ends in the products at -15.34 kcal mol^{-1}. For the HNC–producing reaction, it proceeds through a 13.33 kcal mol^{-1} barrier and ends in the products at -0.37 kcal mol^{-1}. The transition state barrier and reaction enthalpy of the HNC–producing reaction are both higher in energy than the HCN–producing, which follows the Evans–Polanyi principle as stated above. For the abstractions of *trans*–HONO, the HCN–producing reaction

proceeds through a 10.12 kcal mol^{-1} barrier and ends in the products at -46.99 kcal mol^{-1}. For the HNC–producing reaction, it proceeds through a barrier of 6.64 kcal mol^{-1} and ends in the products at -32.01 kcal mol^{-1}. In the case of the *trans*–HONO abstraction, the Evans–Polanyi postulate does not appear to hold as the activation energy qualitatively changes ordering between the HCN and HNC–producing reactions. It is possible this may have resulted from the large geometric differences between the two transition states. As shown in Figure 3.1, the angle of approach of the cyano radical is significantly different in the two transition states, with an angle of 137.4° for the HCN–producing reaction and 154.2° for the HNC–producing. Because of the significant geometric difference between the two transition states, this may make the two *trans*–HONO reactions dissimilar, such that the Evans–Polanyi postulate should not be expected to hold.

Kinetics

In this work, it has been observed that the HCN–producing reactions have lower barrier heights than the corresponding HNC–producing reaction in nearly every case. Because of this, it is expected the HCN–producing reactions will be faster, so rate constants for the HCN reactions are reported below. In the case of CN + *trans*–HONO, rate constants for both the HCN and HNC–producing reactions have been investigated since it was discovered the barrier height for the HNC–producing reaction is lower in energy. Table 3.5 contains the rate constants calculated in this work using the rigid–rotor harmonic oscillator approximation.

$\mathbf{CN + HNCO \rightarrow HCN + NCO}$

The features of the potential energy surface obtained for this reaction can be seen in Figure 3.4. The reaction first proceeds through a pre–reactive complex at -1.56 kcal mol^{-1}, which then leads to a transition state at approximately 6 or 8 kcal

Table 3.5: Rate constants for a selection of the studied hydrogen abstractions in cm^3 $molecule^{-1}$ s^{-1}.

T(K)	HNCO[c]	HNCO[d]	HOCN	*trans*–HONO[a]	*trans*–HONO[b]
200	4.21×10^{-19}	1.21×10^{-17}	2.61×10^{-15}	1.11×10^{-19}	8.18×10^{-18}
225	8.02×10^{-19}	1.92×10^{-17}	3.45×10^{-15}	1.76×10^{-19}	8.66×10^{-18}
250	1.67×10^{-18}	3.30×10^{-17}	4.65×10^{-15}	2.82×10^{-19}	1.03×10^{-17}
275	3.60×10^{-18}	5.84×10^{-17}	6.16×10^{-15}	4.58×10^{-19}	1.32×10^{-17}
295	6.60×10^{-18}	9.21×10^{-17}	7.67×10^{-15}	6.79×10^{-19}	1.68×10^{-17}
298	7.21×10^{-18}	9.85×10^{-17}	7.92×10^{-15}	7.20×10^{-19}	1.74×10^{-17}
300	7.65×10^{-18}	1.03×10^{-16}	8.10×10^{-15}	7.49×10^{-19}	1.79×10^{-17}
325	1.57×10^{-17}	1.78×10^{-16}	1.06×10^{-14}	1.23×10^{-18}	2.48×10^{-17}
350	3.07×10^{-17}	2.97×10^{-16}	1.36×10^{-14}	2.00×10^{-18}	3.47×10^{-17}
375	5.72×10^{-17}	4.82×10^{-16}	1.74×10^{-14}	3.23×10^{-18}	4.86×10^{-17}
400	1.02×10^{-16}	7.57×10^{-16}	2.21×10^{-14}	5.15×10^{-18}	6.76×10^{-17}
500	6.85×10^{-16}	3.46×10^{-15}	5.19×10^{-14}	2.77×10^{-17}	2.24×10^{-16}
1000	9.40×10^{-14}	2.12×10^{-13}	8.58×10^{-13}	3.60×10^{-15}	7.84×10^{-15}
1500	9.19×10^{-13}	1.58×10^{-12}	4.29×10^{-12}	3.62×10^{-14}	4.80×10^{-14}
2000	3.78×10^{-12}	5.69×10^{-12}	1.28×10^{-11}	1.51×10^{-13}	1.56×10^{-13}
3000	2.20×10^{-11}	2.89×10^{-11}	5.46×10^{-11}	8.86×10^{-13}	7.10×10^{-13}
5000	1.50×10^{-10}	1.77×10^{-10}	2.93×10^{-10}	6.06×10^{-12}	3.97×10^{-12}

[a] $CN + trans\text{–}HONO \rightarrow HCN + NO_2$
[b] $CN + trans\text{–}HONO \rightarrow HNC + NO_2$
[c] Includes DBOC for TS.
[d] Does not include DBOC for TS.

mol^{-1}, depending on it the δ_{DBOC} correction was included. The barrier height of the transition state is largely influenced by the magnitude of the δ_{DBOC} correction. The significance of this correction will be discussed later on. The geometric parameters of the transition state can be seen in Figure 3.3 and Table 3.6. After proceeding through the linear transition state, the reaction ends in the set of products, HCN + NCO at -15.34 kcal mol^{-1}. This reaction has been previously studied theoretically.[134,135]

An *ab initio* study by Zhang et al. of the $CN + HNCO \rightarrow HCN + NCO$ reaction reported results at the UMP2/6–311G** level of theory.[134] The energetics and geometric parameters they reported can be found in Table 3.6. They reported a barrier height ($\Delta H^{\ddagger}$) of 4.96 kcal mol^{-1} for the transition state and a reaction enthalpy

(ΔH_r) of -30.94 kcal mol^{-1}.[134] They did not report a pre–reactive complex in their findings. A different theoretical study by Sun et al. investigated the same reaction at the HL//B3LYP/6–311+G(2d,p) level of theory,[135] where HL refers to a higher–level energy calculation. The HL method uses a combination of QCISD(T) and MP2(FC) methods and includes the extrapolation to the CBS limit. Further explanation of this method can be found in their study. They reported a pre–reactive complex at -1.2 kcal mol^{-1}, a $\Delta H^{\ddagger}$ of 8.0 kcal mol^{-1}, and a ΔH_r of -14.7 kcal mol^{-1}.

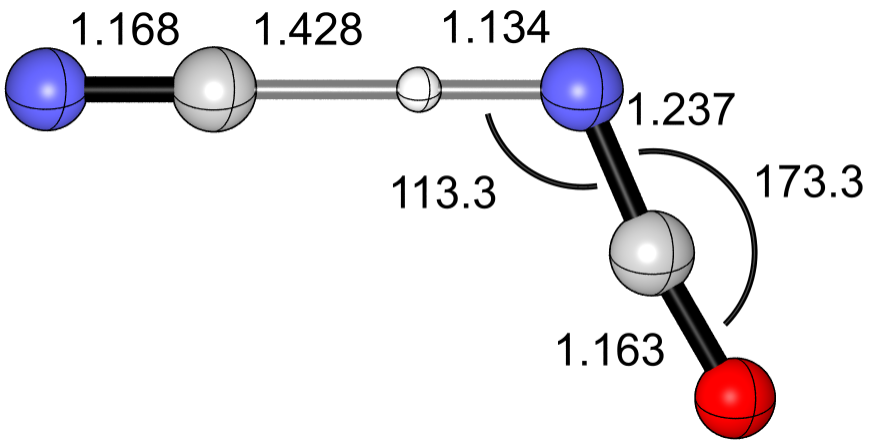

Figure 3.3: C_s symmetric CN + HNCO → HCN + NCO transition state found in this work optimized at the CCSD(T)–F12a/cc–pVTZ–F12 level of theory. Bond angles and distances given in degrees and Angstroms, respectively.

The transition states found in the studies by Zhang et al. and Sun et al. have similar C−H and N−H bond distances, differing by less than 0.1 Å, but the ∠CHN angle differs by nearly 30°. When compared to the transition state found in this study, which may be considered the highest level of theory, the angle of approach of the CN radical increases to linearity. Additionally, the R_{CH} bond length decreases and the R_{NH} bond length increases as the level of theory increases. However, there is not a similar trend between the relative barrier heights as the level of theory increases.

In this research, the diagonal Born–Oppenheimer correction for the transition state for this reaction was found to have a value of 1.62 kcal mol^{-1}, which is unusually

Table 3.6: Comparison of the CN + HNCO → HCN + NCO abstraction at various levels of theory. Enthalpies are given in kcal mol^{-1}, bond distances and angles of the transition state are given in Angstroms and degrees, respectively.

	ΔH_{prc}	$\Delta H^{\ddagger}$	ΔH_r	R_{CN}[d]	R_{NH}[d]	θ_{CNH}[d]	R_{CH}[e]	R_{NH}[e]	θ_{CHN}[e]
Zhang et al.[a]		4.96	−30.94				1.606	1.061	128.90°
Sun et al.[b]	−1.2	8.0	−14.7	2.250	1.010		1.564	1.088	156.35°
This work[c]	−1.56	6.23	−15.34	2.567	1.006	109.9°	1.428	1.134	180.0°

[a] UMP2/6–311G**.[134]
[b] HL//B3LYP/6–311+G(2d,p).[135]
[c] CCSDT(Q)/CBS//CCSD(T)–F12a/cc–pVTZ–F12. The δ_{DBOC} correction is not included for $\Delta H^{\ddagger}$.
[d] Geometric parameters of the pre–reactive complex (if available).
[e] Geometric parameters of the transition state.

large. The adiabatic DBOC is evaluated as:

$$E_{\mathrm{DBOC}} = \langle \Psi_e(\boldsymbol{r};\boldsymbol{R}) | \hat{T}_N | \Psi_e(\boldsymbol{r};\boldsymbol{R}) \rangle \tag{3.7}$$

where $\Psi_e(\boldsymbol{r};\boldsymbol{R})$ is the electronic wavefunction, $\boldsymbol{r}$ is the set of electronic coordinates, $\boldsymbol{R}$ is the set of nuclear coordinates, and $\hat{T}_N$ is the nuclear kinetic energy operator. A previous study by Allen et al. suggested that a diagonal Born–Oppenheimer correction of this magnitude may be used as a diagnostic tool of nearby conical intersections.[30] Meek and Levine recommended the diagonal Born–Oppenheimer correction be ignored in certain cases because the E_{DBOC} is non–integrable over domains including a conical intersection due to the second derivative of the $\hat{T}_n$ operator diverging.[136] For this study, the magnitude of δ_{DBOC} is taken as a signal that there may be a conical intersection nearby. Effort has been put into locating a nearby, symmetry–breaking transition state, but at this point one has not been found. The possibility of a nearby conical intersection should be the topic of future study for this reaction. Neither of the two previous studies on this reaction mentioned above drew any attention to this idea, so it does not seem they had any inclination toward this possibility.

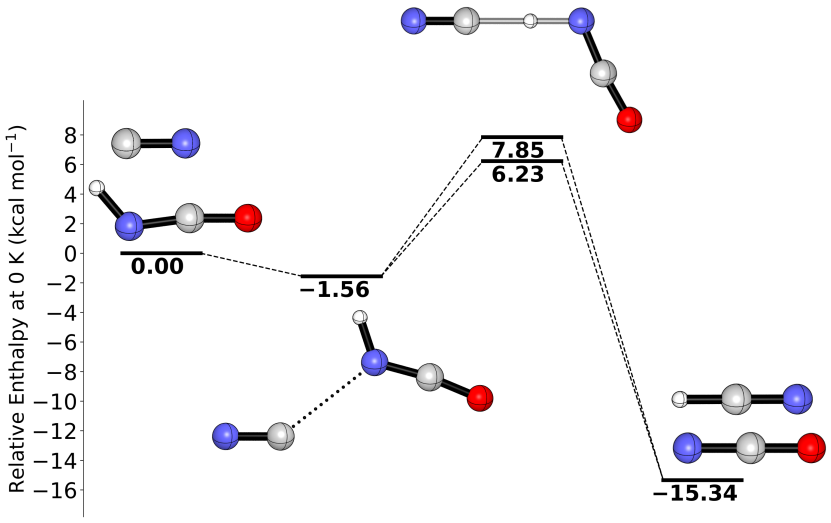

Figure 3.4: Potential energy surface of the CN + HNCO → HCN + NCO reaction at 0 K at the CCSDT(Q)/CBS//CCSD(T)–F12a/cc–pVTZ–F12 level of theory. The transition state energy is included with and without the diagonal Born–Oppenheimer correction of 1.62 kcal mol^{-1}. Internal coordinates for all structures can be found in the supporting information.

Rate constants were obtained for this reaction as outlined in the Methods section. Zhang et al. obtained rate constants using conventional transition state theory (TST) for the temperature range $1000 - 2100$ K.[134] Additionally, Sun et al. obtained rate constants for this reaction using TST with the Eckart method to account for tunneling effects in the temperature range $200 - 2500$ K.[135] They reported rate constants with and without tunneling effects included, and they concluded that tunneling is quite significant for this hydrogen abstraction and thus should be included. Their study used HL//CCSD/6–31+G(d,p) energies for obtaining the rate constants. Their HL//B3LYP/6–311+G(2d,p) transition state had an imaginary frequency of $382i$, which they considered to be too small and were concerned it would lead to incorrect tunneling results. They attempted to reoptimize the transition state to obtain a more reasonable imaginary frequency. Using CCSD/6–31+G(d,p) they obtained an imaginary frequency of $1908i$, which they considered more reasonable so proceeded with calculating their rate constants with this transition state. They did not include

any geometric parameters for this newly optimized transition state, but they reported it had a HL//CCSD/6–31+G(d,p) barrier height of 8.7 kcal mol^{-1}.

A comparison between the rate constants obtained in this work and the previously reported theoretical rate constants can be found in Figure 3.5. Rate constants were reported for the transition state barrier obtained in this work with and without the DBOC for the transition state, . The rate constants reported by Zhang et al. and Sun et al. are both higher than both sets of rate constants obtained in this work in their respective temperature ranges. The transition state barrier reported by Zhang et al. of 4.96 kcal mol^{-1} is much lower than the barriers of 6.23 and 7.85 kcal mol^{-1} (with and without δ_{DBOC}) found in this work, which may explain why their rate constants are faster than those reported here. The barrier reported by Sun et al. of 8.7 kcal mol^{-1} is $1-2$ kcal mol^{-1} higher than the barriers found in this work. However, at room temperature they determined the rate constants for this reaction are faster than those found in this work. A comprehensive chemical kinetic data base was published with data for reactions involving CN, NCO, and HNCO.[137] A rate law for the $\mathrm{CN} + \mathrm{HNCO} \rightarrow \mathrm{HCN} + \mathrm{NCO}$ reaction was reported to be $2 \times 10^{-11} exp(-4456/T)$ with an uncertainty of a factor of 10 at 2500 K and larger at lower temperatures.[137] This rate law was derived on the basis of their estimated rate expression for the reverse reaction. At 2500 K, Tsang's rate law gives a rate constant of 3.36×10^{-12} with an uncertainty of a factor of 10. In this work, the rate for this reaction with δ_{DBOC} included at 2500 K is 1.03×10^{-11}, and without the δ_{DBOC} correction the rate at 2500 K is 1.43×10^{-11}. However, given the amount of uncertainty in the rate law reported, it is difficult to draw any conclusions between this study and the reported expression. The rate constants for this reaction obtained in this work have an uncertainty directly related to the uncertainty of the barrier height, which was determined to be 0.16 kcal mol^{-1}. However, the magnitude of the δ_{DBOC} correction plays a large role in the magnitude of the barrier height as well, which influences the magnitude of the rate

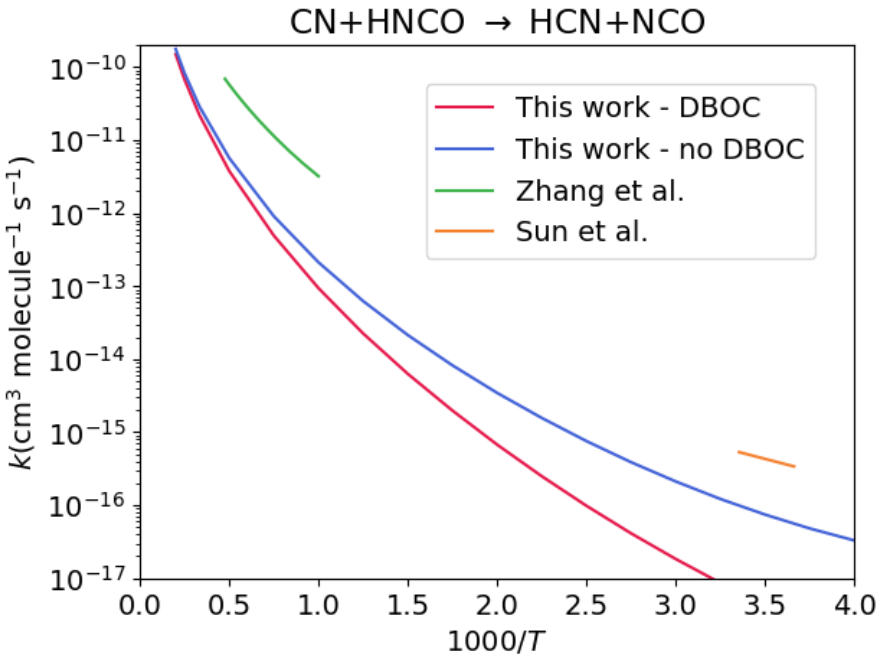

Figure 3.5: Comparison between CN + HNCO → HCN + NCO rate constants obtained in this work and previously reported theoretical rate constants.[134,135]

---

constants. Further investigation of the potential for a conical intersection or some other factor affecting the δ_{DBOC} for this reaction should be conducted to determine how this impacts the rate constants.

CN + HNCO → HNC + NCO

Sun et al. also investigated the CN + HNCO → HNC + NCO reaction at the HL//B3LYP/6–311+G(2d,p) level of theory.[135] The energetics and geometric parameters of their results can be seen in Table 3.7. The reaction mechanism they reported first proceeded to a pre–reactive complex at −2.5 kcal mol^{-1} relative to the reactants, and then proceeded through a transition state barrier of 14.3 kcal mol^{-1}, and ended in the products HNC and NCO at 0.1 kcal mol^{-1}. The potential energy surface features found in this study are qualitatively similar to those found by Sun et al., and they can be seen in Figure 3.7. The reaction first proceeds to a pre–reactive complex

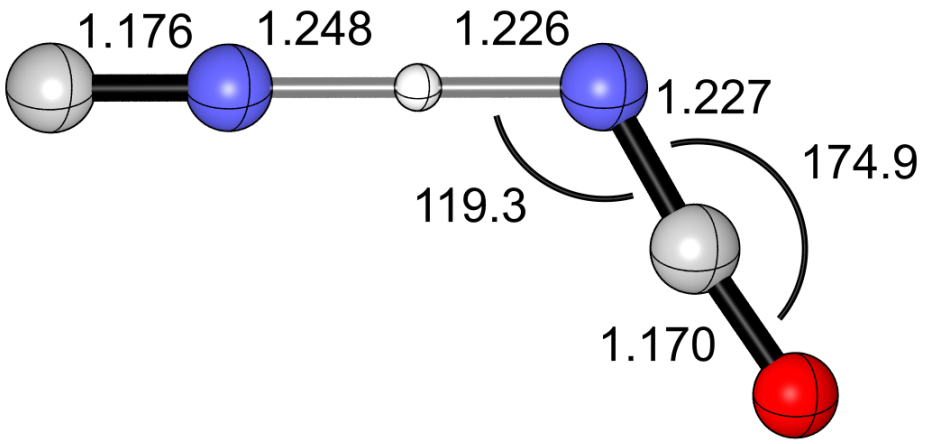

Figure 3.6: C_s symmetric CN + HNCO → HNC + NCO transition state found in this work optimized at the CCSD(T)–F12a/cc–pVTZ–F12 level of theory. Bond angles and distances given in degrees and Angstroms, respectively.

---

at −1.89 kcal mol^{-1} relative to the reactants, which is followed by a transition state barrier of 13.33 kcal mol^{-1}, and the reaction terminates in the products HNC and NCO at −0.37 kcal mol^{-1}.

Table 3.7: Comparison of the CN + HNCO → HNC + NCO abstraction at various levels of theory. Enthalpies are given in kcal mol^{-1}, bond distances and angles are given in Angstroms and degrees, respectively.

	ΔH_{prc}	$\Delta H^{\ddagger}$	ΔH_r	R_{N_1H}[c]	R_{N_2H}[c]	θ_{CHN}[c]	R_{N_1H}[d]	R_{N_2H}[d]	θ_{CHN}[d]
Sun et al.[a]	−2.5	14.3	0.1	2.053	1.016	≤ 180.00°	1.295	1.199	≤ 180.00°
This work[b]	−1.89	13.33	−0.37	2.178	1.009	180.0°	1.248	1.226	180.0°

[a] HL//B3LYP/6–311+G(2d,p).[135]
[b] CCSDT(Q)/CBS//CCSD(T)–F12a/cc–pVTZ–F12.
[c] Geometric parameters of the pre–reactive complex.
[d] Geometric parameters of the transition state.

It was found in this study and the study by Sun et al. that the pre–reactive complex is lower in energy than the resulting set of products. This suggests it is not very favorable for the reaction to proceed past the pre–reactive complex. Qualitatively, the two pre–reactive complexes found line up well. The geometric parameters and energetics have good agreement. Figure 3.6 depicts the transition state found in this

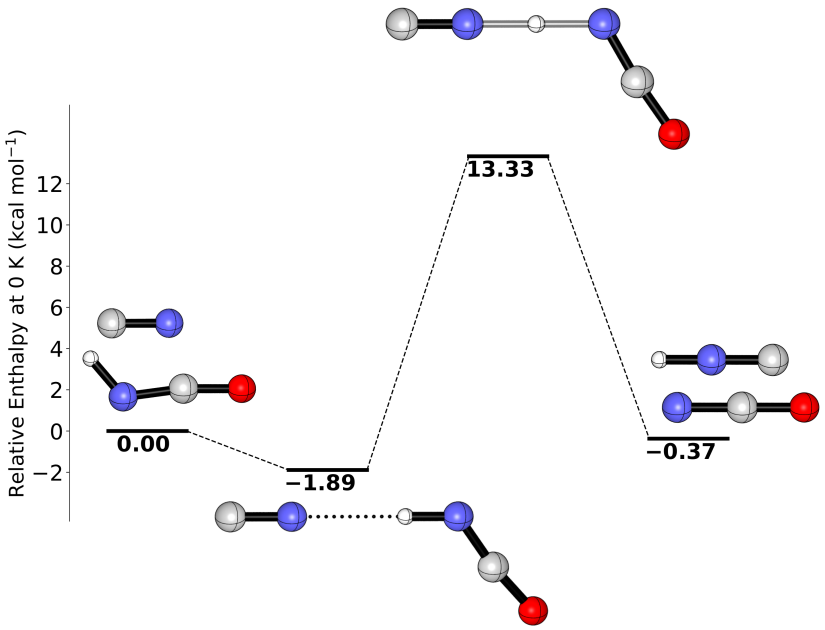

Figure 3.7: Potential energy surface of the CN + HNCO → HNC + NCO reaction at 0 K at the CCSDT(Q)/CBS//CCSD(T)–F12a/cc–pVTZ–F12 level of theory. Internal coordinates for all structures can be found in the supporting information.

---

work. It is similar geometrically to the one found by Sun et al. The reaction enthalpy (ΔH_r) found by Sun et al. was slightly endothermic, while the reaction enthalpy found in this work is slightly exothermic. The two reaction enthalpies are within 0.5 kcal mol^{-1} of each other, but there is a qualitative energetic difference between the two results. This may simply be a result of the levels of theory used by Sun et al. and in this work. The uncertainty in the energetics of the HNC–producing reactions found in this study is expected to be within 0.22 kcal mol^{-1}. Within the amount of uncertainty obtained in this work, the reaction enthalpy still remains slightly exothermic. Additionally, the values from the ATcT suggest that this reaction should result in a set of slightly exothermic products, as can be seen in Table 3.2. Therefore, it may be safely concluded the reaction enthalpy for this reaction should be slightly exothermic rather than slightly endothermic as suggested by Sun et al.

$CN + HOCN \rightarrow HCN + NCO$

To date there have been no other studies of the hydrogen abstraction of HOCN by CN. Since HOCN is present in some of the same environments as CN, though in lower abundance than HNCO, it seemed useful to study this reaction. Therefore, this will simply serve as a report of the findings of this study. This reaction first proceeds from the reactants through a transition state barrier of 4.22 kcal mol^{-1} and ends in the products HCN and NCO at -39.95 kcal mol^{-1} relative to the reactants. The features of the potential energy surface obtained for this reaction can be seen in Figure 3.8.

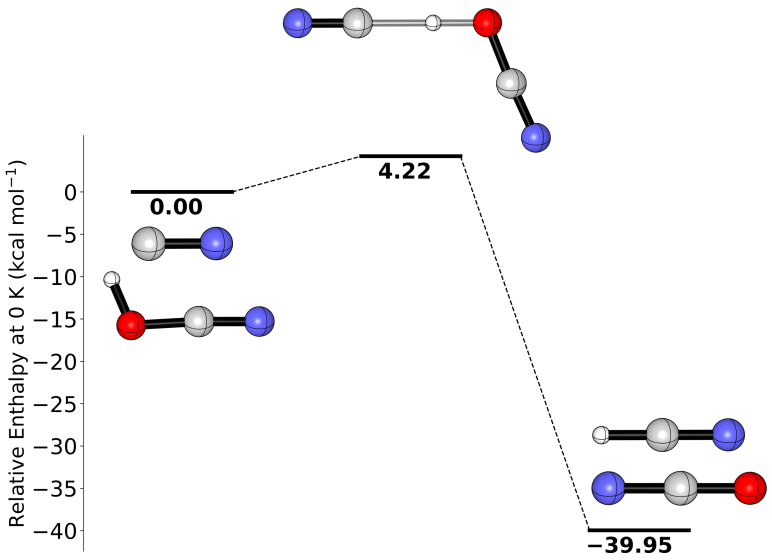

Figure 3.8: Potential energy surface of the $CN + HOCN \rightarrow HCN + NCO$ reaction at 0 K at the CCSDT(Q)/CBS//CCSD(T)–F12a/cc–pVTZ–F12 level of theory. Internal coordinates for all structures can be found in the supporting information.

As mentioned previously, the HCN–producing reaction energetics reported here are expected to be accurate within 0.16 kcal mol^{-1}. The rate constants computed for this reaction can be found in Table 3.5. Expectedly, because of the relatively low barrier height, the rates are quite fast, especially when compared to $CN + HNCO \rightarrow HCN +$

NCO. The computed rate constants and low barrier height suggest this reaction may be favorable in the moderate to high temperature range. Thus far, no transition state for the CN + HOCN → HNC + NCO has been located.

CN + *trans*–HONO

Initially, both the *cis* and *trans* isomers of HONO were investigated. The energy breakdown of the isomerization transition state and the *cis* isomer relative to the *trans* isomer found in this study can be seen in Table 3.8. It was determined that *trans*–HONO is lower in energy than the *cis* isomer by 0.43 kcal mol^{-1}. As shown in Figure 3.9, the transition state barrier for the isomerization of *trans*–HONO to *cis*–HONO was determined to be 10.49 kcal mol^{-1}. A previous study on the CN + HONO reaction utilizing the CCSD(T)/aug–cc–pVTZ//UMP2/6–311++G(d,p) level of theory found that the *trans* isomer is 0.45 kcal mol^{-1} lower in energy than the *cis* isomer, and they found the isomerization barrier to be 9.46 kcal mol^{-1}, which are both in good agreement with our findings.[138] Because the barrier height for isomerization is quite large, only hydrogen abstraction of the *trans* isomer has been studied at this time.

Table 3.8: Enthalpies at 0 K in kcal mol^{-1} for the *cis*–HONO isomer and the *trans*–HONO → *cis*–HONO isomerization transition state relative to *trans*–HONO at the CCSDT(Q)/CBS//CCSD(T)–F12a/cc–pVTZ–F12 level of theory.

Structure	CBS[a]	$\delta_{\mathrm{T(Q)}}$	δ_{CORE}	δ_{REL}	δ_{DBOC}	δ_{ZPVE}	Total
TS	11.65	0.10	0.05	−0.03	0.01	−1.30	10.49
cis–HONO	0.31	0.11	0.01	0.00	0.00	0.01	0.43

[a] CBS denotes the CCSD(T)/CBS relative energy.

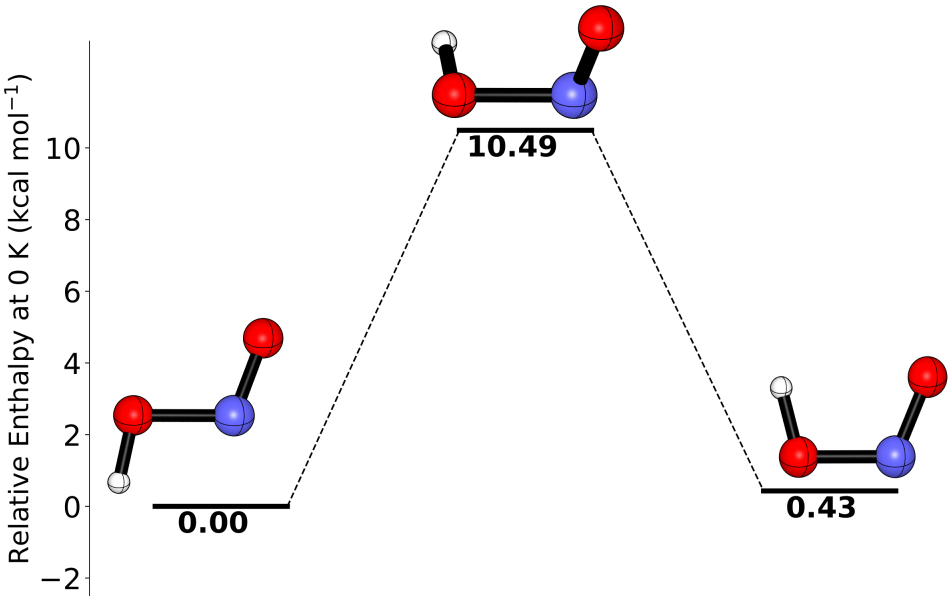

Figure 3.9: Potential energy surface of the HONO isomerization at 0 K at the CCSDT(Q)/CBS//CCSD(T)–F12a/cc–pVTZ–F12 level of theory. Internal coordinates for all structures can be found in the supporting information.

CN + HONO → HCN + NO_2

The studied features of the potential energy surface for this reaction can be found in Figure 3.10. The energetics and geometric parameters of these stationary points are shown in Table 3.9. The reaction first proceeds through a transition state barrier of 10.12 kcal mol^{-1}, then is followed by a post–reactive complex at −48.07 kcal mol^{-1}, which then leads to the products HCN and NO_2 at −46.99 kcal mol^{-1}.

Wang et al. investigated the CN + *trans*–HONO → HCN + NO_2 reaction at the CCSD(T)/aug–cc–pVTZ//UMP2/6–311++G(d,p) level of theory.[138] They found that the transition state has an activation energy of 8.80 kcal mol^{-1}. The reaction then proceeded to a post–reactive complex at −49.87 kcal mol^{-1} relative to the reactants followed by the products HCN and NO_2 at −55.63 kcal mol^{-1}. The post–reactive complex was determined to be higher in energy than the products, which is interesting, but the authors made no comment on this finding.[138] The post–reactive complex

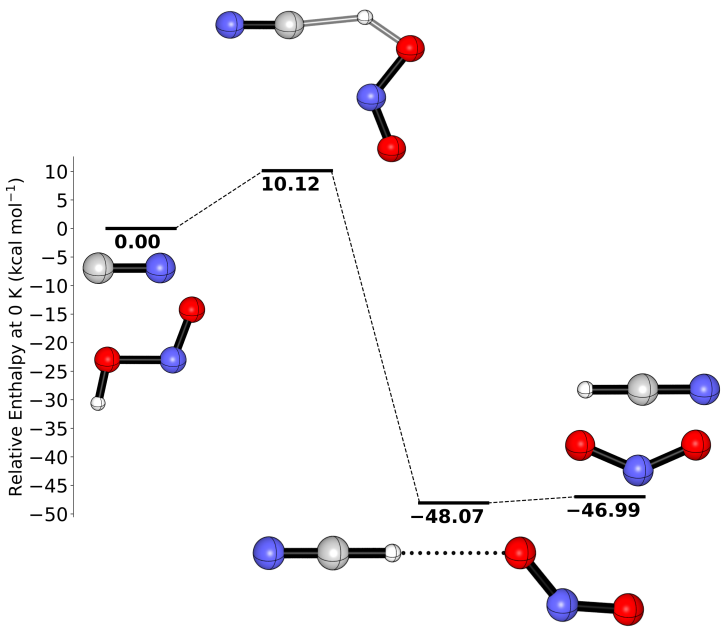

Figure 3.10: Potential energy surface of the CN + *trans*–HONO → HCN + NO_2 reaction at 0 K at the CCSDT(Q)/CBS//CCSD(T)–F12a/cc–pVTZ–F12 level of theory. Internal coordinates for all structures can be found in the supporting information.

---

found in this study has a relative energy 1.08 kcal mol^{-1} below the products. When comparing the relative energies in this study to Wang et al.'s, there is a difference of 1.32, 1.80, and 8.64 kcal mol^{-1} between the two transition states, post–reactive complexes, and products, respectively. The difference between the two sets of products is quite significant. This suggests that Wang et al.'s post–reactive complex being higher in energy than their products may be a result of the relative energy of their products rather than the relative energy of the post–reactive complex itself. Alternatively, it is possible that due to the level of theory utilized by Wang et al. for the optimization of their post–reactive complex geometry, there may have been some impact on the resulting energetics they reported. Either way, due to the level of theory utilized in this study and the various additive energy corrections included in the relative energy, it is expected that the result found in this study is correct.

Table 3.9: Energetic and geometric parameters found in this study and a previous study of the CN + HONO → HCN + NO_2 reaction. All bond distances are reported in Angstroms and bond angles in degrees.

	$\Delta H^{\ddagger}$	ΔH_{post}	ΔH_r	R_{CH}[a]	R_{OH}[a]	∠CHO[a]	R_{CH}[b]	R_{OH}[b]	∠CHO[b]
Wang et al.[c]	8.80	−49.87	−55.63	1.511	1.270	142.9°	1.069	2.372	178.7°
This work[d]	10.12	−48.07	−46.99	1.517	1.119	137.4°	1.069	2.312	180.0°

[a] Geometric parameters of the transition state.
[b] Geometric parameters of the post–reactive complex.
[c] CCSD(T)/aug–cc–pVTZ//UMP2/6–311++G(d,p).[138]
[d] CCSDT(Q)/CBS//CCSD(T)–F12a/cc–pVTZ–F12.

CN + HONO → HNC + NO_2

Wang et al. also investigated the CN + *trans*–HONO → HNC + NO_2 reaction at the CCSD(T)/aug–cc–pVTZ//UMP2/6–311++G(d,p) level of theory.[138] The energetics and geometric parameters for this reaction as studied by Wang et al. may be found in Table 3.10. They found the reaction first proceeded to a pre–reactive complex at −0.29 kcal mol^{-1} relative to the reactants followed by a transition state with a barrier of 4.87 kcal mol^{-1}. This was followed by a post–reactive complex at −36.01 kcal mol^{-1}, and ended in the products HNC and NO_2 at −35.03 kcal mol^{-1}. A previous study of hydrogen abstractions by the cyano radical observed the expected trend that the abstraction by the carbon is accompanied by a lower transition state barrier than the corresponding nitrogen abstraction.[41] This expectation is opposed by Wang et al.'s results as their carbon terminal abstraction barrier height was 8.80 kcal mol^{-1} and their nitrogen terminal abstraction barrier height was 4.87 kcal mol^{-1}.[138]

The results from this study indicate the same unexpected trend. As shown in Figure 3.11, the reaction first proceeds through a pre–reactive complex at −1.72 kcal mol^{-1} relative to the reactants, which is followed by a transition state at 6.64 kcal mol^{-1}, which leads to a post–reactive complex at −33.75 kcal mol^{-1} and ends in the products HNC and NO_2 at −32.45 kcal mol^{-1}. The transition state barrier of

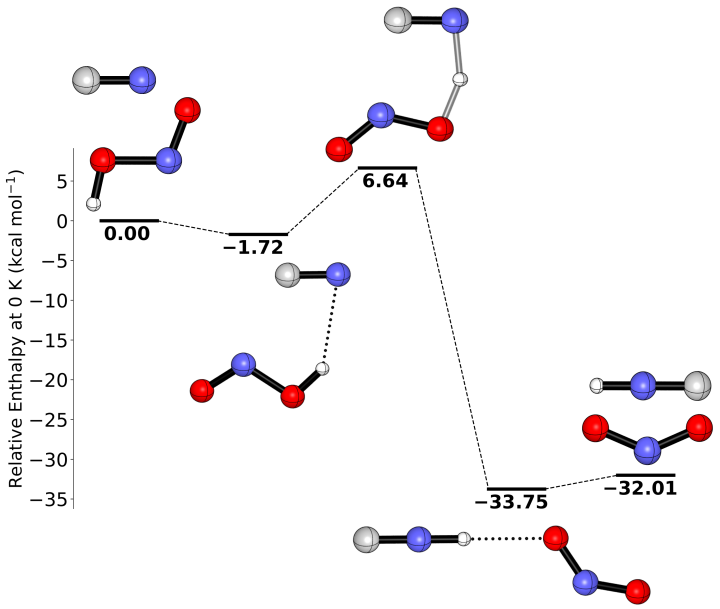

Figure 3.11: Potential energy surface of the CN + *trans*–HONO → HNC + NO_2 reaction at 0 K at the CCSDT(Q)/CBS//CCSD(T)–F12a/cc–pVTZ–F12 level of theory. Internal coordinates for all structures can be found in the supporting information.

6.64 kcal mol^{-1} is 3.48 kcal mol^{-1} lower in energy than the corresponding transition state for the hydrogen abstraction by the carbon found in this study. There is good qualitative agreement between the relative energies found by Wang et al. and those found in this study. Additionally, the geometric parameters of the stationary points match well with the largest differences in the pre–reactive complex where the bond distances differ at a maximum of 0.11 Å and the bond angle for the approach of the cyano radical differs by 16°. The lower barrier height of 6.64 kcal mol^{-1} found for this reaction mechanism, as opposed to the 10.12 kcal mol^{-1} barrier found for the HCN–producing reaction, may be a result of some interaction taking place between the C atom of the CN radical and the N atom of the *trans*–HONO molecule. This finding indicates that as the hydrogen donor size increases for this reaction type, the hydrogen abstraction transition state may become more complicated. Investigating this interaction should be the topic of a future study.

Rate constants were obtained in this study via TST for both this reaction and

Table 3.10: Energetic and geometric parameters found in this study and a previous study of the $CN + HONO \rightarrow HNC + NO_2$ reaction. All bond distances are reported in Angstroms and bond angles in degrees.

	ΔH_{pre}	$\Delta H^{\ddagger}$	R_{NH}[a]	R_{OH}[a]	∠CHO[a]	R_{NH}[b]	R_{OH}[b]	∠CHO[b]
Wang et al.[d]	−0.29	4.87	2.204	0.978	127.0°		1.216	
This work[e]	−1.72	6.64	2.314	0.973	143.4°	1.330	1.194	154.2°
	ΔH_{post}	ΔH_r	R_{NH}[c]	R_{OH}[c]	∠CHO[c]			
Wang et al.[d]	−36.01	−35.03	1.003	2.125	179.9°			
This work[e]	−33.75	−32.45	1.001	2.065	180.0°			

[a] Geometric parameters of the pre–reactive complex.
[b] Geometric parameters of the transition state (if available).
[c] Geometric parameters of the post–reactive complex.
[d] CCSD(T)/aug–cc–pVTZ//UMP2/6–311++G(d,p).[138]
[e] CCSDT(Q)/CBS//CCSD(T)–F12a/cc–pVTZ–F12.

the HCN–producing abstraction of *trans*–HONO, which may be seen in Table 3.5. Due to the difference in energy barriers found for the two reactions, it is expected that the rate constants for $CN + trans\text{–}HONO \rightarrow HNC + NO_2$ are faster than for the HCN–producing reaction. This is in agreement with the computed rate constants. The barrier heights for these two reactions are expected to have an uncertainty of 0.15 and 0.22 kcal mol^{-1}, respectively. This amount of uncertainty in the barrier height should only lead to a small uncertainty in the rate constants, suggesting that the rate constants obtained with these barrier heights are expected to be reliable.

Conclusions

The energetics of the cyano radical hydrogen abstractions of HNCO, HOCN, and *trans*–HONO with both the carbon and nitrogen terminals have been obtained using highly accurate *ab initio* methods. The methods used were developed in a previous study,[41] and they were proven to be a good precedent for studying hydrogen abstractions by the cyano radical. There was good qualitative agreement of the potential energy surface features with previous studies of the reactions investigated above. Re-

liable results for a previously unstudied reaction, $CN + HOCN \rightarrow HCN + NCO$, have been reported. The unexpected trend predicted by a previous study concerning the barrier height energy ordering of the HCN and HNC–producing CN + *trans*–HONO reactions was observed and discussed. For the $CN + HNCO \rightarrow HCN + NCO$ reaction, the rate constants obtained in this work did not agree particularly well with previously reported rate constants, which was likely due to the difference in the calculated barrier heights. Additionally, the possible presence of a conical intersection may further complicate these results, and should be considered in future studies. The rate constants obtained in this study may be useful to guide any future experimental or theoretical study of these reactions.

Chapter 4

Concluding Remarks

In this dissertation, high-level energetics and kinetics were obtained for an array of small molecule reactions. This was accomplished primarily utilizing *ab initio* methods such as coupled cluster and via additive energy corrections. Both of these improved the accuracy of the approximations that must be made in order to obtain useful energetics and rate constants.

In Chapter 2, various hydrogen abstractions by the cyano radical were studied. It was determined that the methods described provided excellent agreement with data obtained from the ATcT database. The rate constants obtained for the $CN + H_2 \rightarrow HCN + H$ reaction had excellent agreement with previous experimental and theoretical results, and the rate constants obtained for the $CN + CH_4 \rightarrow HCN + CH_3$ reaction had good agreement with previous experimental and theoretical results. The observed agreement helped confirm that the methodology chosen to study these reactions was appropriate and useful for modeling hydrogen abstractions by the cyano radical.

This finding led to Chapter 3, which was a study of various hydrogen abstractions by the cyano radical with mid–sized hydrogen donors, such as $HNCO, HOCN,$ and *trans*–HONO. As noted, the abstractions of these larger donor molecules became more complex to study. Additionally, there were not as many previous studies available to compare with these findings. The choice of methods utilized in this study was supported by the excellent agreement found in the previous study and by the excellent agreement found in this study when compared to values from the Active Thermochemical Tables. For a few of the studied reactions, there were previous the-

oretical results present, with which our results had good agreement. There were a few cases where the results differed qualitatively. In these cases, it was expected the results obtained in this study were more accurate due to the choice of methods. At this point, there have been no experimental results published for the reactions investigated in this chapter. Because of this, it was difficult to definitively say how well these results would reproduce experiment. However, there is confidence in the methods utilized here, and these results may guide future studies of these reactions.

The work accomplished in this dissertation may serve to further promote high–level energetic studies of small molecule reactions, particularly hydrogen abstractions. Understanding these reactions is of importance in numerous environments, such as combustion and atmospheric chemistry. Utilizing high–level theoretical results in conjunction with experimental results allows the creation of a useful computational methodology for reproducing experimental results and predicting results for reactions which have no available experimental data. The methodology developed in this dissertation has been proven to provide excellent agreement in the prototypical $CN + H_2 \rightarrow HCN + H$ reaction. This precedent led to the application of this methodology to more complex hydrogen abstractions in an effort to understand their energetics and kinetics. Obtaining highly accurate results for these reactions should be continued in order to better understand the role these reactions play in the world around us.

Chapter A

Energetics and Kinetics of Various Cyano Radical Hydrogen Abstractions: Supporting Information

Reactants

CN ($^2\Sigma^+$)

Level of Theory:

Reference: ROHF

Geometry: CCSD(T)-F12a/aug-cc-pVTZ

Frequencies: CCSD(T)-F12a/aug-cc-pVTZ

Program: Molpro 2010.1

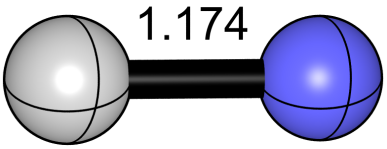

Figure A.1: CN

Wavefunction Diagnostics:

T_1: 0.044

D_1: 0.150

Cartesian Coordinates (Å):

C	0.0000000000	0.0000000000	-0.6319747809
N	0.0000000000	0.0000000000	0.5419298688

Rotational Constants (GHz): 56.7159810, 56.7159810

Harmonic Vibrational Frequencies (cm^{-1}):

a_1: 2071

H_2

Level of Theory:

Reference: ROHF

Geometry: CCSD(T)-F12a/aug-cc-pVTZ

Frequencies: CCSD(T)-F12a/aug-cc-pVTZ

Program: Molpro 2010.1

Figure A.2: H_2

Wavefunction Diagnostics:

T_1: 0.005

D_1: 0.008

Cartesian Coordinates (Å):

H	0.0000000000	0.0000000000	-0.3709824635
H	0.0000000000	0.0000000000	0.3709824635

Rotational Constants (GHz): 1821.5695094, 1821.5695094

Harmonic Vibrational Frequencies (cm^{-1}):

σ_g^+: 4401

CH_4

Level of Theory:

Reference:	ROHF
Geometry:	CCSD(T)-F12a/aug-cc-pVTZ
Frequencies:	CCSD(T)-F12a/aug-cc-pVTZ
Program:	Molpro 2010.1

Wavefunction Diagnostics:

T_1: 0.008

D_1: 0.014

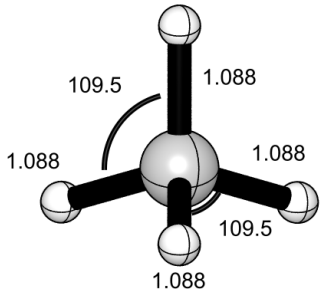

Figure A.3: CH_4

Cartesian Coordinates (Å):

C	-0.0000000000	-0.0000000000	0.0000002049
H	-0.0002218767	0.0000000000	1.0878996099
H	0.5681112097	0.8540231244	-0.3625181658
H	0.4556610391	-0.9189462619	-0.3625411001
H	-1.0235503716	0.0649231378	-0.3628427853

Rotational Constants (GHz): 158.8678663, 158.8678664, 158.8680262

Harmonic Vibrational Frequencies (cm^{-1}):

a_1:		3034
e:		1570
t_2:	3156	1346

NH_3

Level of Theory:

Reference:	ROHF
Geometry:	CCSD(T)-F12a/aug-cc-pVTZ
Frequencies:	CCSD(T)-F12a/aug-cc-pVTZ
Program:	Molpro 2010.1

Wavefunction Diagnostics:

T_1: 0.008

D_1: 0.017

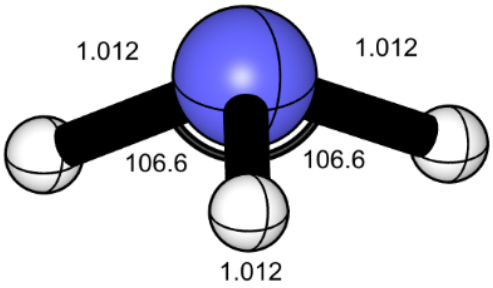

Figure A.4: NH_3

Cartesian Coordinates (Å):

N	-0.0000004029	-0.0679223550	-0.0000000000
H	0.9373304824	0.3146230410	0.0000390111
H	-0.4686962260	0.3146253261	0.8117335062
H	-0.4686286573	0.3146253262	-0.8117725167

Rotational Constants (GHz): 298.5712125, 190.2256925, 298.5726454

Harmonic Vibrational Frequencies (cm^{-1}):

a_1:	3478	1056
e:	3609	1674

H_2O

Level of Theory:

Reference:	ROHF
Geometry:	CCSD(T)-F12a/aug-cc-pVTZ
Frequencies:	CCSD(T)-F12a/aug-cc-pVTZ
Program:	Molpro 2010.1

Wavefunction Diagnostics:

T_1: 0.009

D_1: 0.020

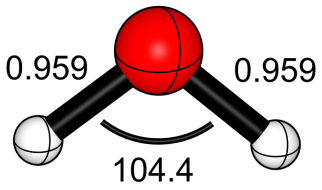

Figure A.5: H_2O

Cartesian Coordinates (Å):

O	0.0000000000	-0.0657136648	0.0000000012
H	0.0000000000	0.5215485163	0.7576575163
H	0.0000000000	0.5215485019	-0.7576575348

Rotational Constants (GHz): $284.7781691, 436.7235659, 818.5133614$

Harmonic Vibrational Frequencies (cm^{-1}):

a_1:	3834	1648
b_2:		3944

HF

Level of Theory:

Reference: ROHF

Geometry: CCSD(T)-F12a/aug-cc-pVTZ

Frequencies: CCSD(T)-F12a/aug-cc-pVTZ

Program: Molpro 2010.1

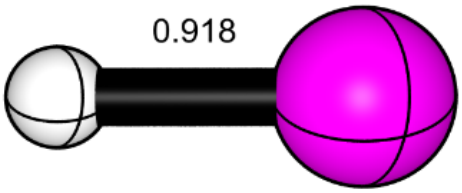

Figure A.6: HF

Wavefunction Diagnostics:

T_1: 0.009

D_1: 0.017

Cartesian Coordinates (Å):

H	0.0000000000	0.0000000000	-0.8713491845
F	0.0000000000	0.0000000000	0.0462285013

Rotational Constants (GHz): 627.1153524, 627.1153524

Harmonic Vibrational Frequencies (cm^{-1}):

σ^+: 4143

HCl

Level of Theory:

Reference: ROHF

Geometry: CCSD(T)-F12a/aug-cc-pVTZ

Frequencies: CCSD(T)-F12a/aug-cc-pVTZ

Program: Molpro 2010.1

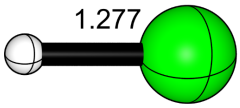

Figure A.7: HCl

Wavefunction Diagnostics:

T_1: 0.005

D_1: 0.013

Cartesian Coordinates (Å):

H	0.0000000000	0.0000000000	-1.2414626581
Cl	0.0000000000	0.0000000000	0.0352951759

Rotational Constants (GHz): 316.3299504, 316.3299504

Harmonic Vibrational Frequencies (cm^{-1}):

σ^+: 2994

C_2H_2

Level of Theory:

Reference:	ROHF
Geometry:	CCSD(T)-F12a/aug-cc-pVTZ
Frequencies:	CCSD(T)-F12a/aug-cc-pVTZ
Program:	Molpro 2010.1

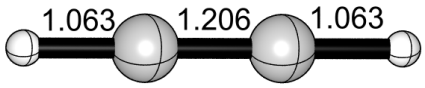

Figure A.8: C_2H_2

Wavefunction Diagnostics:

T_1: 0.012

D_1: 0.030

Cartesian Coordinates (Å):

C	0.0000000000	0.0000000000	-0.6029509599
C	0.0000000000	0.0000000000	0.6029509598
H	0.0000000000	0.0000000000	-1.6662535492
H	0.0000000000	0.0000000000	1.6662535502

Rotational Constants (GHz): 35.2669901, 35.2669901

Harmonic Vibrational Frequencies (cm^{-1}):

σ_g^+:	3503	3409	2008
σ_u^+:		753	615
π_u:			615

SiH_4

Level of Theory:

Reference:	ROHF
Geometry:	CCSD(T)-F12a/aug-cc-pVTZ
Frequencies:	CCSD(T)-F12a/aug-cc-pVTZ
Program:	Molpro 2010.1

Wavefunction Diagnostics:

T_1: 0.009

D_1: 0.019

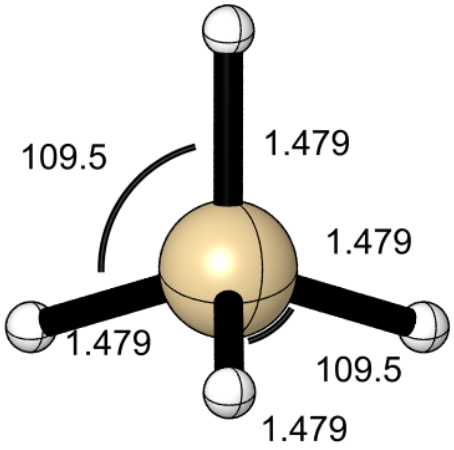

Figure A.9: SiH_4

Cartesian Coordinates (Å):

Si	-0.0000009937	0.0000000027	0.0000000012
H	-1.4791576341	0.0023349088	-0.0000000000
H	0.4908623041	-1.3941102821	0.0584932404
H	0.4940815371	0.6452310537	-1.2359090023
H	0.4942414807	0.7465442442	1.1774157281

Rotational Constants (GHz): 85.9382004, 85.9375520, 85.9375533

Harmonic Vibrational Frequencies (cm^{-1}):

a_1:		2260
e:		982
t_2:	2264	930

PH_3

Level of Theory:

Reference:	ROHF
Geometry:	CCSD(T)-F12a/aug-cc-pVTZ
Frequencies:	CCSD(T)-F12a/aug-cc-pVTZ
Program:	Molpro 2010.1

Wavefunction Diagnostics:

T_1: 0.010

D_1: 0.024

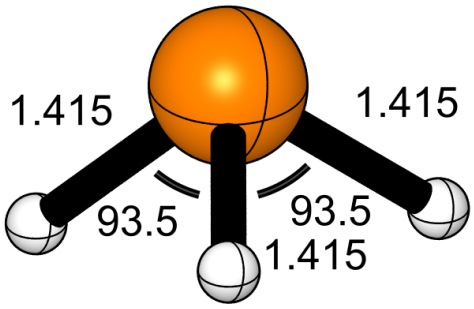

Figure A.10: PH_3

Cartesian Coordinates (Å):

P	0.0000000411	-0.0680918703	-0.0000000155
H	1.1823453802	0.6974829675	-0.1383938055
H	-0.4713206072	0.6974820049	1.0931384206
H	-0.7110260354	0.6974822462	-0.9547441401

Rotational Constants (GHz): 134.5108534, 117.9403831, 134.5108205

Harmonic Vibrational Frequencies (cm^{-1}):

a_1: 2420 1013

e: 2428 1143

H_2S

Level of Theory:

Reference: ROHF

Geometry: CCSD(T)-F12a/aug-cc-pVTZ

Frequencies: CCSD(T)-F12a/aug-cc-pVTZ

Program: Molpro 2010.1

Wavefunction Diagnostics:

T_1: 0.008

D_1: 0.019

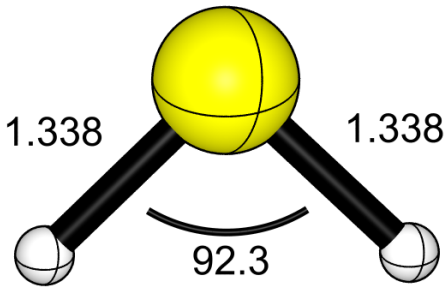

Figure A.11: H_2S

Cartesian Coordinates (Å):

S	0.0000000000	-0.0548731756	-0.0000000001
H	0.0000000000	0.8726878618	0.9652217398
H	0.0000000000	0.8726878649	-0.9652217365

Rotational Constants (GHz): 143.9868205, 269.0904726, 309.7070385

Harmonic Vibrational Frequencies (cm^{-1}):

a_1: 2721 1213

b_2: 2737

HCN

Level of Theory:

Reference: ROHF

Geometry: CCSD(T)-F12a/aug-cc-pVTZ

Frequencies: CCSD(T)-F12a/aug-cc-pVTZ

Program: Molpro 2010.1

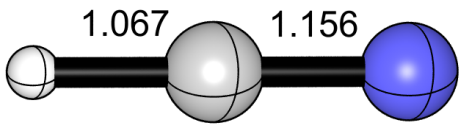

Figure A.12: HCN

Wavefunction Diagnostics:

T_1: 0.013

D_1: 0.030

Cartesian Coordinates (Å):

C	0.0000000000	0.0000000000	0.5591863743
H	0.0000000000	0.0000000000	1.6259526769
N	0.0000000000	0.0000000000	-0.5965181151

Rotational Constants (GHz): 44.3140612, 44.3140612

Harmonic Vibrational Frequencies (cm^{-1}):

σ^+: 3437 2125

π: 729

HNC

Level of Theory:

Reference:	ROHF
Geometry:	CCSD(T)-F12a/aug-cc-pVTZ
Frequencies:	CCSD(T)-F12a/aug-cc-pVTZ
Program:	Molpro 2010.1

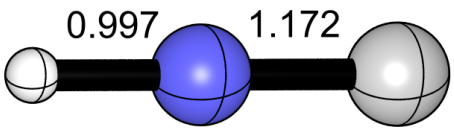

Figure A.13: HNC

Wavefunction Diagnostics:

T_1: 0.014

D_1: 0.034

Cartesian Coordinates (Å):

N	0.0000000000	0.0000000000	0.4834305016
H	0.0000000000	0.0000000000	1.4800462604
C	0.0000000000	0.0000000000	-0.6879580247

Rotational Constants (GHz): 45.2604925, 45.2604925

Harmonic Vibrational Frequencies (cm^{-1}):

σ^+:	3813	2053
π:		465

Products

CH_3 ($^2A_2''$)

Level of Theory:

Reference:	ROHF
Geometry:	CCSD(T)-F12a/aug-cc-pVTZ
Frequencies:	CCSD(T)-F12a/aug-cc-pVTZ
Program:	Molpro 2010.1

Wavefunction Diagnostics:

T_1: 0.006

D_1: 0.011

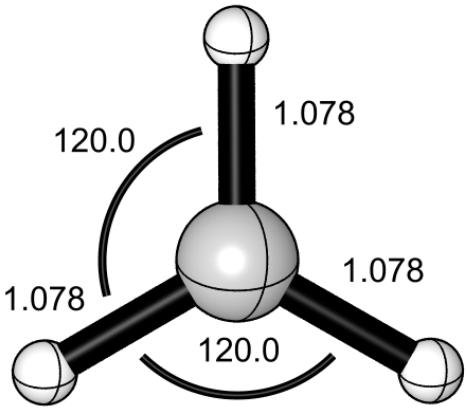

Figure A.14: CH_3

Cartesian Coordinates (Å):

C	0.0000000000	-0.0000000000	-0.0000000000
H	0.0000000000	-1.0777093855	0.0000000000
H	0.0000000000	0.5388546928	0.9333237060
H	0.0000000000	0.5388546929	-0.9333237058

Rotational Constants (GHz): 143.8990480, 287.7980960, 287.7980959

Harmonic Vibrational Frequencies (cm^{-1}):

a_1':		3120
e:	3304	1421
a_2'':		518

NH_2 ($^2B_1$)

Level of Theory:

Reference:	ROHF
Geometry:	CCSD(T)-F12a/aug-cc-pVTZ
Frequencies:	CCSD(T)-F12a/aug-cc-pVTZ
Program:	Molpro 2010.1

Wavefunction Diagnostics:

T_1: 0.007

D_1: 0.014

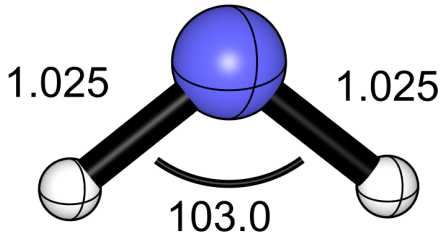

Figure A.15: NH_2

Cartesian Coordinates (Å):

N	0.0000000000	-0.0802397172	-0.0000000000
H	0.0000000000	0.5575201136	0.8025151394
H	0.0000000000	0.5575201139	-0.8025151391

Rotational Constants (GHz): $250.8006512, 389.2656141, 705.0741749$

Harmonic Vibrational Frequencies (cm^{-1}):

a_1:	3375	1541
b_2:		3470

OH ($^2\Pi$)

Level of Theory:

Reference: ROHF

Geometry: CCSD(T)-F12a/aug-cc-pVTZ

Frequencies: CCSD(T)-F12a/aug-cc-pVTZ

Program: Molpro 2010.1

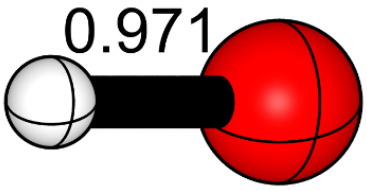

Figure A.16: OH

Wavefunction Diagnostics:

T_1: 0.008

D_1: 0.017

Cartesian Coordinates (Å):

O	0.0000000000	0.0000000000	-0.0575165941
H	0.0000000000	0.0000000000	0.9129819196

Rotational Constants (GHz): 565.8814452, 565.8814452

Harmonic Vibrational Frequencies (cm^{-1}):

σ^+: 3738

SiH_3 ($^2A_1$)

Level of Theory:

Reference: ROHF

Geometry: CCSD(T)-F12a/aug-cc-pVTZ

Frequencies: CCSD(T)-F12a/aug-cc-pVTZ

Program: Molpro 2010.1

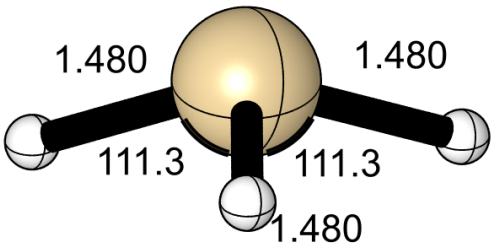

Figure A.17: SiH_3

Wavefunction Diagnostics:

T_1: 0.013

D_1: 0.035

Cartesian Coordinates (Å):

Si	0.0000000003	-0.0435800318	0.0000001886
H	-0.0006845217	0.4047739671	-1.4106892395
H	1.2220361900	0.4047756383	0.7047491830
H	-1.2213516767	0.4047756361	0.7059348018

Rotational Constants (GHz): 142.0588464, 83.9843854, 142.0583091

Harmonic Vibrational Frequencies (cm^{-1}):

a_1: 2227 770

e: 2261 939

$\mathbf{PH_2}$ ($^2B_1$)

Level of Theory:

Reference:	ROHF
Geometry:	CCSD(T)-F12a/aug-cc-pVTZ
Frequencies:	CCSD(T)-F12a/aug-cc-pVTZ
Program:	Molpro 2010.1

Wavefunction Diagnostics:

T_1: 0.009

D_1: 0.022

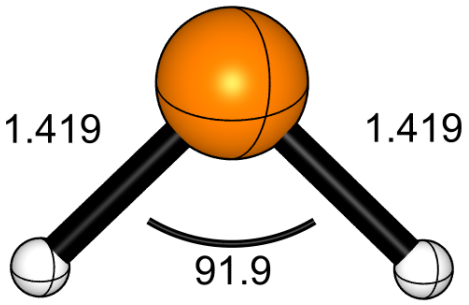

Figure A.18: PH_2

Cartesian Coordinates (Å):

P	0.0000000000	-0.0603505120	-0.0000000001
H	0.0000000000	0.9272785444	1.0196157769
H	0.0000000000	0.9272785471	-1.0196157741

Rotational Constants (GHz): 128.2069785, 241.1456418, 273.7464142

Harmonic Vibrational Frequencies (cm^{-1}):

a_1:	2396	1128
b_2:		2404

SH ($^2\Pi$)

Level of Theory:

Reference: ROHF

Geometry: CCSD(T)-F12a/aug-cc-pVTZ

Frequencies: CCSD(T)-F12a/aug-cc-pVTZ

Program: Molpro 2010.1

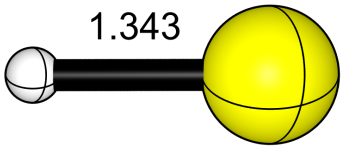

Figure A.19: SH

Wavefunction Diagnostics:

T_1: 0.007

D_1: 0.018

Cartesian Coordinates (Å):

H	0.0000000000	0.0000000000	-1.3018375700
S	0.0000000000	0.0000000000	0.0409287010

Rotational Constants (GHz): 286.8305109, 286.8305109

Harmonic Vibrational Frequencies (cm^{-1}):

σ^+: 2700

C_2H ($^2\Sigma^+$)

Level of Theory:

Reference:	ROHF
Geometry:	CCSD(T)-F12a/aug-cc-pVTZ
Frequencies:	CCSD(T)-F12a/aug-cc-pVTZ
Program:	Molpro 2010.1

Wavefunction Diagnostics:

T_1: 0.014

D_1: 0.032

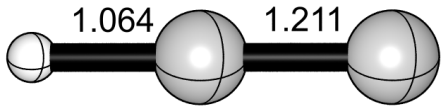

Figure A.20: C_2H

Cartesian Coordinates (Å):

C	0.0000000000	0.0000000000	-0.6725882558
C	0.0000000000	0.0000000000	0.5381060408
H	0.0000000000	0.0000000000	1.6025417027

Rotational Constants (GHz): 43.9464233, 43.9464233

Harmonic Vibrational Frequencies (cm^{-1}):

σ^+:	3445	2020
π^+:		370

Pre-Reactive Complexes

$CN + H_2 \rightarrow HCN + H$

Level of Theory:

Reference:	ROHF
Geometry:	CCSD(T)-F12a/aug-cc-pVTZ
Frequencies:	CCSD(T)-F12a/aug-cc-pVTZ
Program:	Molpro 2010.1

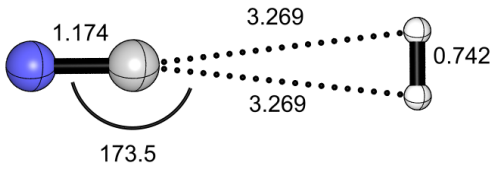

Figure A.21: PRC ($CN + H_2 \rightarrow HCN + H$)

Wavefunction Diagnostics:

T_1: 0.041

D_1: 0.149

Cartesian Coordinates (Å):

C	0.0000000000	0.0000000000	-0.3529809957
N	0.0000000000	0.0000000000	0.8209492554
H	0.0000000000	0.3712222556	-3.6009758503
H	0.0000000000	-0.3712222556	-3.6009758503

Rotational Constants (GHz): 13.5293712, 13.6307420, 1819.2169740

Harmonic Vibrational Frequencies (cm^{-1}):

a_1:	4392	2071	85	$12i$
b_2:				160

Incremental Focal Point Analysis Table (kcal mol^{-1}):

Basis	ROHF	+δMP2	+δCCSD	+δ(T)	+δT	+δ(Q)	Net
aug-cc-pVDZ	−0.08	−0.28	+0.03	−0.04	−0.00	−0.00	[−0.37]
aug-cc-pVTZ	−0.05	−0.27	+0.04	−0.03	[−0.00]	[−0.00]	[−0.32]
aug-cc-pVQZ	−0.02	−0.26	+0.05	−0.03	[−0.00]	[−0.00]	[−0.27]
aug-cc-pV5Z	−0.01	−0.25	+0.04	−0.03	[−0.00]	[−0.00]	[−0.25]
CBS LIMIT	[−0.01]	[−0.23]	[+0.04]	[−0.03]	[−0.00]	[−0.00]	[−0.24]

$$\Delta H_{0K} = \Delta E_{CCSD(T)/CBS} + \delta_{ZPVE} + \delta_{T(Q)} + \delta_{CORE} + \delta_{REL} + \delta_{DBOC}$$
$$= -0.23 + 0.34 - 0.01 + 0.00 - 0.07 + 0.19 = 0.22 \text{ kcal mol}^{-1}$$

$CN + H_2 \rightarrow HNC + H$

Level of Theory:

Reference: ROHF

Geometry: CCSD(T)-F12a/aug-cc-pVTZ

Frequencies: CCSD(T)-F12a/aug-cc-pVTZ

Program: Molpro 2010.1

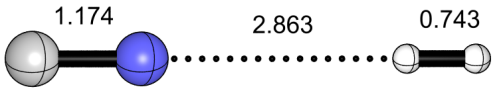

Figure A.22: PRC (CN + H_2)

Wavefunction Diagnostics:

T_1: 0.041

D_1: 0.149

Cartesian Coordinates (Å):

N	0.0000000000	0.0000000000	-0.2702877289
C	0.0000000000	0.0000000000	0.9033919869
H	0.0000000000	0.0000000000	-3.1332849597
H	0.0000000000	0.0000000000	-3.8758644170

Rotational Constants (GHz): 14.0920604, 14.0920604

Harmonic Vibrational Frequencies (cm^{-1}):

σ^+: 4391 2072 108

π: 181 22

Incremental Focal Point Analysis Table (kcal mol^{-1}):

Basis	ROHF	+δMP2	+δCCSD	+δ(T)	+δT	+δ(Q)	Net
aug-cc-pVDZ	−0.17	−0.40	+0.09	−0.05	−0.01	−0.00	[−0.55]
aug-cc-pVTZ	−0.15	−0.40	+0.09	−0.05	[−0.01]	[−0.00]	[−0.52]
aug-cc-pVQZ	−0.07	−0.37	+0.10	−0.04	[−0.01]	[−0.00]	[−0.40]
aug-cc-pV5Z	−0.06	−0.34	+0.10	−0.04	[−0.01]	[−0.00]	[−0.37]
CBS LIMIT	[−0.06]	[−0.31]	[+0.09]	[−0.04]	[−0.01]	[−0.00]	[−0.34]

$$\Delta H_{0K} = \Delta E_{CCSD(T)/CBS} + \delta_{ZPVE} + \delta_{T(Q)} + \delta_{CORE} + \delta_{REL} + \delta_{DBOC}$$
$$= -0.32 + 0.66 - 0.02 + 0.00 + 0.00 + 0.02 = 0.34 \text{ kcal mol}^{-1}$$

Transition States

$CN + H_2 \rightarrow HCN + H$

Level of Theory:

Reference:	ROHF
Geometry:	CCSD(T)-F12a/aug-cc-pVTZ
Frequencies:	CCSD(T)-F12a/aug-cc-pVTZ
Program:	MOLPRO 2010.1

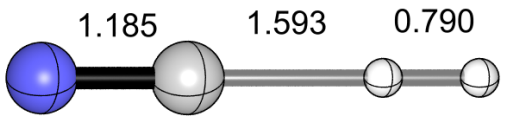

Figure A.23: TS ($CN + H_2 \rightarrow HCN + H$)

Wavefunction Diagnostics:

T_1: 0.028

D_1: 0.097

Cartesian Coordinates (Å):

C	0.0000000000	0.0000000000	-0.4492016545
N	0.0000000000	0.0000000000	0.7358905242
H	0.0000000000	0.0000000000	-2.0417298808
H	0.0000000000	0.0000000000	-2.8316125133

Rotational Constants (GHz): 22.6706911, 22.6706911

Harmonic Vibrational Frequencies (cm^{-1}):

σ^+:	3088	2001	$750i$
π :		431	132

Incremental Focal Point Analysis Table (kcal mol^{-1}):

Basis	ROHF	$+\delta$MP2	$+\delta$CCSD	$+\delta$(T)	$+\delta$T	$+\delta$(Q)	Net
aug-cc-pVDZ	+12.50	−11.14	+2.87	−0.77	+0.21	−0.13	[+3.55]
aug-cc-pVTZ	+13.48	−11.60	+3.07	−0.84	[+0.21]	[−0.13]	[+4.20]
aug-cc-pVQZ	+13.71	−11.67	+3.11	−0.85	[+0.21]	[−0.13]	[+4.38]
aug-cc-pV5Z	+13.74	−11.65	+3.12	−0.85	[+0.21]	[−0.13]	[+4.44]
CBS LIMIT	[+13.74]	[−11.62]	[+3.12]	[−0.85]	[+0.21]	[−0.13]	[+4.48]

$$\Delta H_{0K} = \Delta E_{CCSD(T)/CBS} + \delta_{ZPVE} + \delta_{T(Q)} + \delta_{CORE} + \delta_{REL} + \delta_{DBOC}$$
$$= 4.40 - 0.37 + 0.08 - 0.02 + 0.03 + 0.11 = 4.24 \text{ kcal mol}^{-1}$$

$CN + H_2 \rightarrow HNC + H$

Level of Theory:

Reference:	ROHF
Geometry:	CCSD(T)-F12a/aug-cc-pVTZ
Frequencies:	CCSD(T)-F12a/aug-cc-pVTZ
Program:	MOLPRO 2010.1

Wavefunction Diagnostics:

T_1: 0.059

D_1: 0.213

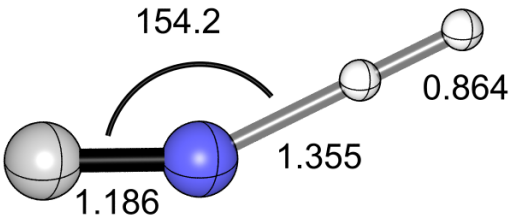

Figure A.24: TS ($CN + H_2 \rightarrow HNC + H$)

Cartesian Coordinates (Å):

N	0.1272018683	0.0000000000	-0.3755122798
C	-0.0912393850	0.0000000000	0.7903786967
H	-0.2272181635	0.0000000000	-1.6832279975
H	-0.4531816168	0.0000000000	-2.5169730828

Rotational Constants (GHz): 26.9974073, 26.1783866, 862.9189757

Harmonic Vibrational Frequencies (cm^{-1}):

a':	$2337i$	2091	1845	779	103
a'':					782

Incremental Focal Point Analysis Table (kcal mol^{-1}):

Basis	ROHF	$+\delta$MP2	$+\delta$CCSD	$+\delta$(T)	$+\delta$T	$+\delta$(Q)	Net
aug-cc-pVDZ	+26.03	−7.30	−0.46	−1.67	+0.06	−0.34	[+16.32]
aug-cc-pVTZ	+26.92	−7.80	−0.05	−1.72	[+0.06]	[−0.34]	[+17.06]
aug-cc-pVQZ	+27.19	−7.99	+0.06	−1.74	[+0.06]	[−0.34]	[+17.23]
aug-cc-pV5Z	+27.23	−7.97	+0.10	−1.74	[+0.06]	[−0.34]	[+17.34]
CBS LIMIT	[+27.24]	[−7.95]	[+0.14]	[−1.74]	[+0.06]	[−0.34]	[+17.41]

$$\Delta H_{0K} = \Delta E_{CCSD(T)/CBS} + \delta_{ZPVE} + \delta_{T(Q)} + \delta_{CORE} + \delta_{REL} + \delta_{DBOC}$$
$$= 17.69 - 1.25 - 0.28 + 0.04 + 0.01 + 0.38 = 16.59 \text{ kcal mol}^{-1}$$

$CN + CH_4 \rightarrow HCN + CH_3$

Level of Theory:

Reference:	ROHF
Geometry:	CCSD(T)-F12a/aug-cc-pVTZ
Frequencies:	CCSD(T)-F12a/aug-cc-pVTZ
Program:	Molpro 2010.1

Wavefunction Diagnostics:

T_1: 0.024

D_1: 0.097

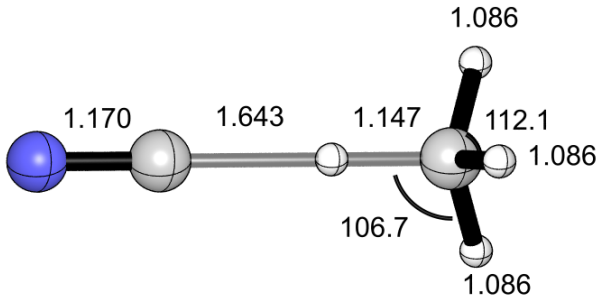

Figure A.25: TS ($CN + CH_4 \rightarrow HCN + CH_3$)

Cartesian Coordinates (Å):

C	-0.0000000000	0.0000000000	0.6694214628
N	-0.0000000000	0.0000000000	1.8394835943
H	0.0000000000	0.0000000000	-0.9735927729
C	0.0000000000	0.0000000000	-2.1205017354
H	1.0407464759	0.0000000000	-2.4323030494
H	-0.5203732379	-0.9013128870	-2.4323030494
H	-0.5203732379	0.9013128870	-2.4323030494

Rotational Constants (GHz): 3.9710148, 3.9710148, 154.3019336

Harmonic Vibrational Frequencies (cm^{-1}):

a':	3189	3068	2115	1852	1481	1274	1214	$307.74i$	263	63
a'':						3189	1481	1274	262	63

Incremental Focal Point Analysis Table (kcal mol^{-1}):

Basis	ROHF	+δMP2	+δCCSD	+δ(T)	+δT	+δ(Q)	Net
aug-cc-pVDZ	+9.57	−9.57	+2.92	−0.89	+0.28	−0.10	[+2.21]
aug-cc-pVTZ	+10.06	−10.13	+3.09	−0.90	[+0.28]	[−0.10]	[+2.29]
aug-cc-pVQZ	+10.24	−10.17	+3.12	−0.91	[+0.28]	[−0.10]	[+2.46]
aug-cc-pV5Z	+10.27	−10.12	+3.12	−0.90	[+0.28]	[−0.10]	[+2.54]
CBS LIMIT	[+10.27]	[−10.06]	[+3.11]	[−0.89]	[+0.28]	[−0.10]	[+2.60]

$$\Delta H_{0K} = \Delta E_{CCSD(T)/CBS} + \delta_{ZPVE} + \delta_{T(Q)} + \delta_{CORE} + \delta_{REL} + \delta_{DBOC}$$
$$= 2.43 - 1.37 - 0.17 - 0.06 - 0.08 + 0.10 = 1.19 \text{ kcal mol}^{-1}$$

$CN + CH_4 \rightarrow HNC + CH_3$

Level of Theory:

Reference:	ROHF
Geometry:	CCSD(T)-F12a/aug-cc-pVTZ
Frequencies:	CCSD(T)-F12a/aug-cc-pVTZ
Program:	MOLPRO 2010.1

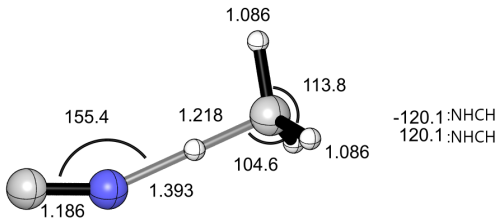

Figure A.26: TS ($CN + CH_4 \rightarrow HNC + CH_3$)

Wavefunction Diagnostics:

T_1: 0.045

D_1: 0.203

Cartesian Coordinates (Å):

N	0.0000000000	-0.2099914824	0.6604948996
C	0.0000000000	0.1707590370	1.7838655116
H	0.0000000000	-0.0668530267	-0.7249558774
C	0.0000000000	0.0583250712	-1.9365666359
H	0.0000000000	1.1302368195	-2.1097668872
H	0.9094848134	-0.4375600668	-2.2620544093
H	-0.9094848134	-0.4375600668	-2.2620544093

Rotational Constants (GHz): 4.7058258, 4.7509181, 116.0661990

Harmonic Vibrational Frequencies (cm^{-1}):

a':	3066	$2040i$	2015	1448	1261	610	379	63	31
a'':						3205	1447	1196	376

Incremental Focal Point Analysis Table (kcal mol^{-1}):

Basis	ROHF	$+\delta$MP2	$+\delta$CCSD	$+\delta$(T)	$+\delta$T	$+\delta$(Q)	Net
aug-cc-pVDZ	+24.36	−7.66	+0.35	−2.12	+0.18	−0.38	[+14.73]
aug-cc-pVTZ	+24.85	−8.14	+0.72	−2.08	[+0.18]	[−0.38]	[+15.14]
aug-cc-pVQZ	+25.16	−8.24	+0.85	−2.09	[+0.18]	[−0.38]	[+15.48]
aug-cc-pV5Z	+25.20	−8.14	+0.88	−2.08	[+0.18]	[−0.38]	[+15.67]
CBS LIMIT	[+25.21]	[−8.04]	[+0.91]	[−2.06]	[+0.18]	[−0.38]	[+15.82]

$$\Delta H_{0K} = \Delta E_{CCSD(T)/CBS} + \delta_{ZPVE} + \delta_{T(Q)} + \delta_{CORE} + \delta_{REL} + \delta_{DBOC}$$
$$= 16.02 - 3.26 - 0.20 + 0.13 + 0.04 + 0.06 = 12.79 \text{ kcal mol}^{-1}$$

$CN + NH_3 \rightarrow HCN + NH_2$

Level of Theory:

Reference:	ROHF
Geometry:	CCSD(T)-F12a/aug-cc-pVTZ
Frequencies:	CCSD(T)-F12a/aug-cc-pVTZ
Program:	MOLPRO 2010.1

Wavefunction Diagnostics:

T_1: 0.045

D_1: 0.205

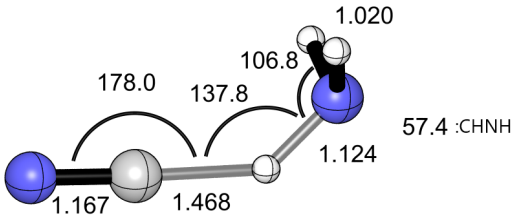

Figure A.27: TS ($CN + NH_3 \rightarrow HCN + NH_2$)

Cartesian Coordinates (Å):

C	-0.1930371157	0.0000000000	0.5665903100
N	0.1240334970	0.0000000000	1.6899509343
H	-0.5417518488	0.0000000000	-0.8589157330
N	-0.0055362110	0.0000000000	-1.8470882501
H	0.5976874709	-0.8219316534	-1.8545773794
H	0.5976874709	0.8219316534	-1.8545773794

Rotational Constants (GHz): 5.0194476, 5.0036654, 166.1713330

Harmonic Vibrational Frequencies (cm^{-1}):

a':	3451	2160	1824	1580	$1067i$	862	380	127
a'':					3551	1453	562	152

Incremental Focal Point Analysis Table (kcal mol^{-1}):

Basis	ROHF	$+\delta$MP2	$+\delta$CCSD	$+\delta$(T)	$+\delta$T	$+\delta$(Q)	Net
aug-cc-pVDZ	+5.39	−2.41	−2.08	−1.65	+0.28	−0.27	[−0.74]
aug-cc-pVTZ	+5.70	−3.21	−2.04	−1.57	[+0.28]	[−0.27]	[−1.13]
aug-cc-pVQZ	+5.97	−3.35	−1.98	−1.59	[+0.28]	[−0.27]	[−0.93]
aug-cc-pV5Z	+6.02	−3.32	−1.97	−1.58	[+0.28]	[−0.27]	[−0.84]
CBS LIMIT	[+6.02]	[−3.29]	[−1.96]	[−1.57]	[+0.28]	[−0.27]	[−0.79]

$$\Delta H_{0K} = \Delta E_{CCSD(T)/CBS} + \delta_{ZPVE} + \delta_{T(Q)} + \delta_{CORE} + \delta_{REL} + \delta_{DBOC}$$
$$= -0.79 - 1.53 + 0.00 - 0.11 - 0.01 + 0.03 = -2.41 \text{ kcal mol}^{-1}$$

$CN + NH_3 \rightarrow HNC + NH_2$

Level of Theory:

Reference:	ROHF
Geometry:	CCSD(T)-F12a/aug-cc-pVTZ
Frequencies:	CCSD(T)-F12a/aug-cc-pVTZ
Program:	Molpro 2010.1

Wavefunction Diagnostics:

T_1: 0.036

D_1: 0.163

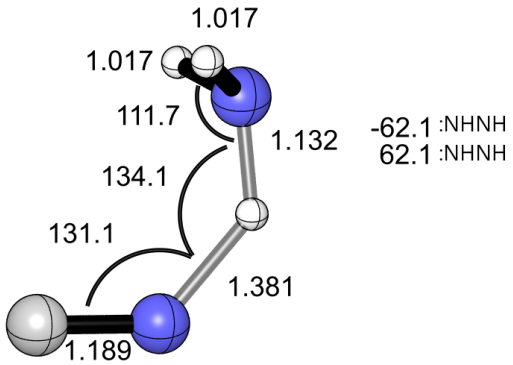

Figure A.28: TS ($CN + NH_3 \rightarrow HNC + NH_2$)

Cartesian Coordinates (Å):

N	-0.5070289888	0.0000000000	-0.6798234275
C	0.4713907010	0.0000000000	-1.3559919725
H	-0.6617303346	0.0000000000	0.6923726031
N	0.0584015653	0.0000000000	1.5660884292
H	0.6393736215	0.8350936388	1.5751441262
H	0.6393736215	-0.8350936388	1.5751441262

Rotational Constants (GHz): 7.2401786, 6.6515466, 56.2229513

Harmonic Vibrational Frequencies (cm^{-1}):

a':	3476	1992	1903	1586	$902i$	794	409	132
a'':					3586	1450	513	154

Incremental Focal Point Analysis Table (kcal mol^{-1}):

Basis	ROHF	+δMP2	+δCCSD	+δ(T)	+δT	+δ(Q)	Net
aug-cc-pVDZ	+4.91	+6.01	−1.44	−1.04	+0.01	−0.00	[+8.45]
aug-cc-pVTZ	+5.46	+5.31	−1.53	−0.78	[+0.01]	[−0.00]	[+8.47]
aug-cc-pVQZ	+5.76	+5.22	−1.51	−0.76	[+0.01]	[−0.00]	[+8.72]
aug-cc-pV5Z	+5.82	+5.28	−1.52	−0.74	[+0.01]	[−0.00]	[+8.84]
CBS LIMIT	[+5.83]	[+5.33]	[−1.53]	[−0.72]	[+0.01]	[−0.00]	[+8.91]

$$\Delta H_{0K} = \Delta E_{CCSD(T)/CBS} + \delta_{ZPVE} + \delta_{T(Q)} + \delta_{CORE} + \delta_{REL} + \delta_{DBOC}$$
$$= 8.91 - 1.68 + 0.00 + 0.04 - 0.01 + 0.01 = 7.27 \text{ kcal mol}^{-1}$$

$CN + H_2O \rightarrow HCN + OH$

Level of Theory:

Reference:	ROHF
Geometry:	CCSD(T)/aug-cc-pVTZ
Frequencies:	CCSD(T)/aug-cc-pVTZ
Program:	Molpro 2010.1

Wavefunction Diagnostics:

T_1: 0.107

D_1: 0.503

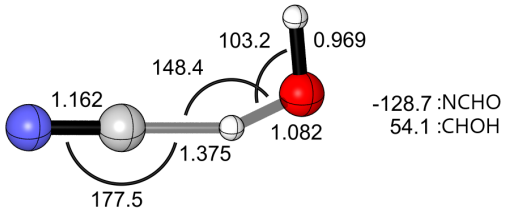

Figure A.29: TS ($CN + H_2O \rightarrow HCN + OH$)

Cartesian Coordinates (Å):

C	0.5792365172	0.1057568987	0.0528501648
N	1.7251151012	-0.0677374396	-0.0349319533
H	-0.7706839662	0.3092592014	0.2160713101
O	-1.7829938575	0.0190036440	-0.0332787295
H	-1.7981330206	-0.9289223997	0.1681652006

Rotational Constants (GHz): 5.0247066, 4.9739375, 384.4788250

Harmonic Vibrational Frequencies (cm^{-1}):

a': 3767 2248 1563i 1514 1062 576 329 171 135

Incremental Focal Point Analysis Table (kcal mol^{-1}):

Basis	ROHF	$+\delta$MP2	$+\delta$CCSD	$+\delta$(T)	$+\delta$T	$+\delta$(Q)	Net
aug-cc-pVDZ	+18.84	+6.47	−12.89	−2.20	+0.11	−0.67	[+9.66]
aug-cc-pVTZ	+18.47	+5.98	−12.81	−2.25	[+0.11]	[−0.67]	[+8.83]
aug-cc-pVQZ	+18.77	+6.16	−12.81	−2.32	[+0.11]	[−0.67]	[+9.25]
aug-cc-pV5Z	+18.81	+6.35	−12.85	−2.32	[+0.11]	[−0.67]	[+9.43]
CBS LIMIT	[+18.81]	[+6.54]	[−12.89]	[−2.31]	[+0.11]	[−0.67]	[+9.59]

$$\Delta H_{0K} = \Delta E_{CCSD(T)/CBS} + \delta_{ZPVE} + \delta_{T(Q)} + \delta_{CORE} + \delta_{REL} + \delta_{DBOC}$$
$$= 10.14 - 2.42 - 0.55 - 0.13 - 0.05 + 0.16 = 7.15 \text{ kcal mol}^{-1}$$

$CN + H_2O \rightarrow HNC + OH$

Level of Theory:

Reference:	ROHF
Geometry:	CCSD(T)-F12a/aug-cc-pVTZ
Frequencies:	CCSD(T)-F12a/aug-cc-pVTZ
Program:	MOLPRO 2010.1

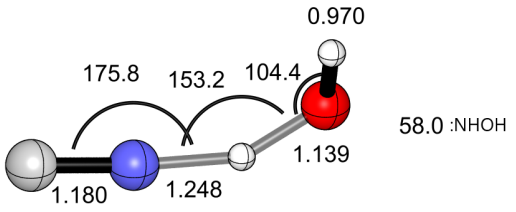

Figure A.30: TS ($CN + H_2O \rightarrow HNC + OH$)

Wavefunction Diagnostics:

T_1: 0.095

D_1: 0.448

Cartesian Coordinates (Å):

N	0.0765387670	-0.1209349038	0.6115065409
C	-0.0635843563	0.1036718763	1.7613306402
H	0.1722998898	-0.2863148744	-0.6220040517
O	-0.0475444582	-0.0105527527	-1.7054502020
H	0.2764757917	0.8989840034	-1.7931704866

Rotational Constants (GHz): 5.3821932, 5.4377410, 335.4231434

Harmonic Vibrational Frequencies (cm^{-1}):

a: $3863i$ 3751 2123 1386 945 646 397 142 106

Incremental Focal Point Analysis Table (kcal mol^{-1}):

Basis	ROHF	+δMP2	+δCCSD	+δ(T)	+δT	+δ(Q)	Net
aug-cc-pVDZ	+42.69	−14.59	−2.26	−4.66	−0.24	−1.45	[+19.50]
aug-cc-pVTZ	+42.93	−14.94	−1.83	−5.75	[−0.24]	[−1.45]	[+18.73]
aug-cc-pVQZ	+43.33	−14.85	−1.46	−5.92	[−0.24]	[−1.45]	[+19.41]
aug-cc-pV5Z	+43.38	−14.66	−1.38	−5.98	[−0.24]	[−1.45]	[+19.68]
CBS LIMIT	[+43.39]	[−14.46]	[−1.30]	[−6.04]	[−0.24]	[−1.45]	[+19.90]

$$\Delta H_{0K} = \Delta E_{CCSD(T)/CBS} + \delta_{ZPVE} + \delta_{T(Q)} + \delta_{CORE} + \delta_{REL} + \delta_{DBOC}$$
$$= 21.59 - 2.86 - 1.69 - 0.09 - 0.05 + 0.01 = 16.91 \text{ kcal mol}^{-1}$$

CN + HF → HCN + F

Level of Theory:

Reference: ROHF

Geometry: CCSD(T)-F12a/aug-cc-pVTZ

Frequencies: CCSD(T)-F12a/aug-cc-pVTZ

Program: Molpro 2010.1

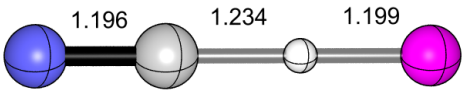

Figure A.31: TS (CN + HF → HCN + F)

Wavefunction Diagnostics:

T_1: 0.045

D_1: 0.198

Cartesian Coordinates (Å):

C	0.0000000000	0.0000000000	0.6675335023
N	0.0000000000	0.0000000000	1.8631375133
H	0.0000000000	0.0000000000	-0.5665099344
F	0.0000000000	0.0000000000	-1.7655770898

Rotational Constants (GHz): 4.4519066, 4.4519066

Harmonic Vibrational Frequencies (cm^{-1}):

σ^+: $7998i$ 2106 1136 1101 566 164 49

Incremental Focal Point Analysis Table (kcal mol^{-1}):

Basis	ROHF	+δMP2	+δCCSD	+δ(T)	+δT	+δ(Q)	Net
aug-cc-pVDZ	+26.56	+5.48	−8.66	−2.09	−0.10	−0.54	[+20.65]
aug-cc-pVTZ	+27.00	+5.94	−8.59	−1.71	[−0.10]	[−0.54]	[+22.00]
aug-cc-pVQZ	+27.42	+6.66	−8.54	−1.69	[−0.10]	[−0.54]	[+23.20]
aug-cc-pV5Z	+27.48	+7.05	−8.58	−1.66	[−0.10]	[−0.54]	[+23.64]
CBS LIMIT	[+27.48]	[+7.46]	[−8.62]	[−1.64]	[−0.10]	[−0.54]	[+24.03]

$$\Delta H_{0K} = \Delta E_{CCSD(T)/CBS} + \delta_{ZPVE} + \delta_{T(Q)} + \delta_{CORE} + \delta_{REL} + \delta_{DBOC}$$
$$= 24.67 - 1.53 - 0.64 + 0.09 - 0.09 + 0.02 = 22.53 \text{ kcal mol}^{-1}$$

CN + HF → HNC + F

Level of Theory:

Reference:	ROHF
Geometry:	CCSD(T)-F12a/aug-cc-pVTZ
Frequencies:	CCSD(T)-F12a/aug-cc-pVTZ
Program:	MOLPRO 2010.1

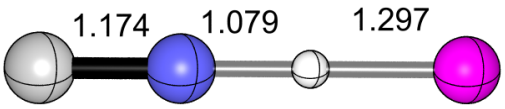

Figure A.32: TS (CN + HF → HNC + F)

Wavefunction Diagnostics:

T_1: 0.044

D_1: 0.203

Cartesian Coordinates (Å):

N	0.0000000000	0.0000000000	0.6978316756
C	0.0000000000	0.0000000000	1.8719375340
H	0.0000000000	0.0000000000	-0.3807731160
F	0.0000000000	0.0000000000	-1.6777391342

Rotational Constants (GHz): 4.9289799, 4.9289799

Harmonic Vibrational Frequencies (cm^{-1}):

σ^+:	$2706i$	2084	626
π:		366	197

Incremental Focal Point Analysis Table (kcal mol^{-1}):

Basis	ROHF	+δMP2	+δCCSD	+δ(T)	+δT	+δ(Q)	Net
aug-cc-pVDZ	+59.29	−39.89	+16.09	−4.05	+0.40	−1.35	[+30.51]
aug-cc-pVTZ	+59.93	−40.58	+16.46	−4.45	[+0.40]	[−1.35]	[+30.41]
aug-cc-pVQZ	+60.45	−40.49	+16.81	−4.65	[+0.40]	[−1.35]	[+31.18]
aug-cc-pV5Z	+60.55	−40.29	+16.91	−4.72	[+0.40]	[−1.35]	[+31.51]
CBS LIMIT	[+60.57]	[−40.08]	[+17.02]	[−4.78]	[+0.40]	[−1.35]	[+31.78]

$$\Delta H_{0K} = \Delta E_{CCSD(T)/CBS} + \delta_{ZPVE} + \delta_{T(Q)} + \delta_{CORE} + \delta_{REL} + \delta_{DBOC}$$
$$= 32.72 - 3.40 - 0.94 - 0.03 - 0.08 - 0.01 = 28.25 \text{ kcal mol}^{-1}$$

$CN + HCl \rightarrow HCN + Cl$

Level of Theory:

Reference:	ROHF
Geometry:	CCSD(T)-F12a/aug-cc-pVTZ
Frequencies:	CCSD(T)-F12a/aug-cc-pVTZ
Program:	MOLPRO 2010.1

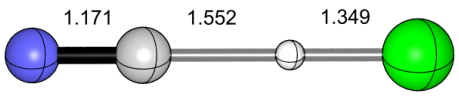

Figure A.33: TS (CN + HCl → HCN + Cl)

Wavefunction Diagnostics:

T_1: 0.027

D_1: 0.137

Cartesian Coordinates (Å):

C	0.0000000000	0.0000000000	1.4085685018
N	0.0000000000	0.0000000000	2.5793511730
H	0.0000000000	0.0000000000	-0.1429663500
Cl	0.0000000000	0.0000000000	-1.4921843807

Rotational Constants (GHz): 2.5787448, 2.5787448

Harmonic Vibrational Frequencies (cm^{-1}):

σ^+:	2114	1148	$518i$
π:		235	93

Incremental Focal Point Analysis Table (kcal mol^{-1}):

Basis	ROHF	+δMP2	+δCCSD	+δ(T)	+δT	+δ(Q)	Net
aug-cc-pV(D+d)Z	+16.77	−13.47	+2.92	−1.59	+0.20	−0.21	[+4.62]
aug-cc-pV(T+d)Z	+16.96	−14.03	+3.30	−1.75	[+0.20]	[−0.21]	[+4.46]
aug-cc-pV(Q+d)Z	+17.15	−13.95	+3.46	−1.80	[+0.20]	[−0.21]	[+4.86]
aug-cc-pV(5+d)Z	+17.18	−13.89	+3.50	−1.80	[+0.20]	[−0.21]	[+4.98]
CBS LIMIT	[+17.18]	[−13.83]	[+3.55]	[−1.81]	[+0.20]	[−0.21]	[+5.08]

$$\Delta H_{0K} = \Delta E_{CCSD(T)/CBS} + \delta_{ZPVE} + \delta_{T(Q)} + \delta_{CORE} + \delta_{REL} + \delta_{DBOC}$$
$$= 5.09 - 1.64 - 0.01 - 0.09 + 0.06 + 0.06 = 3.47 \text{ kcal mol}^{-1}$$

$CN + HCl \rightarrow HNC + Cl$

Level of Theory:

Reference: ROHF

Geometry: CCSD(T)-F12a/aug-cc-pVTZ

Frequencies: CCSD(T)-F12a/aug-cc-pVTZ

Program: Molpro 2010.1

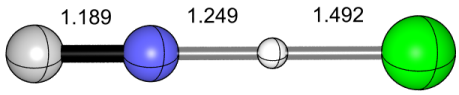

Figure A.34: TS (CN + HCl → HNC + Cl)

Wavefunction Diagnostics:

T_1: 0.014

D_1: 0.044

Cartesian Coordinates (Å):

N	0.0000000000	0.0000000000	1.3470922075
C	0.0000000000	0.0000000000	2.5365431003
H	0.0000000000	0.0000000000	0.0980425130
Cl	0.0000000000	0.0000000000	-1.3943405797

Rotational Constants (GHz): 2.9445216, 2.9445216

Harmonic Vibrational Frequencies (cm^{-1}):

σ^+: $2285i$ 1962 408

π: 537 207

Incremental Focal Point Analysis Table (kcal mol^{-1}):

Basis	ROHF	+δMP2	+δCCSD	+δ(T)	+δT	+δ(Q)	Net
aug-cc-pV(D+d)Z	+34.69	−34.80	+14.94	−4.10	+0.87	−1.28	[+10.32]
aug-cc-pV(T+d)Z	+35.27	−35.85	+15.89	−4.49	[+0.87]	[−1.28]	[+10.41]
aug-cc-pV(Q+d)Z	+35.66	−36.00	+16.18	−4.61	[+0.87]	[−1.28]	[+10.82]
aug-cc-pV(5+d)Z	+35.74	−35.92	+16.27	−4.64	[+0.87]	[−1.28]	[+11.03]
CBS LIMIT	[+35.76]	[−35.84]	[+16.35]	[−4.67]	[+0.87]	[−1.28]	[+11.19]

$$\Delta H_{0K} = \Delta E_{CCSD(T)/CBS} + \delta_{ZPVE} + \delta_{T(Q)} + \delta_{CORE} + \delta_{REL} + \delta_{DBOC}$$
$$= 11.60 - 1.73 - 0.41 + 0.07 - 0.15 + 0.09 = 9.47 \text{ kcal mol}^{-1}$$

$CN + C_2H_2 \rightarrow HCN + C_2H$

Level of Theory:

Reference: ROHF

Geometry: CCSD(T)-F12a/aug-cc-pVTZ

Frequencies: CCSD(T)-F12a/aug-cc-pVTZ

Program: MOLPRO 2010.1

Figure A.35: TS ($CN + C_2H_2 \rightarrow HCN + C_2H$)

Wavefunction Diagnostics:

T_1: 0.024

D_1: 0.083

Cartesian Coordinates (Å):

C	0.0000000000	0.0000000000	1.3015250371
C	0.0000000000	0.0000000000	2.5107935879
H	0.0000000000	0.0000000000	3.5761496032
H	0.0000000000	0.0000000000	-0.0321240518
C	0.0000000000	0.0000000000	-1.2710182629
N	0.0000000000	0.0000000000	-2.4342438807

Rotational Constants (GHz): 2.3911160, 2.3911160

Harmonic Vibrational Frequencies (cm^{-1}):

σ^+:	3439	2210	2049	$1669i$	450
π:		705	594	184	66

Incremental Focal Point Analysis Table (kcal mol^{-1}):

Basis	ROHF	$+\delta$MP2	$+\delta$CCSD	$+\delta$(T)	$+\delta$T	$+\delta$(Q)	Net
aug-cc-pVDZ	+29.45	−14.75	+3.34	−1.33	+0.39	−0.19	[+16.91]
aug-cc-pVTZ	+30.19	−14.90	+3.78	−1.34	[+0.39]	[−0.19]	[+17.94]
aug-cc-pVQZ	+30.48	−14.78	+3.90	−1.33	[+0.39]	[−0.19]	[+18.47]
aug-cc-pV5Z	+30.51	−14.62	+3.89	−1.32	[+0.39]	[−0.19]	[+18.67]
CBS LIMIT	[+30.51]	[−14.46]	[+3.89]	[−1.30]	[+0.39]	[−0.19]	[+18.84]

$$\Delta H_{0K} = \Delta E_{CCSD(T)/CBS} + \delta_{ZPVE} + \delta_{T(Q)} + \delta_{CORE} + \delta_{REL} + \delta_{DBOC}$$
$$= 18.64 - 3.55 + 0.20 - 0.11 + 0.05 + 0.02 = 15.25 \text{ kcal mol}^{-1}$$

$CN + C_2H_2 \rightarrow HNC + C_2H$

Level of Theory:

Reference: ROHF

Geometry: CCSD(T)-F12a/aug-cc-pVTZ

Frequencies: CCSD(T)-F12a/aug-cc-pVTZ

Program: MOLPRO 2010.1

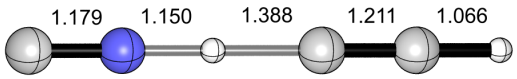

Figure A.36: TS ($CN + C_2H_2 \rightarrow HNC + C_2H$)

Wavefunction Diagnostics:

T_1: 0.059

D_1: 0.291

Cartesian Coordinates (Å):

C	0.0000000000	0.0000000000	1.2436611786
C	0.0000000000	0.0000000000	2.4545628572
H	0.0000000000	0.0000000000	3.5201551011
H	0.0000000000	0.0000000000	-0.1443349062
N	0.0000000000	0.0000000000	-1.2939076582
C	0.0000000000	0.0000000000	-2.4726181587

Rotational Constants (GHz): 2.5226526, 2.5226526

Harmonic Vibrational Frequencies (cm^{-1}):

σ^+:	3434	$2519i$	2106	2028	441
π:		712	359	140	$38i$

Incremental Focal Point Analysis Table (kcal mol^{-1}):

Basis	ROHF	$+\delta$MP2	$+\delta$CCSD	$+\delta$(T)	$+\delta$T	$+\delta$(Q)	Net
aug-cc-pVDZ	+62.51	−37.68	+10.38	−4.71	+0.10	−0.27	[+30.33]
aug-cc-pVTZ	+63.64	−38.01	+11.17	−5.06	[+0.10]	[−0.27]	[+31.57]
aug-cc-pVQZ	+64.02	−37.97	+11.45	−5.15	[+0.10]	[−0.27]	[+32.17]
aug-cc-pV5Z	+64.19	−37.75	+11.33	−5.17	[+0.10]	[−0.27]	[+32.43]
CBS LIMIT	[+64.26]	[−37.51]	[+11.20]	[−5.19]	[+0.10]	[−0.27]	[+32.59]

$$\Delta H_{0K} = \Delta E_{CCSD(T)/CBS} + \delta_{ZPVE} + \delta_{T(Q)} + \delta_{CORE} + \delta_{REL} + \delta_{DBOC}$$
$$= 32.76 - 4.71 - 0.17 + 0.07 - 0.04 - 0.01 = 27.91 \text{ kcal mol}^{-1}$$

$CN + SiH_4 \rightarrow HCN + Si\,H_3$

Level of Theory:

Reference:	ROHF
Geometry:	CCSD(T)-F12a/aug-cc-pVTZ
Frequencies:	CCSD(T)-F12a/aug-cc-pVTZ
Program:	Molpro 2010.1

Wavefunction Diagnostics:

T_1: 0.027

D_1: 0.135

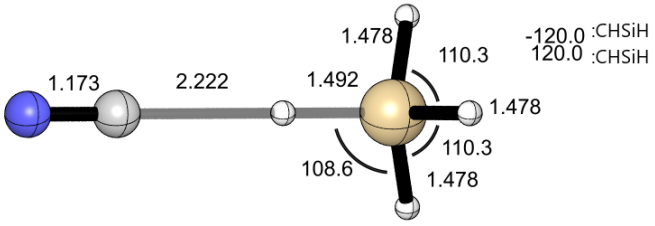

Figure A.37: TS ($CN + SiH_4 \rightarrow HCN + SiH_3$)

Cartesian Coordinates (Å):

C	-0.0000002528	0.0000000000	1.7678150806
N	0.0000010680	0.0000000000	2.9411044838
H	-0.0000027540	0.0000000000	-0.4539749625
Si	-0.0000044339	0.0000000000	-1.9462478910
H	1.4007158027	0.0000000000	-2.4172983873
H	-0.7003006651	-1.2130971099	-2.4172960221
H	-0.7003006651	1.2130971099	-2.4172960221

Rotational Constants (GHz): 1.7675309, 1.7675332, 85.1840170

Harmonic Vibrational Frequencies (cm^{-1}):

a':	2274	2264	2113	2088	968	919	913	844i	750	66	19
a'':								2274	969	919	70

Incremental Focal Point Analysis Table (kcal mol^{-1}):

Basis	ROHF	+δMP2	+δCCSD	+δ(T)	+δT	+δ(Q)	Net
aug-cc-pV(D+d)Z	+1.46	−2.74	+0.62	−0.35	+0.06	−0.03	[−0.97]
aug-cc-pV(T+d)Z	+1.60	−2.96	+0.70	−0.36	[+0.06]	[−0.03]	[−0.98]
aug-cc-pV(Q+d)Z	+1.77	−2.97	+0.74	−0.36	[+0.06]	[−0.03]	[−0.78]
aug-cc-pV(5+d)Z	+1.78	−2.90	+0.73	−0.35	[+0.06]	[−0.03]	[−0.71]
CBS LIMIT	[+1.78]	[−2.84]	[+0.71]	[−0.35]	[+0.06]	[−0.03]	[−0.66]

$$\Delta H_{0K} = \Delta E_{CCSD(T)/CBS} + \delta_{ZPVE} + \delta_{T(Q)} + \delta_{CORE} + \delta_{REL} + \delta_{DBOC}$$
$$= -0.69 + 1.02 + 0.03 - 0.04 + 0.02 + 0.01 = 0.35 \text{ kcal mol}^{-1}$$

$CN + SiH_4 \rightarrow HNC + SiH_3$

Level of Theory:

Reference:	ROHF
Geometry:	CCSD(T)-F12a/aug-cc-pVTZ
Frequencies:	CCSD(T)-F12a/aug-cc-pVTZ
Program:	MOLPRO 2010.1

Wavefunction Diagnostics:

T_1: 0.062

D_1: 0.333

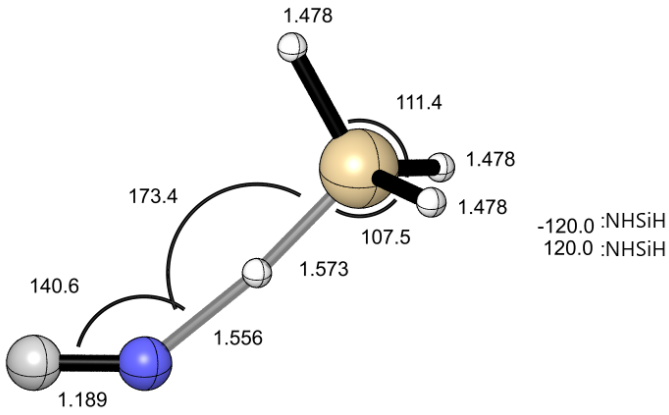

Figure A.38: TS ($CN + SiH_4 \rightarrow HNC + SiH_3$)

Cartesian Coordinates (Å):

N	-0.0000000002	-0.3642314968	1.5069492427
C	0.0000000001	0.3236017559	2.4763922149
H	-0.0000000001	-0.2532467191	-0.0451714263
Si	0.0000000000	0.0391624289	-1.5907206166
H	0.0000000006	1.5067088210	-1.7636266496
H	1.2208278307	-0.5696819122	-2.1588532246
H	-1.2208278306	-0.5696819105	-2.1588532275

Rotational Constants (GHz): 2.5886166, 2.6312269, 55.1085223

Harmonic Vibrational Frequencies (cm^{-1}):

a: 2276 2254 1985 1455i 949 912 886 879 529 229 187 82 14

Incremental Focal Point Analysis Table (kcal mol^{-1}):

Basis	ROHF	+δMP2	+δCCSD	+δ(T)	+δT	+δ(Q)	Net
aug-cc-pV(D+d)Z	+17.25	−1.83	−5.25	−1.70	+0.21	−0.44	[+8.23]
aug-cc-pV(T+d)Z	+17.34	−2.46	−4.91	−1.82	[+0.21]	[−0.44]	[+7.92]
aug-cc-pV(Q+d)Z	+17.61	−2.53	−4.84	−1.88	[+0.21]	[−0.44]	[+8.14]
aug-cc-pV(5+d)Z	+17.65	−2.44	−4.84	−1.88	[+0.21]	[−0.44]	[+8.26]
CBS LIMIT	[+17.65]	[−2.35]	[−4.85]	[−1.88]	[+0.21]	[−0.44]	[+8.35]

$$\Delta H_{0K} = \Delta E_{CCSD(T)/CBS} + \delta_{ZPVE} + \delta_{T(Q)} + \delta_{CORE} + \delta_{REL} + \delta_{DBOC}$$
$$= 8.57 - 2.09 - 0.22 - 0.01 - 0.04 + 0.15 = 6.36 \text{ kcal mol}^{-1}$$

$CN + PH_3 \rightarrow HCN + PH_2$

Level of Theory:

Reference:	ROHF
Geometry:	CCSD(T)-F12a/aug-cc-pVTZ
Frequencies:	CCSD(T)-F12a/aug-cc-pVTZ
Program:	MOLPRO 2010.1

Wavefunction Diagnostics:

T_1: 0.026

D_1: 0.121

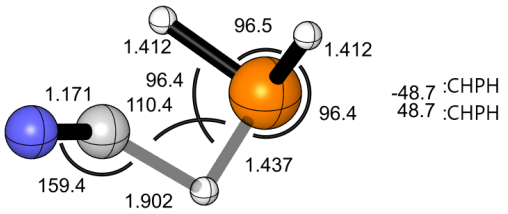

Figure A.39: TS ($CN + PH_3 \rightarrow HCN + PH_2$)

Cartesian Coordinates (Å):

C	-0.0000000075	-0.0873996942	1.2534072381
N	0.0000000047	0.0573260226	2.4149894681
H	-0.0000000827	-0.9717416765	-0.4304532155
P	-0.0000000009	-0.0113581518	-1.4992755206
H	1.0532921202	0.7828199651	-0.9964066048
H	-1.0532919865	0.7828201520	-0.9964066140

Rotational Constants (GHz): 2.8928410, 2.8943724, 110.6984739

Harmonic Vibrational Frequencies (cm^{-1}):

a: 2458 2444 2234 2112 1113 1095 822 $423i$ 307 187 67 55

Incremental Focal Point Analysis Table (kcal mol^{-1}):

Basis	ROHF	+δMP2	+δCCSD	+δ(T)	+δT	+δ(Q)	Net
aug-cc-pV(D+d)Z	+6.38	−12.04	+3.69	−1.44	+0.28	−0.21	[−3.34]
aug-cc-pV(T+d)Z	+6.55	−13.07	+3.94	−1.53	[+0.28]	[−0.21]	[−4.03]
aug-cc-pV(Q+d)Z	+6.69	−13.25	+3.94	−1.56	[+0.28]	[−0.21]	[−4.11]
aug-cc-pV(5+d)Z	+6.71	−13.26	+3.92	−1.57	[+0.28]	[−0.21]	[−4.13]
CBS LIMIT	[+6.71]	[−13.28]	[+3.90]	[−1.57]	[+0.28]	[−0.21]	[−4.16]

$$\Delta H_{0K} = \Delta E_{CCSD(T)/CBS} + \delta_{ZPVE} + \delta_{T(Q)} + \delta_{CORE} + \delta_{REL} + \delta_{DBOC}$$
$$= -4.24 + 0.35 + 0.08 - 0.15 + 0.36 + 0.01 = -3.59 \text{ kcal mol}^{-1}$$

$CN + PH_3 \rightarrow HNC + PH_2$

Level of Theory:

Reference:	ROHF
Geometry:	CCSD(T)-F12a/aug-cc-pVTZ
Frequencies:	CCSD(T)-F12a/aug-cc-pVTZ
Program:	MOLPRO 2010.1

Wavefunction Diagnostics:

T_1: 0.076

D_1: 0.413

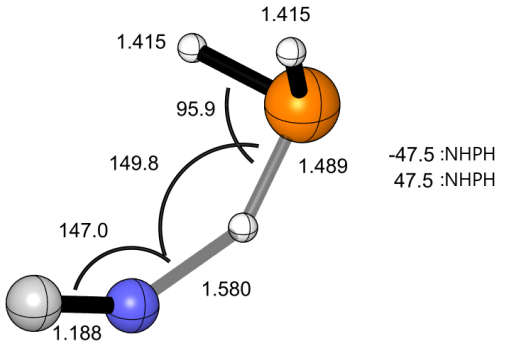

Figure A.40: TS ($CN + PH_3 \rightarrow HNC + PH_2$)

Cartesian Coordinates (Å):

N	0.0000000001	-0.3995602301	1.4499044769
C	-0.0000000001	0.3634013428	2.3605469525
H	0.0000000001	-0.5894027024	-0.1187295886
P	-0.0000000000	-0.0014967831	-1.4862294390
H	1.0385583404	0.9287012664	-1.2436852534
H	-1.0385583397	0.9287012661	-1.2436852567

Rotational Constants (GHz): 2.9072600, 2.9711302, 62.5039513

Harmonic Vibrational Frequencies (cm^{-1}):

a: 2434 2424 2024 1240 1195i 1094 1048 774 295 246 81 51

Incremental Focal Point Analysis Table (kcal mol^{-1}):

Basis	ROHF	+δMP2	+δCCSD	+δ(T)	+δT	+δ(Q)	Net
aug-cc-pV(D+d)Z	+16.93	−1.71	−8.05	−2.52	+0.79	−0.75	[+4.70]
aug-cc-pV(T+d)Z	+17.12	−1.47	−8.30	−2.75	[+0.79]	[−0.75]	[+4.65]
aug-cc-pV(Q+d)Z	+17.35	−1.44	−8.34	−2.84	[+0.79]	[−0.75]	[+4.77]
aug-cc-pV(5+d)Z	+17.39	−1.33	−8.38	−2.86	[+0.79]	[−0.75]	[+4.87]
CBS LIMIT	[+17.40]	[−1.20]	[−8.42]	[−2.87]	[+0.79]	[−0.75]	[+4.94]

$$\Delta H_{0K} = \Delta E_{CCSD(T)/CBS} + \delta_{ZPVE} + \delta_{T(Q)} + \delta_{CORE} + \delta_{REL} + \delta_{DBOC}$$
$$= 4.90 - 1.33 + 0.04 + 0.06 + 0.33 + 0.25 = 4.25 \text{ kcal mol}^{-1}$$

$CN + H_2S \rightarrow HCN + SH$

Level of Theory:

Reference:	ROHF
Geometry:	CCSD(T)-F12a/aug-cc-pVTZ
Frequencies:	CCSD(T)-F12a/aug-cc-pVTZ
Program:	MOLPRO 2010.1

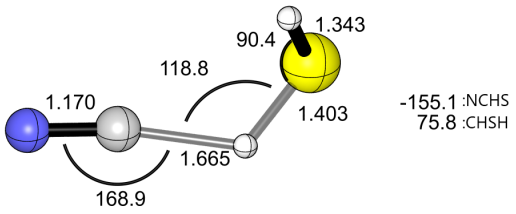

Figure A.41: TS ($CN + H_2S \rightarrow HCN + SH$)

Wavefunction Diagnostics:

T_1: 0.025

D_1: 0.119

Cartesian Coordinates (Å):

C	-0.1359836200	-0.1005558394	1.2089899538
N	0.0873703345	0.0761492502	2.3434820405
H	-0.5004497750	-0.6596782401	-0.3163543654
S	-0.0096611295	0.0399881260	-1.4284198163
H	1.2140488054	-0.4721776587	-1.2219206511

Rotational Constants (GHz): 3.1116089, 3.0896794, 169.1724787

Harmonic Vibrational Frequencies (cm^{-1}):

a: 2705 2130 2005 1129 $987i$ 428 226 100 85

Incremental Focal Point Analysis Table (kcal mol^{-1}):

Basis	ROHF	+δMP2	+δCCSD	+δ(T)	+δT	+δ(Q)	Net
aug-cc-pV(D+d)Z	+12.67	−16.58	+5.05	−1.93	+0.34	−0.29	[−0.73]
aug-cc-pV(T+d)Z	+12.84	−17.69	+5.59	−2.05	[+0.34]	[−0.29]	[−1.26]
aug-cc-pV(Q+d)Z	+13.02	−17.88	+5.74	−2.09	[+0.34]	[−0.29]	[−1.15]
aug-cc-pV(5+d)Z	+13.05	−17.88	+5.75	−2.09	[+0.34]	[−0.29]	[−1.11]
CBS LIMIT	[+13.06]	[−17.88]	[+5.77]	[−2.10]	[+0.34]	[−0.29]	[−1.10]

$$\Delta H_{0K} = \Delta E_{CCSD(T)/CBS} + \delta_{ZPVE} + \delta_{T(Q)} + \delta_{CORE} + \delta_{REL} + \delta_{DBOC}$$
$$= -1.15 + 0.09 + 0.05 - 0.17 + 0.33 + 0.10 = -0.75 \text{ kcal mol}^{-1}$$

$CN + H_2S \rightarrow HNC + SH$

Level of Theory:

Reference:	ROHF
Geometry:	CCSD(T)-F12a/aug-cc-pVTZ
Frequencies:	CCSD(T)-F12a/aug-cc-pVTZ
Program:	MOLPRO 2010.1

Wavefunction Diagnostics:

T_1: 0.050

D_1: 0.268

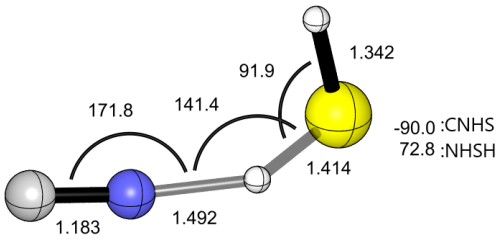

Figure A.42: TS ($CN + H_2S \rightarrow HNC + SH$)

Cartesian Coordinates (Å):

N	-0.0866746370	0.1559174450	1.3010528157
C	0.0845121161	-0.1344158069	2.4350777736
H	-0.4243077877	0.3475393272	-0.1394762715
S	0.0309875258	0.0110286547	-1.4356594988
H	-0.3639429663	-1.2632677345	-1.2930813036

Rotational Constants (GHz): 3.0627876, 3.0957117, 178.6773960

Harmonic Vibrational Frequencies (cm^{-1}):

a: 2711 2481i 2035 1248 982 406 280 62 23

Incremental Focal Point Analysis Table (kcal mol^{-1}):

Basis	ROHF	+δMP2	+δCCSD	+δ(T)	+δT	+δ(Q)	Net
aug-cc-pV(D+d)Z	+30.25	−23.28	+5.47	−3.90	+0.47	−1.22	[+7.79]
aug-cc-pV(T+d)Z	+30.61	−24.21	+6.37	−4.22	[+0.47]	[−1.22]	[+7.80]
aug-cc-pV(Q+d)Z	+30.88	−24.37	+6.59	−4.33	[+0.47]	[−1.22]	[+8.02]
aug-cc-pV(5+d)Z	+30.93	−24.29	+6.63	−4.35	[+0.47]	[−1.22]	[+8.16]
CBS LIMIT	[+30.94]	[−24.21]	[+6.67]	[−4.38]	[+0.47]	[−1.22]	[+8.27]

$$\Delta H_{0K} = \Delta E_{CCSD(T)/CBS} + \delta_{ZPVE} + \delta_{T(Q)} + \delta_{CORE} + \delta_{REL} + \delta_{DBOC}$$
$$= 9.03 - 1.45 - 0.76 - 0.04 + 0.67 + 0.03 = 7.47 \text{ kcal mol}^{-1}$$

CN + HCN → HCN + CN

Level of Theory:

Reference: ROHF

Geometry: CCSD(T)-F12a/aug-cc-pVTZ

Frequencies: CCSD(T)-F12a/aug-cc-pVTZ

Program: Molpro 2010.1

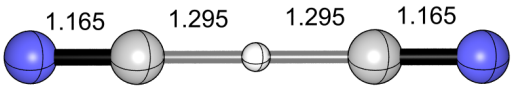

Figure A.43: TS (CN + HCN → HCN + CN)

Wavefunction Diagnostics:

T_1: 0.026

D_1: 0.118

Cartesian Coordinates (Å):

C	0.0000000000	0.0000000000	1.2951575493
N	0.0000000000	0.0000000000	2.4604921202
H	0.0000000000	0.0000000000	0.0000000006
C	0.0000000000	0.0000000000	-1.2951575492
N	0.0000000000	0.0000000000	-2.4604921203

Rotational Constants (GHz): 2.4078391, 2.4078391

Harmonic Vibrational Frequencies (cm^{-1}):

σ^+: 2198 2156 1895i 419

π: 829 224 102

Incremental Focal Point Analysis Table (kcal mol^{-1}):

Basis	ROHF	+δMP2	+δCCSD	+δ(T)	+δT	+δ(Q)	Net
aug-cc-pVDZ	+36.50	−23.34	+5.79	−2.60	+0.32	−0.33	[+16.34]
aug-cc-pVTZ	+37.45	−23.58	+6.42	−2.79	[+0.32]	[−0.33]	[+17.50]
aug-cc-pVQZ	+37.71	−23.45	+6.61	−2.83	[+0.32]	[−0.33]	[+18.04]
aug-cc-pV5Z	+37.75	−23.28	+6.62	−2.83	[+0.32]	[−0.33]	[+18.26]
CBS LIMIT	[+37.75]	[−23.09]	[+6.64]	[−2.83]	[+0.32]	[−0.33]	[+18.47]

$$\Delta H_{0K} = \Delta E_{CCSD(T)/CBS} + \delta_{ZPVE} + \delta_{T(Q)} + \delta_{CORE} + \delta_{REL} + \delta_{DBOC}$$
$$= 18.47 - 2.87 - 0.00 + 0.02 - 0.00 + 0.15 = 15.77 \text{ kcal mol}^{-1}$$

CN + HCN → HNC + CN

Level of Theory:

Reference: ROHF

Geometry: CCSD(T)-F12a/aug-cc-pVTZ

Frequencies: CCSD(T)-F12a/aug-cc-pVTZ

Program: Molpro 2010.1

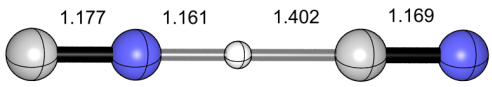

Figure A.44: TS (CN + HCN → HNC + CN)

Wavefunction Diagnostics:

T_1: 0.033

D_1: 0.154

Cartesian Coordinates (Å):

C	0.0000000000	0.0000000000	1.2420848948
N	0.0000000000	0.0000000000	2.4106568533
H	0.0000000000	0.0000000000	-0.1603100495
N	0.0000000000	0.0000000000	-1.3214007314
C	0.0000000000	0.0000000000	-2.4988745718

Rotational Constants (GHz): 2.5343572, 2.5343572

Harmonic Vibrational Frequencies (cm^{-1}):

σ^+: $2827i$ 2153 2064 431

π: 871 185 62

Incremental Focal Point Analysis Table (kcal mol^{-1}):

Basis	ROHF	+δMP2	+δCCSD	+δ(T)	+δT	+δ(Q)	Net
aug-cc-pVDZ	+57.41	−40.72	+15.24	−5.37	+0.57	−0.26	[+26.86]
aug-cc-pVTZ	+58.41	−41.15	+16.25	−5.72	[+0.57]	[−0.26]	[+28.10]
aug-cc-pVQZ	+58.78	−41.06	+16.52	−5.82	[+0.57]	[−0.26]	[+28.73]
aug-cc-pV5Z	+58.85	−40.90	+16.57	−5.84	[+0.57]	[−0.26]	[+28.99]
CBS LIMIT	[+58.86]	[−40.72]	[+16.62]	[−5.86]	[+0.57]	[−0.26]	[+29.21]

$$\Delta H_{0K} = \Delta E_{CCSD(T)/CBS} + \delta_{ZPVE} + \delta_{T(Q)} + \delta_{CORE} + \delta_{REL} + \delta_{DBOC}$$
$$= 28.90 - 2.81 + 0.31 + 0.04 - 0.08 + 0.02 = 26.37 \text{ kcal mol}^{-1}$$

CN + HNC → HCN + CN

Level of Theory:

Reference: ROHF

Geometry: CCSD(T)-F12a/aug-cc-pVTZ

Frequencies: CCSD(T)-F12a/aug-cc-pVTZ

Program: Molpro 2010.1

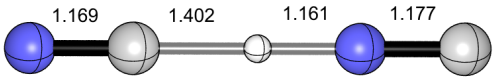

Figure A.45: TS (CN + HNC → HCN + CN)

Wavefunction Diagnostics:

T_1: 0.033

D_1: 0.154

Cartesian Coordinates (Å):

C	0.0000000000	0.0000000000	1.2420848948
N	0.0000000000	0.0000000000	2.4106568533
H	0.0000000000	0.0000000000	-0.1603100495
N	0.0000000000	0.0000000000	-1.3214007314
C	0.0000000000	0.0000000000	-2.4988745718

Rotational Constants (GHz): 2.5343572, 2.5343572

Harmonic Vibrational Frequencies (cm^{-1}):

σ^+: $2827i$ 2153 2064 431

π: 871 185 62

Incremental Focal Point Analysis Table (kcal mol^{-1}):

Basis	ROHF	+δMP2	+δCCSD	+δ(T)	+δT	+δ(Q)	Net
aug-cc-pVDZ	+47.44	−48.31	+18.46	−5.57	+0.73	−0.59	[+12.16]
aug-cc-pVTZ	+48.66	−49.12	+19.47	−6.06	[+0.73]	[−0.59]	[+13.08]
aug-cc-pVQZ	+49.13	−49.08	+19.78	−6.19	[+0.73]	[−0.59]	[+13.78]
aug-cc-pV5Z	+49.19	−48.97	+19.84	−6.22	[+0.73]	[−0.59]	[+13.98]
CBS LIMIT	[+49.20]	[−48.85]	[+19.90]	[−6.26]	[+0.73]	[−0.59]	[+14.13]

$$\Delta H_{0K} = \Delta E_{CCSD(T)/CBS} + \delta_{ZPVE} + \delta_{T(Q)} + \delta_{CORE} + \delta_{REL} + \delta_{DBOC}$$
$$= 13.99 - 2.83 + 0.14 + 0.04 - 0.08 + 0.02 = 11.27 \text{ kcal mol}^{-1}$$

CN + HNC → HNC + CN

Level of Theory:

Reference: ROHF

Geometry: CCSD(T)-F12a/aug-cc-pVTZ

Frequencies: CCSD(T)-F12a/aug-cc-pVTZ

Program: Molpro 2010.1

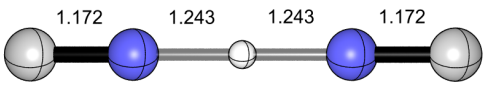

Figure A.46: TS (CN + HNC → HNC + CN)

Wavefunction Diagnostics:

T_1: 0.016

D_1: 0.039

Cartesian Coordinates (Å):

N	0.0000000000	0.0000000000	1.2433472207
C	0.0000000000	0.0000000000	2.4156903194
H	0.0000000000	0.0000000000	-0.0000000002
N	0.0000000000	0.0000000000	-1.2433472207
C	0.0000000000	0.0000000000	-2.4156903194

Rotational Constants (GHz):2.7542879, 2.7542879

Harmonic Vibrational Frequencies (cm^{-1}):

σ^+:	$4232i$	2131	2062	473
π:		1078	198	97

Incremental Focal Point Analysis Table (kcal mol^{-1}):

Basis	ROHF	+δMP2	+δCCSD	+δ(T)	+δT	+δ(Q)	Net
aug-cc-pVDZ	+51.07	−51.52	+21.84	−6.86	+1.12	−1.45	[+14.20]
aug-cc-pVTZ	+52.01	−52.62	+23.11	−7.35	[+1.12]	[−1.45]	[+14.83]
aug-cc-pVQZ	+52.53	−52.73	+23.41	−7.48	[+1.12]	[−1.45]	[+15.40]
aug-cc-pV5Z	+52.59	−52.58	+23.44	−7.50	[+1.12]	[−1.45]	[+15.63]
CBS LIMIT	[+52.59]	[−52.42]	[+23.48]	[−7.53]	[+1.12]	[−1.45]	[+15.80]

$$\Delta H_{0K} = \Delta E_{CCSD(T)/CBS} + \delta_{ZPVE} + \delta_{T(Q)} + \delta_{CORE} + \delta_{REL} + \delta_{DBOC}$$
$$= 16.13 - 2.08 - 0.33 + 0.06 + 0.00 + 0.07 = 13.85 \text{ kcal mol}^{-1}$$

Chapter B

Energetics and Kinetics of Various Cyano Radical Hydrogen Abstractions from Mid-Sized Donors: Supporting Information

Reactants

CN ($^2\Sigma^+$)

Level of Theory:

Reference: ROHF

Geometry: CCSD(T)-F12a/cc-pVTZ-F12

Frequencies: CCSD(T)-F12a/cc-pVTZ-F12

Program: Molpro 2010.1

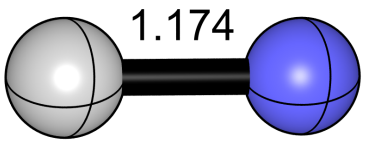

Figure B.1: CN

Wavefunction Diagnostics:

T_1: 0.043

D_1: 0.147

Cartesian Coordinates (Å):

C	0.0000000000	0.0000000000	-0.6318990142
N	0.0000000000	0.0000000000	0.5418648975

Rotational Constants (GHz): 56.7295827, 56.729827

Harmonic Vibrational Frequencies (cm^{-1}):

σ^+: 2069

HNCO

Level of Theory:

Reference:	RHF
Geometry:	CCSD(T)-F12a/cc-pVTZ-F12
Frequencies:	CCSD(T)-F12a/cc-pVTZ-F12
Program:	Molpro 2010.1

Wavefunction Diagnostics:

T_1: 0.015

D_1: 0.051

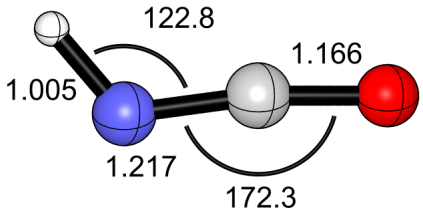

Figure B.2: HNCO

Cartesian Coordinates (Å):

N	0.0000000000	-0.0805830178	-1.2072193296
C	0.0000000000	0.0389685309	0.0042517563
H	0.0000000000	0.7064005187	-1.8321928650
O	0.0000000000	-0.0032100084	1.1690958170

Rotational Constants (GHz): $10.9207550, 11.0671927, 825.3482644$

Harmonic Vibrational Frequencies (cm^{-1}):

a':	3687	2304	1312	823	570
a'':					633

HOCN

Level of Theory:

Reference:	RHF
Geometry:	CCSD(T)-F12a/cc-pVTZ-F12
Frequencies:	CCSD(T)-F12a/cc-pVTZ-F12
Program:	Molpro 2010.1

Wavefunction Diagnostics:

T_1: 0.013

D_1: 0.034

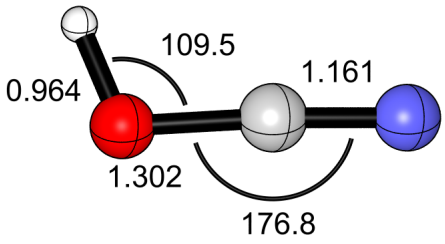

Figure B.3: HOCN

Cartesian Coordinates (Å):

H	-0.8272763892	0.0000000000	-1.5265026461
O	0.0626978984	0.0000000000	-1.1554868333
C	-0.0076924426	0.0000000000	0.1448694170
N	-0.0054895060	0.0000000000	1.3054961233

Rotational Constants (GHz): 10.5652042, 10.4012845, 670.3998303

Harmonic Vibrational Frequencies (cm^{-1}):

a':	3803	2327	1266	1081	432
a'':					491

trans−HONO

Level of Theory:

Reference:	RHF
Geometry:	CCSD(T)-F12a/cc-pVTZ-F12
Frequencies:	CCSD(T)-F12a/cc-pVTZ-F12
Program:	Molpro 2010.1

Wavefunction Diagnostics:

T_1: 0.018

D_1: 0.059

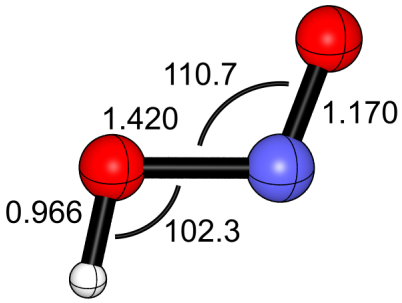

Figure B.4: *trans*-HONO

Cartesian Coordinates (Å):

O	0.0000000000	0.2389954013	-1.0581505977
N	0.0000000000	-0.4950235781	-0.1465575416
O	0.0000000000	0.2249056778	1.0772857181
H	0.0000000000	-0.4846440999	1.7328780214

Rotational Constants (GHz): 11.1804445, 12.6948300, 93.7237218

Harmonic Vibrational Frequencies (cm^{-1}):

a':	3780	1733	1319	835	635
a'':					573

Products

HCN

Level of Theory:

Reference: RHF

Geometry: CCSD(T)-F12a/cc-pVTZ-F12

Frequencies: CCSD(T)-F12a/cc-pVTZ-F12

Program: Molpro 2010.1

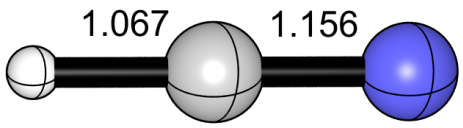

Figure B.5: HCN

Wavefunction Diagnostics:

T_1: 0.013

D_1: 0.031

Cartesian Coordinates (Å):

C	0.0000000000	0.0000000000	-0.5591192471
N	0.0000000000	0.0000000000	0.5964610701
H	0.0000000000	0.0000000000	-1.6259598727

Rotational Constants (GHz): 44.3211780, 44.3211780

Harmonic Vibrational Frequencies (cm^{-1}):

σ^+: 3436 2125

π: 728

HNC

Level of Theory:

Reference: RHF

Geometry: CCSD(T)-F12a/cc-pVTZ-F12

Frequencies: CCSD(T)-F12a/cc-pVTZ-F12

Program: Molpro 2010.1

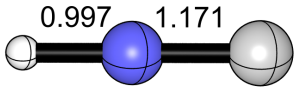

Figure B.6: HNC

Wavefunction Diagnostics:

T_1: 0.014

D_1: 0.033

Cartesian Coordinates (Å):

N	0.0000000000	0.0000000000	-0.4833928329
C	0.0000000000	0.0000000000	0.6879182209
H	0.0000000000	0.0000000000	-1.4800954013

Rotational Constants (GHz): 45.2646325, 45.2646325

Harmonic Vibrational Frequencies (cm^{-1}):

σ^+: 3810 2053

π: 462

NCO

Level of Theory:

Reference: ROHF

Geometry: CCSD(T)-F12a/cc-pVTZ-F12

Frequencies: CCSD(T)-F12a/cc-pVTZ-F12

Program: Molpro 2010.1

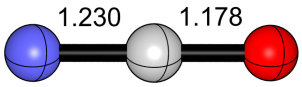

Figure B.7: NCO

Wavefunction Diagnostics:

T_1: 0.028

D_1: 0.109

Cartesian Coordinates (Å):

N	0.0000000000	0.0000000000	-1.2680494213
C	0.0000000000	0.0000000000	-0.0385048718
O	0.0000000000	0.0000000000	1.1390220786

Rotational Constants (GHz): 11.6723698, 11.6723698

Harmonic Vibrational Frequencies (cm^{-1}):

σ^+: 1977 1269

π: 581 503

NO_2

Level of Theory:

Reference:	ROHF
Geometry:	CCSD(T)-F12a/cc-pVTZ-F12
Frequencies:	CCSD(T)-F12a/cc-pVTZ-F12
Program:	Molpro 2010.1

Wavefunction Diagnostics:

T_1: 0.022

D_1: 0.065

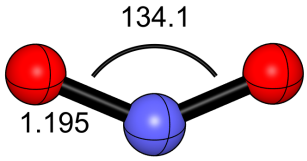

Figure B.8: NO_2

Cartesian Coordinates (Å):

N	0.0000000000	0.0000000000	-0.3242150824
O	0.0000000000	1.1003698053	0.1419173030
O	0.0000000000	-1.1003698053	0.1419173030

Rotational Constants (GHz): $12.3681338, 238.7475191, 13.0438611$

Harmonic Vibrational Frequencies (cm^{-1}):

a_1:	1359	763
b_2:		1682

Pre-Reactive Complexes

CN + HNCO → HCN + NCO

Level of Theory:

Reference:	ROHF
Geometry:	CCSD(T)-F12a/cc-pVTZ-F12
Frequencies:	CCSD(T)-F12a/cc-pVTZ-F12
Program:	Molpro 2010.1

Wavefunction Diagnostics:

T_1: 0.026

D_1: 0.122

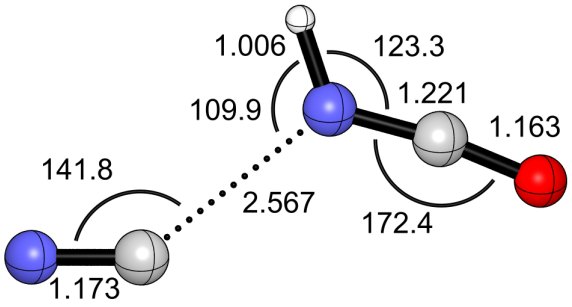

Figure B.9: PRC (CN + HNCO → HCN + NCO)

Cartesian Coordinates (Å):

N	0.0000000000	-0.0971330461	-3.0127853593
C	0.0000000000	-0.3604822803	-1.8698517046
N	0.0000000000	0.7341899031	0.4523336409
H	0.0000000000	1.7359520564	0.3591754879
C	0.0000000000	0.1607888320	1.5298778426
O	0.0000000000	-0.5170322787	2.4746058723

Rotational Constants (GHz): 1.6026585, 1.6932769, 29.9469455

Harmonic Vibrational Frequencies (cm^{-1}):

a': 3671 2299 2075 1309 846 579 116 69 51

a'': 629 57

Incremental Focal Point Analysis Table (kcal mol^{-1}):

Basis	ROHF	+δMP2	+δCCSD	+δ(T)	+δT	+δ(Q)	Net
aug-cc-pVDZ	−0.71	−2.53	+1.18	−0.43	+0.15	−0.05	[−2.39]
aug-cc-pVTZ	−0.46	−2.66	+1.20	−0.39	[+0.15]	[−0.05]	[−2.21]
aug-cc-pVQZ	−0.39	−2.61	+1.21	−0.38	[+0.15]	[−0.05]	[−2.07]
aug-cc-pV5Z	−0.37	−2.55	+1.20	−0.37	[+0.15]	[−0.05]	[−1.99]
CBS LIMIT	[−0.36]	[−2.48]	[+1.19]	[−0.36]	[+0.15]	[−0.05]	[−1.93]

$$\Delta H_{0K} = \Delta E_{CCSD(T)/CBS} + \delta_{ZPVE} + \delta_{T(Q)} + \delta_{CORE} + \delta_{REL} + \delta_{DBOC}$$
$$= 2.02 + 0.38 + 0.09 - 0.02 + 0.01 + 0.00 = -1.56 \text{ kcal mol}^{-1}$$

$CN + HNCO \rightarrow HNC + NCO$

Level of Theory:

Reference:	ROHF
Geometry:	CCSD(T)-F12a/cc-pVTZ-F12
Frequencies:	CCSD(T)-F12a/cc-pVTZ-F12
Program:	MOLPRO 2010.1

Wavefunction Diagnostics:

T_1: 0.026

D_1: 0.129

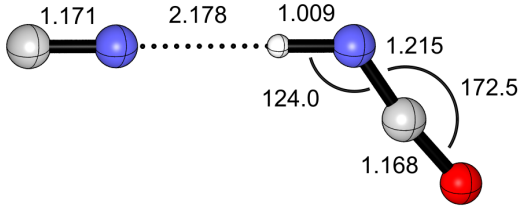

Figure B.10: PRC ($CN + HNCO \rightarrow HNC + NCO$)

Cartesian Coordinates (Å):

N	-0.0132963371	0.0000000000	2.3043704471
C	-0.3304701016	0.0000000000	3.4311215865
H	0.5767988330	0.0000000000	0.2080734655
N	0.8501092141	0.0000000000	-0.7628542019
C	0.0641888837	0.0000000000	-1.6888955121
O	-0.5690252029	0.0000000000	-2.6705475543

Rotational Constants (GHz): 1.3573145, 1.2980424, 29.7248330

Harmonic Vibrational Frequencies (cm^{-1}):

a':	2303	2090	1314	838	603	114	83	52
a'':						3620	640	299

Incremental Focal Point Analysis Table (kcal mol^{-1}):

Basis	ROHF	$+\delta$MP2	$+\delta$CCSD	$+\delta$(T)	$+\delta$T	$+\delta$(Q)	Net
aug-cc-pVDZ	−3.11	−0.61	+0.60	−0.08	+0.06	+0.01	[−3.13]
aug-cc-pVTZ	−3.12	−0.69	+0.61	−0.03	[+0.06]	[+0.01]	[−3.15]
aug-cc-pVQZ	−3.00	−0.57	+0.62	−0.01	[+0.06]	[+0.01]	[−2.89]
aug-cc-pV5Z	−2.98	−0.49	+0.61	+0.00	[+0.06]	[+0.01]	[−2.79]
CBS LIMIT	[−2.98]	[−0.40]	[+0.59]	[+0.02]	[+0.06]	[+0.01]	[−2.70]

$$\Delta H_{0K} = \Delta E_{CCSD(T)/CBS} + \delta_{ZPVE} + \delta_{T(Q)} + \delta_{CORE} + \delta_{REL} + \delta_{DBOC}$$
$$= -2.77 + 0.80 + 0.07 - 0.04 + 0.02 + 0.03 = -1.89 \text{ kcal mol}^{-1}$$

$CN + \textit{trans}-HONO \rightarrow HNC + NO_2$

Level of Theory:

Reference:	ROHF
Geometry:	CCSD(T)-F12a/cc-pVTZ-F12
Frequencies:	CCSD(T)-F12a/cc-pVTZ-F12
Program:	MOLPRO 2010.1

Wavefunction Diagnostics:

T_1: 0.027

D_1: 0.129

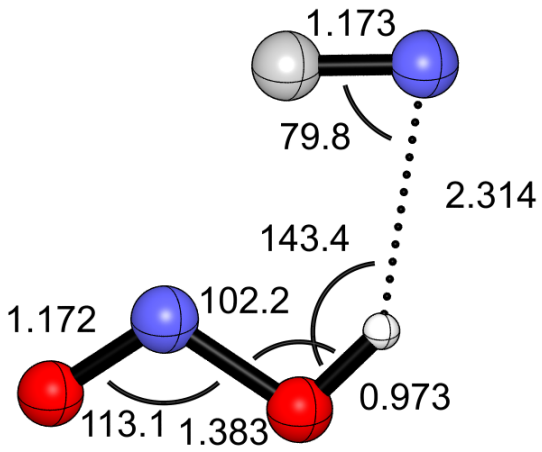

Figure B.11: PRC ($CN + t$–$HONO \rightarrow HNC + NO_2$)

Cartesian Coordinates (Å):

C	0.0000000000	-0.7477995205	1.5819834910
N	0.0000000000	0.1631974603	2.3212097775
H	0.0000000000	1.2794004208	0.2936717693
O	0.0000000000	1.1470957079	-0.6706138461
N	0.0000000000	-0.2316087147	-0.7771281405
O	0.0000000000	-0.6064206140	-1.8872755435

Rotational Constants (GHz): 2.3540707, 2.8351308, 13.8737294

Harmonic Vibrational Frequencies (cm^{-1}):

a':	3661	2069	1735	1383	893	683	208	118
a'':						673	150	96

Incremental Focal Point Analysis Table (kcal mol^{-1}):

Basis	ROHF	+δMP2	+δCCSD	+δ(T)	+δT	+δ(Q)	Net
aug-cc-pVDZ	+0.25	−3.45	+1.53	−0.86	+0.06	−0.05	[−2.51]
aug-cc-pVTZ	+0.37	−4.09	+1.63	−0.83	[+0.06]	[−0.05]	[−2.91]
aug-cc-pVQZ	+0.43	−4.15	+1.66	−0.83	[+0.06]	[−0.05]	[−2.87]
aug-cc-pV5Z	+0.47	−4.09	+1.64	−0.82	[+0.06]	[−0.05]	[−2.78]
CBS LIMIT	[+0.49]	[−4.03]	[+1.63]	[−0.81]	[+0.06]	[−0.05]	[−2.71]

$$\Delta H_{0K} = \Delta E_{CCSD(T)/CBS} + \delta_{ZPVE} + \delta_{T(Q)} + \delta_{CORE} + \delta_{REL} + \delta_{DBOC}$$
$$= -2.73 + 1.04 + 0.02 - 0.09 + 0.05 - 0.01 = -1.72 \text{ kcal mol}^{-1}$$

Post-Reactive Complexes

CN + *trans*−HONO → HCN + NO_2

Level of Theory:

Reference:	ROHF
Geometry:	CCSD(T)-F12a/cc-pVTZ-F12
Frequencies:	CCSD(T)-F12a/cc-pVTZ-F12
Program:	Molpro 2010.1

Wavefunction Diagnostics:

T_1: 0.019

D_1: 0.065

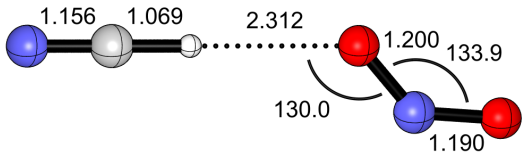

Figure B.12: PRC (CN + *t*−HONO → $HCN + NO_2$)

Cartesian Coordinates (Å):

C	-0.0142681307	0.0000000000	2.5305630830
N	0.1598644258	0.0000000000	3.6731904427
H	-0.1753025228	0.0000000000	1.4738835852
O	-0.5235789635	0.0000000000	-0.8114454644
N	0.2689560164	0.0000000000	-1.7119747306
O	0.1699225548	0.0000000000	-2.8980898634

Rotational Constants (GHz): 1.1330418, 1.0979228, 80.8276926

Harmonic Vibrational Frequencies (cm^{-1}):

a':	3412	2123	1684	1361	768	759	91	75
a'':							759	81

Incremental Focal Point Analysis Table (kcal mol^{-1}):

Basis	ROHF	+δMP2	+δCCSD	+δ(T)	+δT	+δ(Q)	Net
aug-cc-pVDZ	−42.86	−15.42	+14.37	−1.57	+0.82	−0.28	[−44.92]
aug-cc-pVTZ	−44.43	−16.06	+13.79	−1.43	[+0.82]	[−0.28]	[−47.59]
aug-cc-pVQZ	−44.38	−16.16	+13.69	−1.40	[+0.82]	[−0.28]	[−47.71]
aug-cc-pV5Z	−44.37	−16.15	+13.62	−1.39	[+0.82]	[−0.28]	[−47.74]
CBS LIMIT	[−44.37]	[−16.14]	[+13.56]	[−1.38]	[+0.82]	[−0.28]	[−47.78]

$$\Delta H_{0K} = \Delta E_{CCSD(T)/CBS} + \delta_{ZPVE} + \delta_{T(Q)} + \delta_{CORE} + \delta_{REL} + \delta_{DBOC}$$
$$= -48.33 + 0.24 + 0.55 - 0.66 + 0.10 + 0.02 = -48.07 \text{ kcal mol}^{-1}$$

$CN + \textit{trans}-HONO \rightarrow HNC + NO_2$

Level of Theory:

Reference:	ROHF
Geometry:	CCSD(T)-F12a/cc-pVTZ-F12
Frequencies:	CCSD(T)-F12a/cc-pVTZ-F12
Program:	MOLPRO 2010.1

Wavefunction Diagnostics:

T_1: 0.019

D_1: 0.065

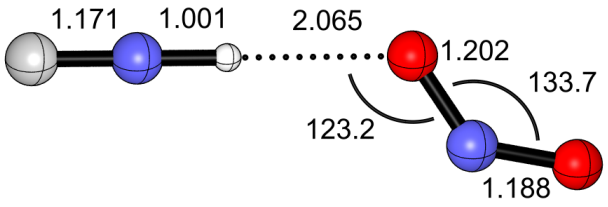

Figure B.13: PRC (CN + t–HONO → HNC + NO_2)

Cartesian Coordinates (Å):

N	0.0049624038	0.0000000000	2.3255496470
C	-0.2245776482	0.0000000000	3.4738527052
H	0.2012536546	0.0000000000	1.3435779104
O	0.6060948080	0.0000000000	-0.6816910145
N	-0.2510489099	0.0000000000	-1.5243627547
O	-0.2347427330	0.0000000000	-2.7122284579

Rotational Constants (GHz): 1.3292749, 1.3009130, 60.9716525

Harmonic Vibrational Frequencies (cm^{-1}):

a':	3725	2056	1686	1359	769	582	124	103
a'':						570	109	55

Incremental Focal Point Analysis Table (kcal mol^{-1}):

Basis	ROHF	+δMP2	+δCCSD	+δ(T)	+δT	+δ(Q)	Net
aug-cc-pVDZ	−33.63	−8.47	+11.35	−1.42	+0.67	+0.04	[−31.46]
aug-cc-pVTZ	−35.21	−8.79	+10.78	−1.16	[+0.67]	[+0.04]	[−33.68]
aug-cc-pVQZ	−35.27	−8.82	+10.64	−1.10	[+0.67]	[+0.04]	[−33.83]
aug-cc-pV5Z	−35.25	−8.72	+10.57	−1.07	[+0.67]	[+0.04]	[−33.76]
CBS LIMIT	[−35.24]	[−8.62]	[+10.49]	[−1.05]	[+0.67]	[+0.04]	[−33.70]

$$\Delta H_{0K} = \Delta E_{CCSD(T)/CBS} + \delta_{ZPVE} + \delta_{T(Q)} + \delta_{CORE} + \delta_{REL} + \delta_{DBOC}$$
$$= -34.41 + 0.28 + 0.71 - 0.47 + 0.14 + 0.00 = -33.75 \text{ kcal mol}^{-1}$$

Transition States

CN + HNCO → HCN + NCO

Level of Theory:

Reference:	ROHF
Geometry:	CCSD(T)-F12a/cc-pVTZ-F12
Frequencies:	CCSD(T)-F12a/cc-pVTZ-F12
Program:	Molpro 2010.1

Wavefunction Diagnostics:

T_1: 0.025

D_1: 0.117

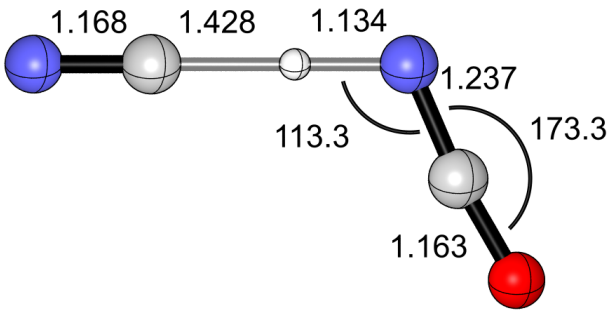

Figure B.14: TS (CN + HNCO → HCN + NCO)

Cartesian Coordinates (Å):

C	0.0371787605	0.0000000000	1.8138519943
N	-0.3878228626	0.0000000000	2.9020809460
H	0.5566956144	0.0000000000	0.4836140593
N	0.9693833820	0.0000000000	-0.5730849092
C	0.0886472995	0.0000000000	-1.4417797389
O	-0.6386587191	0.0000000000	-2.3487107394

Rotational Constants (GHz): 1.8341026, 1.6972481, 22.7462455

Harmonic Vibrational Frequencies (cm^{-1}):

a':	2183	2143	1361i	1309	910	696	488	199	69
a'':							596	502	148

Incremental Focal Point Analysis Table (kcal mol^{-1}):

Basis	ROHF	+δMP2	+δCCSD	+δ(T)	+δT	+δ(Q)	Net
aug-cc-pVDZ	+25.14	−20.45	+5.81	−2.58	+0.47	−0.45	[+7.94]
aug-cc-pVTZ	+25.81	−21.03	+6.30	−2.76	[+0.47]	[−0.45]	[+8.33]
aug-cc-pVQZ	+26.13	−20.78	+6.46	−2.80	[+0.47]	[−0.45]	[+9.03]
aug-cc-pV5Z	+26.18	−20.61	+6.47	−2.80	[+0.47]	[−0.45]	[+9.25]
CBS LIMIT	[+26.18]	[−20.44]	[+6.49]	[−2.80]	[+0.47]	[−0.45]	[+9.45]

$$\Delta H_{0K} = \Delta E_{CCSD(T)/CBS} + \delta_{ZPVE} + \delta_{T(Q)} + \delta_{CORE} + \delta_{REL} + \delta_{DBOC}$$
$$= 9.43 - 3.08 + 0.02 + 0.06 - 0.20 + 1.62 = 7.85 \text{ kcal mol}^{-1}$$

CN + HNCO → HNC + NCO

Level of Theory:

Reference:	ROHF
Geometry:	CCSD(T)-F12a/cc-pVTZ-F12
Frequencies:	CCSD(T)-F12a/cc-pVTZ-F12
Program:	MOLPRO 2010.1

Wavefunction Diagnostics:

T_1: 0.026

D_1: 0.128

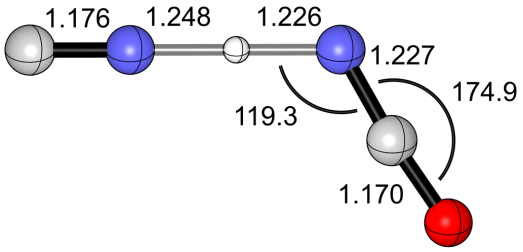

Figure B.15: TS (CN + HNCO → HNC + NCO)

Cartesian Coordinates (Å):

N	0.0050163224	0.0000000000	1.8379016731
C	-0.4132630546	0.0000000000	2.9373304391
H	0.4489387886	0.0000000000	0.6710711864
N	0.8849276522	0.0000000000	-0.4749061785
C	0.0974060592	0.0000000000	-1.4163411846
O	-0.5702665887	0.0000000000	-2.3773435516

Rotational Constants (GHz): 1.8782095, 1.7571351, 27.2581898

Harmonic Vibrational Frequencies (cm^{-1}):

a':	$3439i$	2114	2044	1306	1015	669	459	156	66
a'':							754	599	114

Incremental Focal Point Analysis Table (kcal mol^{-1}):

Basis	ROHF	+δMP2	+δCCSD	+δ(T)	+δT	+δ(Q)	Net
aug-cc-pVDZ	+41.67	−38.05	+16.01	−5.10	+0.96	−1.10	[+14.39]
aug-cc-pVTZ	+42.26	−38.75	+16.82	−5.45	[+0.96]	[−1.10]	[+14.73]
aug-cc-pVQZ	+42.72	−38.65	+17.11	−5.55	[+0.96]	[−1.10]	[+15.49]
aug-cc-pV5Z	+42.79	−38.46	+17.16	−5.57	[+0.96]	[−1.10]	[+15.77]
CBS LIMIT	[+42.80]	[−38.26]	[+17.20]	[−5.59]	[+0.96]	[−1.10]	[+16.01]

$$\Delta H_{0K} = \Delta E_{CCSD(T)/CBS} + \delta_{ZPVE} + \delta_{T(Q)} + \delta_{CORE} + \delta_{REL} + \delta_{DBOC}$$
$$= 16.15 - 3.01 - 0.14 + 0.15 - 0.07 + 0.24 = 13.33 \text{ kcal mol}^{-1}$$

CN + HOCN → HCN + NCO

Level of Theory:

Reference:	ROHF
Geometry:	CCSD(T)-F12a/cc-pVTZ-F12
Frequencies:	CCSD(T)-F12a/cc-pVTZ-F12
Program:	Molpro 2010.1

Wavefunction Diagnostics:

T_1: 0.034

D_1: 0.184

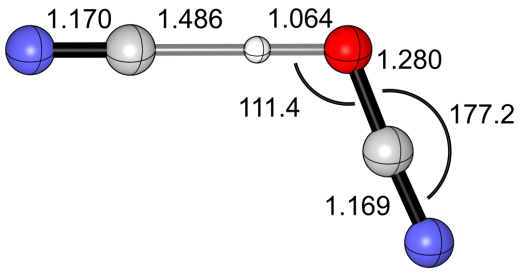

Figure B.16: TS (CN + HOCN → HCN + NCO)

Cartesian Coordinates (Å):

C	0.0243240242	0.0000000000	1.7415399022
N	-0.4075222113	0.0000000000	2.8293615972
H	0.5725646225	0.0000000000	0.3605205305
O	0.9652868015	0.0000000000	-0.6287475730
C	0.0302629987	0.0000000000	-1.5024939718
N	-0.7831055005	0.0000000000	-2.3420933481

Rotational Constants (GHz): 1.9515750, 1.7724398, 19.3097192

Harmonic Vibrational Frequencies (cm^{-1}):

a': 2240 2134i 2128 1202 1110 591 425 172 56

a'': 531 497 141

Incremental Focal Point Analysis Table (kcal mol^{-1}):

Basis	ROHF	+δMP2	+δCCSD	+δ(T)	+δT	+δ(Q)	Net
aug-cc-pVDZ	+26.92	−20.53	+4.14	−3.23	+0.27	−0.97	[+6.62]
aug-cc-pVTZ	+27.01	−20.92	+4.53	−3.51	[+0.27]	[−0.97]	[+6.41]
aug-cc-pVQZ	+27.33	−20.69	+4.69	−3.57	[+0.27]	[−0.97]	[+7.07]
aug-cc-pV5Z	+27.39	−20.52	+4.71	−3.58	[+0.27]	[−0.97]	[+7.30]
CBS LIMIT	[+27.40]	[−20.33]	[+4.72]	[−3.60]	[+0.27]	[−0.97]	[+7.50]

$$\Delta H_{0K} = \Delta E_{CCSD(T)/CBS} + \delta_{ZPVE} + \delta_{T(Q)} + \delta_{CORE} + \delta_{REL} + \delta_{DBOC}$$
$$= 8.19 - 3.40 - 0.69 - 0.03 - 0.03 + 0.18 = 4.22 \text{ kcal mol}^{-1}$$

$CN + \textit{trans}-HONO \rightarrow HCN + NO_2$

Level of Theory:

Reference: ROHF

Geometry: CCSD(T)-F12a/cc-pVTZ-F12

Frequencies: CCSD(T)-F12a/cc-pVTZ-F12

Program: MOLPRO 2010.1

Wavefunction Diagnostics:

T_1: 0.029

D_1: 0.135

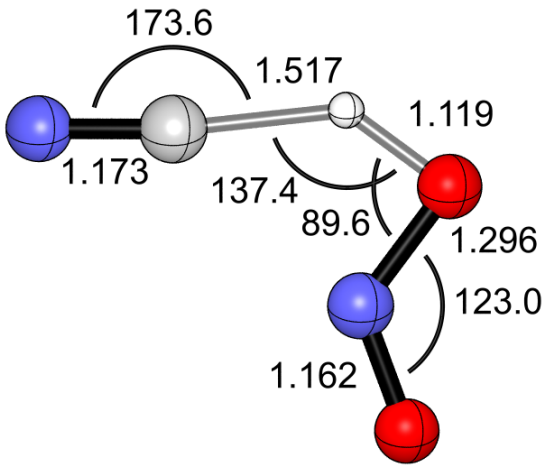

Figure B.17: TS (CN + *t*-HONO → HCN + NO_2)

Cartesian Coordinates (Å):

C	0.0000000000	0.2239344140	1.4415028162
N	0.0000000000	-0.4157840984	2.4245323474
H	0.0000000000	1.1878950060	0.2699870264
O	0.0000000000	1.1262654871	-0.8472682816
N	0.0000000000	-0.1673825523	-0.7677813704
O	0.0000000000	-0.8586781284	-1.7023045124

Rotational Constants (GHz): 2.4019474, 2.9132878, 13.6847477

Harmonic Vibrational Frequencies (cm^{-1}):

a':	2194i	2091	2013	1805	1178	848	458	332	117
a'':							1115	288	155

Incremental Focal Point Analysis Table (kcal mol^{-1}):

Basis	ROHF	+δMP2	+δCCSD	+δ(T)	+δT	+δ(Q)	Net
aug-cc-pVDZ	+31.93	−29.52	+15.11	−4.59	+0.46	−0.95	[+12.45]
aug-cc-pVTZ	+31.37	−30.67	+15.27	−4.71	[+0.46]	[−0.95]	[+10.78]
aug-cc-pVQZ	+31.61	−30.81	+15.36	−4.78	[+0.46]	[−0.95]	[+10.89]
aug-cc-pV5Z	+31.67	−30.71	+15.33	−4.79	[+0.46]	[−0.95]	[+11.01]
CBS LIMIT	[+31.70]	[−30.61]	[+15.30]	[−4.80]	[+0.46]	[−0.95]	[+11.10]

$$\Delta H_{0K} = \Delta E_{CCSD(T)/CBS} + \delta_{ZPVE} + \delta_{T(Q)} + \delta_{CORE} + \delta_{REL} + \delta_{DBOC}$$
$$= 11.59 - 0.78 - 0.49 - 0.29 + 0.05 + 0.03 = 10.12 \text{ kcal mol}^{-1}$$

$CN + \textit{trans}-HONO \rightarrow HNC + NO_2$

Level of Theory:

Reference:	ROHF
Geometry:	CCSD(T)-F12a/cc-pVTZ-F12
Frequencies:	CCSD(T)-F12a/cc-pVTZ-F12
Program:	MOLPRO 2010.1

Wavefunction Diagnostics:

T_1: 0.028

D_1: 0.129

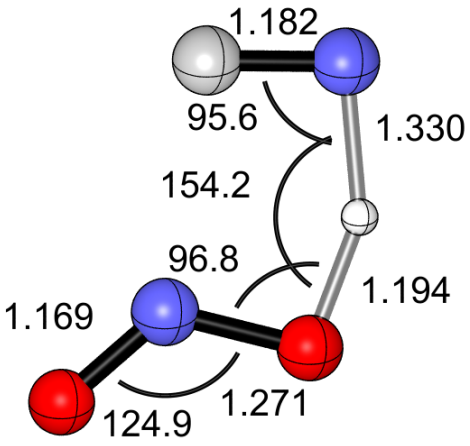

Figure B.18: TS (CN + *t*-HONO → HNC + NO_2)

Cartesian Coordinates (Å):

C	-0.8865914232	0.0000000000	-1.3447181912
N	0.1426495322	0.0000000000	-1.9252831565
H	0.9059513024	0.0000000000	-0.8360483000
O	1.0971629435	0.0000000000	0.3424308986
N	-0.1250416230	0.0000000000	0.6926781573
O	-0.5040734322	0.0000000000	1.7988259711

Rotational Constants (GHz): 3.7516223, 2.9938317, 14.8216743

Harmonic Vibrational Frequencies (cm^{-1}):

a':	2029	1779i	1761	1581	1224	834	515	366	165
a'':							1101	296	180

Incremental Focal Point Analysis Table (kcal mol^{-1}):

Basis	ROHF	+δMP2	+δCCSD	+δ(T)	+δT	+δ(Q)	Net
aug-cc-pVDZ	+28.43	−26.77	+13.59	−5.04	+0.25	−0.48	[+9.98]
aug-cc-pVTZ	+27.89	−28.26	+13.69	−5.10	[+0.25]	[−0.48]	[+7.99]
aug-cc-pVQZ	+28.08	−28.55	+13.69	−5.18	[+0.25]	[−0.48]	[+7.80]
aug-cc-pV5Z	+28.14	−28.47	+13.62	−5.18	[+0.25]	[−0.48]	[+7.88]
CBS LIMIT	[+28.17]	[−28.38]	[+13.54]	[−5.19]	[+0.25]	[−0.48]	[+7.91]

$$\Delta H_{0K} = \Delta E_{CCSD(T)/CBS} + \delta_{ZPVE} + \delta_{T(Q)} + \delta_{CORE} + \delta_{REL} + \delta_{DBOC}$$
$$= 8.14 - 1.27 - 0.23 - 0.28 + 0.12 + 0.15 = 6.64 \text{ kcal mol}^{-1}$$

cis−HONO → *trans*−HONO

Level of Theory:

Reference:	ROHF
Geometry:	CCSD(T)-F12a/cc-pVTZ-F12
Frequencies:	CCSD(T)-F12a/cc-pVTZ-F12
Program:	Molpro 2010.1

Wavefunction Diagnostics:

T_1: 0.020

D_1: 0.055

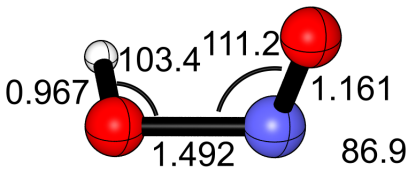

Figure B.19: TS (*c*-HONO → *trans*-HONO)

Cartesian Coordinates (Å):

O	0.0045185894	0.2738091964	-1.0531912164
N	-0.0180740089	-0.5095275327	-0.1959315342
O	0.0652811830	0.1499766463	1.1398108755
H	-0.8567943095	0.3536719259	1.3477901922

Rotational Constants (GHz):10.9334590, 12.1152392, 82.3782869

Harmonic Vibrational Frequencies (cm^{-1}):

a: 3773 1731 1120 788 $596i$ 555

Incremental Focal Point Analysis Table (kcal mol^{-1}):

Basis	ROHF	+δMP2	+δCCSD	+δ(T)	+δT	+δ(Q)	Net
aug-cc-pVDZ	+11.75	+0.19	−0.81	+0.21	+0.09	+0.01	[+11.43]
aug-cc-pVTZ	+11.58	+0.32	−0.70	+0.19	[+0.09]	[+0.01]	[+11.50]
aug-cc-pVQZ	+11.64	+0.43	−0.67	+0.19	[+0.09]	[+0.01]	[+11.68]
aug-cc-pV5Z	+11.65	+0.45	−0.66	+0.19	[+0.09]	[+0.01]	[+11.72]
CBS LIMIT	[+11.65]	[+0.48]	[−0.65]	[+0.18]	[+0.09]	[+0.01]	[+11.75]

$$\Delta H_{0K} = \Delta E_{CCSD(T)/CBS} + \delta_{ZPVE} + \delta_{T(Q)} + \delta_{CORE} + \delta_{REL} + \delta_{DBOC}$$
$$= 11.65 - 1.30 + 0.10 + 0.05 - 0.03 + 0.01 = 10.49 \text{ kcal mol}^{-1}$$

Bibliography

[1] Schrödinger, E. *Phys. Rev.* **1926**, *28*, 1049.

[2] Born, M.; Oppenheimer, R. *Ann. Phys.* **1927**, *389*, 457–484.

[3] Pauli, W. *Z. Phys.* **1925**, *31*, 765–783.

[4] Slater, J. C. *Phys. Rev.* **1929**, *34*, 1293.

[5] Roothan, C. C. J. *Rev. Mod. Phys.* **1951**, *23*, 69.

[6] Pople, J.; Nesbet, R. *J. Chem. Phys.* **1954**, *22*, 571–572.

[7] Roothan, C. C. J. *Rev. Mod. Phys.* **1960**, *32*, 179.

[8] Segal, G. A. *J. Chem. Phys.* **1970**, *52*, 3530–3533.

[9] Boys, S. F. *Proc. R. Soc. Lond. A* **1950**, *200*, 542–554.

[10] Raffenetti, R. C. *J. Chem. Phys.* **1973**, *58*, 4452–4458.

[11] Hehre, W. J.; Stewart, R. F.; Pople, J. A. *J. Chem. Phys.* **1969**, *51*, 2657–2664.

[12] Hariharan, P. C.; Pople, J. A. *Theor. Chim. Acta* **1973**, *28*, 213–222.

[13] Dunning, T. H. *J. Chem. Phys.* **1989**, *90*, 1007–1023.

[14] Dunning, T. H.; Peterson, K. A.; Wilson, A. K. *J. Chem. Phys.* **2001**, *114*, 9244–9253.

[15] Sherrill, C. D.; Schaefer III, H. F. *Adv. Quant. Chem.* **1999**, *34*, 143–269.

[16] Langhoff, S. R.; Davidson, E. R. *Int. J. Quant. Chem.* **1974**, *8*, 61–72.

[17] Čížek, J. *J. Chem. Phys.* **1966**, *45*, 4256–4266.

[18] Noga, J.; Bartlett, R. J. *J. Chem. Phys.* **1987**, *86*, 7041–7050.

[19] Raghavachari, K.; Trucks, G. W.; Pople, J. A.; Head-Gordon, M. *Chem. Phys. Lett.* **1989**, *157*, 479–483.

[20] Tajti, A.; Szalay, P. G.; Császár, A. G.; Kállay, M.; Gauss, J.; Valeev, E. F.; Flowers, B. A.; Vázquez, J.; Stanton, J. F. *J. Chem. Phys.* **2004**, *121*, 11599–11613.

[21] Boese, A. D.; Oren, M.; Atasoylu, A.; Martin, J. M. L.; Kállay, M.; Gauss, J. *J. Chem. Phys.* **2004**, *120*, 4129–4141.

[22] Karton, A.; Rabinovich, E.; Martin, J. M. L.; Ruscic, B. *J. Chem. Phys.* **2006**, *125*, 114108.

[23] East, A. L. L.; Allen, W. D. *J. Chem. Phys.* **1993**, *99*, 4638–4650.

[24] Császár, A. G.; Allen, W. D.; Schaefer III, H. F. *J. Chem. Phys.* **1998**, *108*, 9751–9764.

[25] Martin, J. M. L.; de Oliveira, G. *J. Chem. Phys.* **1999**, *111*, 1843–1856.

[26] Feller, D. *J. Chem. Phys.* **1993**, *98*, 7059.

[27] Helgaker, T.; Klopper, W.; Koch, H.; Noga, J. *J. Chem. Phys.* **1997**, *106*, 9639.

[28] Klippenstein, S. J.; Harding, L. B.; Ruscic, B. *J. Chem. Phys. A* **2017**, *121*, 6580–6602.

[29] Valeev, E. F.; Sherrill, C. D. *J. Chem. Phys.* **2003**, *118*, 3921–3927.

[30] Bartlett, M. A.; Liang, T.; Pu, L.; Schaefer III, H. F.; Allen, W. D. *J. Chem. Phys.* **2018**, *148*, 094303.

[31] Truhlar, D. G.; Garrett, B. C.; Klippenstein, S. J. *J. Phys. Chem.* **1996**, *100*, 12771–12800.

[32] Eyring, H. *J. Chem. Phys.* **1935**, *3*, 107–115.

[33] Cramer, C. J. *Essentials of Computational Chemistry: Theories and Models*; John Wiley and Sons, Ltd., 2004; pp 524–547.

[34] Wigner, E. P. *Z. Phys. Chem.* **1932**, *19*, 203–216.

[35] Ecakart, C. *Phys. Rev.* **1930**, *35*, 1303.

[36] Skodje, R. T.; Truhlar, D. G.; Garrett, B. C. *J. Phys. Chem.* **1981**, *85*, 3019–3023.

[37] Johnston, H. S.; Heicklen, J. *J. Phys. Chem.* **1962**, *66*, 532–533.

[38] Zhang, F.; Dibble, T. S. *Phys. Chem. Chem. Phys.* **2011**, *13*, 17969–17977.

[39] Sirjean, B.; Dames, E.; Wang, H.; Tsang, W. *J. Phys. Chem. A* **2012**, *116*, 319–332.

[40] Sha, Y.; Dibble, T. S. *J. Phys. Chem. A* **2012**, *116*, 319–332.

[41] Burke, A. D.; Bowman, M. C.; Turney, J. M.; Schaefer III, H. F. *Phys. Chem. Chem. Phys.* **2021**, *23*, 3389–3400.

[42] Bowman, M. C.; Burke, A. D.; Turney, J. M.; Schaefer III, H. F. *Mol. Phys.* **2020**, *118*, e1769214.

[43] Gopalsamy, K.; Thripati, S.; Ramabhadran, R. O. *ACS Earth Sp. Chem.* **2019**, *3*, 1080–1095.

[44] McKellar, A. *Publ. Astron. Soc. Pac.* **1940**, *52*, 187–192.

[45] Clarke, D. W.; Ferris, J. P. *Orig. Life Evol. Biosph.* **1997**, *27*, 225–248.

[46] Fukuzawa, K.; Osamura, Y.; Schaefer, H. F. *Astrophys. J.* **1998**, *505*, 278.

[47] Huang, L. C. L.; Asvany, O.; Chang, A. H. H.; Balucani, N.; Lin, S. H.; Lee, Y. T.; Kaiser, R. I. *J. Chem. Phys.* **2000**, *113*, 8656.

[48] Bair, R. A.; Dunning Jr., T. H. *J. Chem. Phys.* **1985**, *82*, 2280–2294.

[49] Sims, I. R.; Queffelec, J. L.; Travers, D.; Bertrand, R. R.; Herbert, L. B.; Karthäuser, J.; Smith, I. W. M. *Chem. Phys. Lett.* **1993**, *211*, 461–468.

[50] Wooldridge, S. T.; Hanson, R. K.; Bowman, C. T. *Int. J. Chem. Kin.* **1996**, *28*, 245–258.

[51] Miller, J. A.; Bowman, C. T. *Prog. Energy Combust. Sci.* **1989**, *15*, 287–338.

[52] Borget, F.; Müller, S.; Grote, D.; Theulé, P.; Vinogradoff, V.; Chiavassa, T.; Sander, W. *Astron. Astrophys.* **2017**, *598*.

[53] Talbi, D. *Chem. Phys. Lett.* **1999**, *313*, 626–632.

[54] Irvine, W. M.; Schloerb, F. P. *Astrophys. J.* **1984**, *282*, 516–521.

[55] Arunan, E.; Manke II, G.; Setser, D. W. *Chem. Phys. Lett.* **1993**, *207*, 81–87.

[56] Meads, R. F.; Maclagan, R. G. A. R.; Phillips, L. F. *J. Chem. Phys.* **1993**, *97*, 3257–3265.

[57] Atakan, B.; Wolfrum, J. *Chem. Phys. Lett.* **1991**, *186*.

[58] ter Horst, M. A.; Schatz, G. C.; Harding, L. B. *J. Chem. Phys.* **1996**, *105*, 558–571.

[59] Balla, R. J.; Casleton, K. H.; Adams, J. S.; Pasternack, L. *J. Phys. Chem.* **1991**, *95*, 8694–8701.

[60] Knizia, G.; Adler, T. B.; Werner, H. J. *J. Chem. Phys.* **2009**, *130*, 054104.

[61] Papajak, E.; Zheng, J.; Xu, X.; Leverentz, H. R.; Truhlar, D. G. *J. Chem. Theory Comput.* **2011**, *7*, 3027–3034.

[62] Werner, H. J. et al. 2019; see https://www.molpro.net.

[63] Bomble, Y. J.; Stanton, J. F.; Kállay, M.; Gauss, J. *J. Chem. Phys.* **2005**, *123*, 054101.

[64] Kállay, M. et al. *J. Chem. Phys.* **2020**, *152*, 074107.

[65] Feller, D. *J. Chem. Phys.* **1992**, *96*, 6104–6114.

[66] Helgaker, T.; Klopper, W.; Koch, H.; Noga, J. *J. Chem. Phys.* **1997**, *106*, 9639–9646.

[67] Cheng, L.; Gauss, J. *J. Chem. Phys.* **2011**, *135*, 084114.

[68] http://slater.chemie.uni-mainz.de/cfour/index.php?n=Main.RecontractedCorrelation-consistentBasisFunctions, Accessed: 2020-05-06.

[69] Sellers, H.; Pulay, P. *Chem. Phys. Lett.* **1984**, *103*, 463–465.

[70] Handy, N. C.; Yamaguchi, Y.; Schaefer III, H. F. *J. Chem. Phys.* **1986**, *84*, 4481–4484.

[71] Matthews, D. A.; Cheng, L.; Harding, M. E.; Lipparini, F.; Stopkowicz, S.; Jagau, T. C.; Szalay, P. G.; Gauss, J.; Stanton, J. F. *J. Chem. Phys.* **2020**, *152*, 214108.

[72] Huber, K. P.; Herzberg, G. *Molecular Spectra and Molecular Structure: IV, Constants of Diatomic Molecules*; 2013.

[73] Moore, C. E. *Atomic Energy Levels as Derived from the Analyses of Optical Spectra, Vol. 1*; 1949.

[74] Møller, C.; Plesset, M. S. *Phys. Rev.* **1934**, *46*, 618–622.

[75] Pople, J. A.; Binkley, J. S.; Seeger, R. *Int. J. Quantum Chem., Symp.* **1976**, *10*, 1–19.

[76] Dunning Jr., T. H. *J. Chem. Phys.* **1989**, *90*, 1007–1023.

[77] Nielson, H. H. *Rev. Mod. Phys.* **1951**, *23*, 90–136.

[78] Watson, J. K. G. In *Vibrational Spectra and Structure*; Durig, J. R., Ed.; Elsevier: Amsterdam, 1977; Vol. 6; p 1.

[79] Mills, I. M. In *Molecular Spectroscopy: Modern Research*; Rao, K. N., Matthew, C. W., Eds.; Academic: New York, 1972; Vol. 1; p 115.

[80] Papousek, D.; Aliev, M. R. *Molecular Vibrational-Rotational Spectra*; Elsevier, Amsterdam, 1982.

[81] Clabo Jr., D. A.; Allen, W. D.; Remington, R. B.; Yamaguchi, Y.; Schaefer III, H. F. *Chem. Phys.* **1988**, *123*, 187–239.

[82] Allen, W. D.; Yamaguchi, Y.; Császár, A. G.; Clabo Jr., D. A.; Remington, R. B.; Schaefer III, H. F. *Chem. Phys.* **1990**, *145*, 427–466.

[83] Eyring, H. *J. Chem. Phys.* **1935**, *3*, 107–115.

[84] Truhlar, D. G.; Garrett, B. C.; Klippenstein, S. J. *J. Phys. Chem.* **1996**, *100*, 12771–12800.

[85] Ruscic, B.; Pinzon, R. E.; Morton, M. L.; von Laszevski, G.; Bittner, S. J.; Nijsure, S. G.; Amin, K. A.; Minkoff, M.; Wagner, A. F. *J. Phys. Chem. A* **2004**, *108*, 9979–9997.

[86] Ruscic, B.; Pinzon, R. E.; von Laszewski, G.; Kodeboyina, D.; Burcat, A.; Leahy, D.; Montoy, D.; Wagner, A. F. *J. Phys. Conf. Ser.* **2005**, *16*, 561–570.

[87] Ruscic, B.; Bross, D. H. https://atct.anl.gov/, 2019.

[88] Lee, T. J.; Rendell, A. P. *Chem. Phys. Lett.* **1991**, *177*, 491–497.

[89] Quapp, W.; Zech, A. *J. Comp. Chem.* **2009**, *31*, 573–585.

[90] Bowman, J. M.; Gazdy, B.; Bentley, J. A.; Lee, T. J.; Dateo, C. E. *J. Chem. Phys.* **1993**, *99*, 308–323.

[91] Gazdy, B.; Musaev, D. G.; Bowman, J. M.; Morokuma, K. *Chem. Phys. Lett.* **1995**, *237*, 27–32.

[92] Talbi, D.; Ellinger, Y. *Chem. Phys. Lett.* **1996**, *263*, 385–392.

[93] Contreras, R.; Safont, V. S.; Pérez, P.; Andrés, J.; Moliner, V.; Tapia, O. *J. Mol. Struc.-Theochem.* **1998**, *426*, 277–288.

[94] Isaacson, A. D. *J. Phys. Chem. A.* **2005**, *110*, 379–388.

[95] DePrince III, A. E.; Mazziotti, D. A. *J. Phys. Chem. B.* **2008**, *112*, 16158–16162.

[96] Gutiérrez-Oliva, S.; Díaz, S.; Toro-Labbé, A.; Lane, P.; Murray, J. S.; Politzer, P. *Mol. Phys.* **2013**, *112*, 349–354.

[97] Lin, M. C.; He, Y.; Melius, C. F. *Int. J. Chem. Kin.* **1992**, *24*, 1103–1107.

[98] Pearson, P. K.; Schaefer III, H. F.; Wahlgren, U. *J. Chem. Phys.* **1975**, *62*, 350–354.

[99] Sun, Q.; Yang, D. L.; Wang, N. S.; Bowman, J. M.; Lin, M. C. *J. Chem. Phys.* **1990**, *93*, 4730–4739.

[100] Sims, I. R.; Smith, I. W. M. *Chem. Phys. Lett.* **1988**, *149*, 565–571.

[101] Choi, N.; Blitz, M. A.; McKee, K.; Pilling, M. J.; Seakins, P. W. *Chem. Phys. Lett.* **2004**, *384*, 68–72.

[102] Li, X.; Sayah, N.; Jackson, W. M. *J. Chem. Phys.* **2004**, *81*, 833–840.

[103] He, G.; Tokue, I.; Macdonald, R. G. *J. Chem. Phys. A*. **1998**, *102*, 4585–4591.

[104] Atakan, B.; Jacobs, A.; Wahl, M.; Weller, R.; Wolfrum, J. *Chem. Phys. Lett.* **1989**, *154*, 449–453.

[105] Wagner, A. F.; Bair, R. A. *Int. J. Chem. Kin.* **1986**, *18*, 473–486.

[106] Albernaz, A. F.; Barreto, P. R. P. *Theor. Chem. Acc.* **2019**, *138*, 1–10.

[107] Carvalho-Silva, V. H.; Aquilanti, V.; de Oliveira, H. C. B.; Mundim, K. C. *J. Comp. Chem.* **2017**, *38*, 178–188.

[108] Coletti, C.; Billing, G. D. *J. Chem. Phys.* **2000**, *113*, 11101–11108.

[109] Zhang, D. H.; Lee, S. Y. *J. Chem. Phys.* **2000**, *112*, 203–211.

[110] Kaledin, A. L.; Heaven, M. C.; Bowman, J. M. *J. Chem. Phys.* **1999**, *110*, 10380–10392.

[111] He, G.; Tokue, I.; Harding, L. B.; Macdonald, R. G. *J. Phys. Chem. A*. **1998**, *102*, 7653–7661.

[112] Ju, L. P.; Han, K. L.; Zhang, J. Z. H. *J. Theor. Comp. Chem.* **2006**, *5*, 769–777.

[113] Zhao, R.; Gao, D.; Pan, X.; Song, L.; Yu, H.; Yu, S.; Yao, L. *Chem. Phys.* **2019**, *516*, 38–47.

[114] Jursic, B. S. *J. Mol. Struc.-Theochem.* **1998**, *428*, 55–59.

[115] Espinosa-Garcia, J.; Rangel, C.; Suleimanov, Y. V. *Phys. Chem. Chem. Phys.* **2017**, *19*, 19341–19351.

[116] Yang, D. L.; Yu, T.; Lin, M. C.; Melius, C. F. *Chem. Phys.* **1993**, *177*, 271–280.

[117] Herbert, L.; Smith, I. W. M.; Spencer-Smith, R. D. *Int. J. Chem. Kin.* **1992**, *24*, 791–802.

[118] Sayah, N.; Li, X.; Caballero, J. F.; Jackson, W. M. *J. Photochem. Photobiol. A.* **1988**, *45*, 177–194.

[119] Copeland, L. R.; Mohammad, F.; Zahedi, M.; Volman, D. H.; Jackson, W. M. *J. Chem. Phys.* **1992**, *96*, 5817–5826.

[120] Bethardy, G. A.; Northrup, F. J.; Macdonald, R. G. *J. Chem. Phys.* **1996**, *105*, 4533–4549.

[121] de Juan, J.; Smith, I. W. M.; Veyret, B. *J. Phys. Chem.* **1987**, *91*, 69–72.

[122] Sims, I. R.; Queffelec, J. L.; Defrance, A.; Rebrion-Rowe, C.; Travers, D.; Bocherel, P.; Rowe, B. R.; Smith, I. W. M. *J. Chem. Phys.* **1994**, *100*, 4229–4241.

[123] Faure, A.; Rist, C.; Valiron, P. *Chem. Phys.* **1999**, *241*, 29–42.

[124] Faure, A.; Rist, C.; Valiron, P. *Astron. Astrophys.* **1999**, *348*, 972–977.

[125] Talbi, D.; Smith, I. W. M. *Phys. Chem. Chem. Phys.* **2009**, *11*, 8477–8483.

[126] Jacobs, A.; Wahl, M.; Weller, R.; Wolfrum, J. *Chem. Phys. Lett.* **1988**, *144*, 203–207.

[127] Wooldridge, S. T.; Hanson, R. K.; Bowman, C. T. *Int. J. Chem. Kin.* **1995**, *27*, 1075–1087.

[128] Szekely, A.; Hanson, R. K.; Bowman, C. T. *Int. J. Chem. Kin.* **1984**, *16*, 1609–1621.

[129] Wang, C. Y.; Zhang, S.; Li, Q. S. *Theo. Chem. Acc.* **2002**, *108*, 341–346.

[130] Peterson, K. A.; Adler, T. B.; Werner, H.-J. *J. Chem. Phys.* **2008**, *128*, 084102.

[131] Bartlett, R. J. *Ann. Rev. Phys. Chem.* **1981**, *32*, 359–401.

[132] Purvis, G. D.; Bartlett, R. J. *J. Chem. Phys.* **1982**, *76*, 1910–1918.

[133] Bolman, P. S. H.; Brown, J. M.; Carrington, A.; Kopp, I.; Ramsay, D. A. *Proc. Math. Phys. Eng. Sci.* **1975**, *343*, 17–44.

[134] Zhang, X.; Zhen, Z.; Liu, X. *Sci. China, Ser. B: Chem.* **2005**, *48*, 279–285.

[135] Sun, C.; Liu, Y.; Xu, B.; Li, X.; Meng, L.; Zhang, S. *Comput. Theor. Chem.* **2013**, *1014*, 43–48.

[136] Meek, G. A.; Levine, B. G. *J. Chem. Phys.* **2016**, *144*, 184109.

[137] Tsang, W. *J. Phys. Chem. Ref. Data* **1992**, *21*, 753–791.

[138] Wang, D. Q.; Li, J. L.; Huang, X. R.; Geng, C. Y.; Sun, C. C. *THEOCHEM* **2008**, *857*, 20–26.